Spring 2016

Dynamic impact of ageing dump truck suspension systems on whole-body vibrations in high-impact shovel loading operations

Saeid R. Dindarloo

DYNAMIC IMPACT OF AGEING DUMP TRUCK SUSPENSION SYSTEMS ON WHOLE-BODY VIBRATIONS IN HIGH-IMPACT SHOVEL LOADING OPERATIONS

by

SAEID REZA DINDARLOO

A DISSERTATION

Presented to the Faculty of the Graduate School of the

MISSOURI UNIVERSITY OF SCIENCE AND TECHNOLOGY

In Partial Fulfilment of the Requirements for the Degree

DOCTOR OF PHILOSOPHY

in

MINING ENGINEERING

2016

Approved by

Samuel Frimpong, Advisor

Nassib Aouad, Co-advisor

Grzegorz Galecki

Ralph Flori

K. Chandrashekhara

ABSTRACT

Surface mining operations typically deploy large shovels, with 100+ tons per pass capacity, to load dump trucks in a phenomenon described as high-impact shovel loading operations (HISLO). The HISLO phenomenon causes excessive shock and vibrations in the dump truck assembly resulting in whole body vibration (WBV) exposures to operators. The truck suspension system performance deteriorates with time; therefore their effectiveness in attenuating vibrations reduces. No research has been conducted to study the impact of ageing suspension mechanisms on the magnitudes of WBV in HISLO operations.

This study is a pioneering effort to provide fundamental and applied knowledge for understanding the impact of ageing on the magnitudes of WBV exposures. The effects of underlying ageing processes on a suspension performance index are mathematically modeled. The effects of scheduled maintenance and corrective maintenance on improving the performance index (PI) are also modeled. Finally, the proposed mathematical ageing model is linked to the truck operator's exposure to WBVs via a virtual prototype CAT 793D truck model in the MSC ADAMS environment. The effects of suspension system ageing in increasing the WBV levels are examined in the form of both the vertical and horizontal accelerations under HISLO conditions.

This study shows that the hydro-pneumatic suspension strut ageing results in deteriorating stiffness-damping parameters. The deteriorating suspension performance (with time) introduces more severe and prolonged WBVs in HISLO operations. The RMS accelerations increase significantly with time (suspension ageing). The vertical RMS accelerations increase to severe magnitudes of over 3.45, 3.75, and 4.0 m/s^2 after 3, 5, and 7 years, respectively. These acceleration magnitudes are well beyond the ISO limits for the human body's exposure to WBVs. This pioneering research effort provides a frontier for further research to provide safe and healthy working environments for HISLO operations.

ACKNOWLEDGMENTS

I would like to thank my PhD advisor, Dr. Samuel Frimpong, and co-advisor, Dr. Nassib Aouad, as well as my other PhD examination committee members. Also, I would like to express my sincere gratitude to my loving wife, Elnaz, for all her supports and encouragements. I would also like to extend my gratitude to my parents, brothers, and sister for their continuous support. The department's administrative assistants, Shirley Hall, Judy Russell, and Tina Alobaidan are acknowledged for being there for me.

TABLE OF CONTENTS

LIST OF ILLUSTRATIONS

LIST OF TABLES

1. INTRODUCTION

1.1. RESEARCH BACKGROUND

Large mining dump trucks expose operators to extreme levels of accelerations and vertical displacements during high impact shovel loading operation (HISLO) (Frimpong, 2011). Long-time exposure to high amplitudes of vibrations under HISLO conditions makes dump trucks operators vulnerable to a range of health threatening consequences (Aziz et al., 2014).

ISO 2631-1 standard has addressed the vibration exposure issue and set maximum tolerable WBV exposures to ensure operator comfort, safety and health (Abdeen and Abbas, 2011). Frimpong and Aouad (2009) formulized the dynamics of the induced vibrations under the HISLO conditions for heavy mining dump trucks. They have developed a comprehensive model of the problem with 37 degrees of freedom (DOF). This virtual prototype model included all the effective parameters in the system response to the impulse force excitation due to material dumping.

In their study, the governing equations of motions were set and solved analytically and numerically. However, all the system characteristics, such as suspension stiffness and damping coefficients were considered as deterministic variables based on the manufacturer's nominal values. On the other hand, there are different types of uncertainties in this problem, which result in unrealistic outputs derived from only deterministic considerations. The major sources of uncertainty in this problem include:

(i) Uncertainties due to manufacturing processes (e.g. different stiffness rates for the same manufacturing design specification of a suspension spring).

(ii) Uncertainties due to operational alterations such as mechanical fatigue, ageing, tear and wear (e.g. reduction of suspension damping coefficient after some years of operation).

(iii) Uncertainties due to simplifications in modeling and calculations (e.g. primary assumptions and simplifications in problem modeling and solution).

Thus, for robust and realistic numerical simulation results, all these uncertainties should be incorporated into the problem to characterize the WBV exposures under HISLO conditions. Since a dump truck is designed to operate for several years in a mining environment, it must meet all safety and health requirements during its useful lifetime. Therefore, a prediction method for anticipating future suspension system performance under HISLO is important for the long-term safety and health of operators.

1.2. STATEMENT OF THE PROBLEM

Surface mining operations around the world deploy large capacity shovels and dump trucks to achieve economic bulk production targets. These large shovels load dump trucks with 100+ tons passes under gravity causing severe vibrations in the dump trucks. These vibrations are propagated through shockwaves in the truck bodies. A component of the shockwaves generated from these vibrations is propagated into the operator's cabin. The severe magnitudes of the cabin shockwaves expose the operator to high levels of whole body vibrations (WBV). Long-term WBV exposures cause musculoskeletal and other diseases of the joints and limbs, and chronic lower back, neck and shoulder pains and injuries [ISO 2631].

The International Standards Organization (ISO) 2631-1 provides recommendations on safe limits beyond which long-term exposure causes health problems and long-term disabilities (Frimpong, 2011). Frimpong and Aouad (2009) have addressed the dynamics of the induced vibrations under HISLO conditions for large dump trucks. The results from their work showed that the lower back region of the operator is exposed to extreme levels of RMS accelerations of 3.56 m/s^2 compared to the limit defined by ISO 2631-1 as extreme (i.e., 2.5 m/s^2). However, their

models utilized deterministic variables to simulate the WBV exposures. The stiffness and damping variables for many dump truck components, within the HISLO environments, are random and must be addressed using stochastic process formulation.

In addition, mining trucks are designed and manufactured with operating lives from 15 to 20 years with effective preventive maintenance (PM) schemes and rebuilds within appropriate time frames. The ability of the suspension mechanism to effectively attenuate the impact of vibrations from HISLO conditions also deteriorates as the truck ages. In cases of poor PM schemes and shovel care practices, the effects can be severely pronounced exposing operators to safety and health risks. Thus, for a sustainable modification of vibration attenuation characteristics of a system, a good knowledge of the time-performance of the suspension system is required for effective PM schemes, replacement of system components and rebuilds.

Discussions with Dr. Jeffrey L. Kohler, Associate Director for Mining, and Director, Office of Mine Safety and Health Research at CDC-NIOSH, after his visit to several large scale surface mining operations in Colombia, provided impetus for this research study. Dr. Kohler observed severe cases of injuries among truck operators due to high WBV exposures mainly from old dump trucks. This problem also persists in the surface mining industry of the United States and the world. This research study is a component of the proposal funded by CDC-NIOSH entitled, “Engineered Solutions: Dump Truck Vibrations and Impact on Operator Safety in High Impact Shovel Loading Operations (Contract Award #: 200-2011-40817)”.

In today’s competitive markets for raw materials, there is an urgent need for producers to reduce mining costs. The use of heavy mining machinery is therefore imperative. However, there is a greater need and requirement to provide safe and healthy operating environments for operators to perform their duties. This research provides a pioneering effort toward this important requirement using fundamental and applied research methods. The current state-of-art technology in large mining dump trucks exposure the truck operators to vertical accelerations of

over 3.50 $^{m}/_{s^2}$ in magnitude, under the HISLO conditions, which is far from the ISO recommended dose of accelerations for the health and comfort of operators. However, this poor performance exacerbates even more with time.

Hydro-pneumatic suspension struts, like other mechanical systems/components/ suffer from mechanical fatigue, wear, ageing, deterioration, creep and chemical reactions which deteriorate their performance with age. If not maintained and repaired adequately these ageing suspensions expose the operators to extremely high magnitudes of vertical acceleration (i.e., even greater than 4.0 $^{m}/_{s^2}$) that result in life-long disabilities of the truck operators. Aside from their long term consequences, the vibrations cause human fatigue and lack of concentration which not only reduce the operators' productivity but they introduce higher risks of accidents.

1.3. RESEARCH OBJECTIVES AND SCOPE

The primary objective of this research study is to provide understanding into the impact of ageing on suspension system performance of large dump trucks in random fields and under HISLO conditions. The elements of this primary objective include:

(i) developing stochastic functional relationship between the suspension system performance and determinant variables for a large mining truck;

(ii) developing time-dependent functional relationship between the suspension system performance and determinant variables for a large mining truck;

(iii) co-simulating the stochastic-time dependent suspension models in the MSC.ADAMS environment;

(iv) providing greater understanding into the performance of truck suspension system under coupled random-time constraints; and

(v) providing a paradigm shift for planning PMs, component replacements and rebuilds.

This research is limited to the study of ageing characteristics of hydro-pneumatic suspension performance in large mining trucks in random fields under HISLO conditions in a surface mining environment.

1.4. RESEARCH METHODOLOGY

This research will combine the use of analytical survey of the required literature and mathematical techniques to model temporal behavior of ageing hydro-pneumatic suspension systems in large mining dump trucks under both the HISLO and normal haulage operations. The developed mathematical model(s) will be validated using numerical examples and (if accessible) real suspension performance data from surface mines. Critical review and analysis of the relevant literature will provide the current body of knowledge and the research frontier in (hydro-pneumatic) suspension mechanism of large mining dump trucks with the ultimate goal of minimizing the dump truck operators' exposure to health-threatening whole-body vibrations due to aged malfunctioning suspension struts. This process ultimately places the research study at the frontiers of this research paradigm and provides a rational for the PhD research. Mathematical models will be developed to capture the effect of ageing and maintenance qualities on performance of the hydro-pneumatic suspension struts in energy dissipation.

The suspension performance deteriorates due to effects of two broad categories of continuous-minor-effect and sudden-major-effect processes. The former category encompasses the ageing processes such as hydraulic oil contamination, oil-nitrogen mixing, and gas accumulator's diaphragm rupture (polymeric deteriorations). The latter category encompasses the shocks which happen discretely, such as the shocks due to HISLO or passing on bumps in mine roads and ramps. Both processes will be mathematically modeled to capture the actual underlying physical processes and their effects on suspensions condition.

The effects of the above deteriorating processes are compensated by maintenance. Two major types of maintenance, i.e., scheduled or fixed-interval inspection and maintenance, and

condition-base maintenance will be combined mathematically together. Finally, the proposed mathematical framework will be verified and validated using actual suspension data from operating US surface mines. The results will be in the form of temporal characterization of typical hydro-pneumatic suspension struts in large mining haul trucks. The outputs will be used to modify current suspensions technologies, reschedule maintenance, and increasing the operators' health and safety through providing relevant training.

1.5. SCIENTIFIC AND INDUSTRIAL CONTRIBUTIONS

This research effort is expected to expand frontiers and advance knowledge with impact on the use of large mining trucks in surface mining operations in the area of reducing WBV exposures and their negative effects. The research will originally develop understanding into the mechanisms underlying and governing the ageing process of the suspension systems in very large mining dump trucks. The new knowledge will be broadly employed in designing and manufacturing more robust suspensions. Thus, the long term health and safety of operators will be improved considerably. The findings of the research study can be used in designing new inter-disciplinary graduate level courses in mining and mechanical engineering. Mining machinery reliability analysis and application of statistical methods in machine-human health and longevity are the two promising courses that can be constructed based on the experience, knowledge, and results obtained from this research initiative.

1.6. STRUCTURE OF THE PHD DISSERTATION

Sections 1.1-1.5 contain an introduction to the PhD dissertation. The introduction lays the groundwork by providing the underlying suspension ageing problem in large mining dump trucks. The objectives and the scope of the research study, the research methodology and its scientific and industrial contributions are discussed in this chapter. Sections 2.1-2.7 provide a critical review and analysis of the relevant literature and provide a rational for the PhD

dissertation on the current frontiers of the ageing suspension problem using mathematical modeling of the underlying processes. Sections 3.1-3.4 contain the mechanics, thermodynamics and working principals of hydro-pneumatic suspension struts in large mining dump trucks.

Sections 4.1-4.3 present the methodology and mathematical modeling scheme of the suspension under different deteriorating phenomenon. The effects of maintenance on ameliorating the influence of ageing and shock process are discussed, elaborated and modeled in this chapter. Sections 5.1-5.3 contain model validation using a numerical example. The proposed methodology and developed models in chapter 4 are verified and validated using numerical examples in this chapter. Sections 6.1 -6.6 discuss the experimentations and the experiment environment. Sections 7.1-7.5 summarize the experimentation results, including the importance of the results. Sections 8.1-8.4 summarize the findings and present the conclusions, contributions of this PhD research, as well as, the recommendations for future work .The references that have been used during the study and the development of the solution of the suspension ageing problem are listed at the end of this dissertation.

2. LITERATURE REVIEW

The author has critically reviewed and summarized the contributions and limitations over 500 technical publications. This section outlines the summary contributions from a segment of the published work with significant impact. This review focuses on (i) vibration and suspension systems modeling; (ii) ageing suspension systems performance, (iii) ergonomics; (iv) vibration transmissibility through human body; and (v) health risks associated with higher WBV levels. To find technical solutions to the WBV exposure problems, it is essential to first evaluate truck vibrations through detailed mathematical modeling and application of numerical methods to solve complex equations of motions associated with HISLO vibrations.

Aouad (2008) covered the mechanics of dump truck vibrations under HISLO conditions. This work is among the few studies conducted specifically on truck vibrations, which provides a comprehensive knowledge of the mechanics of the system. Numerous researchers have addressed health risks associated with vehicular vibrations in a wide range of vehicles from forklift trucks to military aircrafts. Others have developed more efficient solutions to minimize vibration exposure and enhance human health conditions through fabrication of more effective ergonomic seats (Huston et al., 1999), measurement of whole body vibration magnitudes (Howard et al., 2009), vibration transmissibility through human body (Abdeen and Abbas, 2011) and mathematical modeling of suspension systems (Gomez et al., 2012).

2.1. OPERATOR'S HEALTH RISKS

Exposure to high levels of vibration affects the health of operators, and contributes to low efficiency and productivity of operations due to extreme human fatigue and lack of concentration. Many researchers have studied different aspects of WBV exposures in different industries from underground mining to aircrafts industries. Although there are differences in the mechanics of

vibrations, there is a unique standard for maximum vibration levels defined by the International Organization for Standardization (ISO).

ISO (2004) addresses the issue comprehensively and discusses evidence, which suggests that long-term exposure to WBV containing multiple shocks can lead to adverse effects on the lumbar spine. Various structures in the low back, including the intervertebral discs, paraspinal ligaments and muscles are at risk of injury in WBV environments containing multiple shocks. The main reasons are as following:

(i) increased mechanical stress caused by seated postures,

(ii) changes to the way the body responds to multiple loads caused by various postures,

(iii) pressure changes, tearing, buckling, or softening of the intervertebral discs with exposure to multiple loads,

(iv) potential changes to the neuromuscular control system which will affect passive and active stabilization,

(v) unexpected sudden loading can lead to an overcompensation in the trunk mussels response, and

(vi) buckling events can occur due to an inability of the neuromuscular control system to respond in a quick and coordinated fashion to sudden loading (ISO 2631-5, 2004).

WBV exposure causes an acceleration of the human body with related dynamic forces acting on the spine. The significant effects of posture and backrest contact on the transmissibility of WBV to the head suggest the interaction between the subject and the seat to have an effect on the associated dynamic internal forces. Seidel (2005) found that the combination of anatomy-based finite element models with *in-vitro* data seems to be the best suited approach to establish quantitative exposure-effect relationships. Manufacturers could use model predictions for an assessment of different designs. Up to now, major uncertainties result from the nonlinearity of human bio-dynamics, insufficient knowledge on the effects of WBV in the x- and y-axes, the unknown strength of the spine for shear loads, the influence of the coupling characteristics

between the seat and operator, the significance of posture and muscle activity, and missing reliable data on material properties of the spinal structures.

Smets et al. (2010) conducted an experiment to measure WBV levels experienced by operators of haulage trucks in a surface mine during one hour of normal operation. They measured WBV on eight trucks in three size classes of 35, 100, and 150 tons. As expected, they found the highest levels of vibration and displacement in the vertical direction. Their results are valid only for that particular mine and for measured trucks with capacities up to 150 tons. They did not relate vibration and shock wave propagation to type, make, and age of trucks, which are important in vibration exposure.

One of the most reported complaints of operators who are exposed to WBV is lower and back pain especially in seated positions, because weight of the upper body, which constitutes the majority of the whole body weight, is acting on lower back. The lower back (buttocks) is the first part in contact with the source of vibration (seat). Leelavathy et al. (2011) reviewed selected papers that had studied exposure to WBV and lower back pain among operators of mobile equipment. They found that the most frequently reported adverse effects of WBV exposure are lower back pain (LBP), early degeneration of the spine and intervertebral discs. Almost all findings, in different studies showed a strong tendency that long term exposure to WBV is harmful to the spinal system.

Leelavathy et al. (2011) suggested that relevant information be gathered to assist in designing better working conditions for operators, which will enhance their health and wellbeing, productivity, morale, and efficiency in performing their jobs. Work modifications and adequate suspension seats would be beneficial for primary prevention of unnecessary exposure to vibration and shocks. Hence, there is a current need to do research focusing on ergonomic exposure data. They found only few studies that had specifically examined the issue by developing models. Since application of mathematical models provides a platform for conducting more accurate and

comprehensive investigations it was suggested to develop robust mathematical models of the problem.

Howard et al. (2009) implemented a series of assessments in order to aid in the further development of an in-house health and safety program. They conducted this study for a large open pit mining facility interested in reducing back pain among its operators. The WBV magnitudes were characterized for a range of jobs. They employed both male and female operators ranging in age, height, and weight to provide the widest range of exposure characterization. The results of their experiments, in that specified surface mine, revealed different vibration exposures for different small to medium size mining vehicles, such as: haul trucks (average root mean squares (A_{RMS}) = 0.6 ± 0.1 m/s^2), graders (A_{RMS} = 0.5 ± 0.3 m/s^2), tracked dozers (A_{RMS} = 0.7 ± 0.1 m/s^2), and personal vehicles (A_{RMS} = 0.8 ± 0.1 m/s^2), which were all found to produce WBV levels falling in the moderate health risk exposure range.

The wheeled dozers group (A_{RMS} = 1.0 ± 0.1 m/s^2), the wheeled loaders group (A_{RMS} = 0.9±0.2 m/s^2), kress haul truck group (A_{RMS} =1.1± 0.6 m/s^2), and the utility vehicles job group (A_{RMS} = 1.0 ± 0.1 m/s^2) were found to produce WBV levels above the moderate/high health risk boundary. As a result of their research, the authors recommended that those workers exposed to WBV with ARMS values above the upper health caution limit, be given awareness training, be placed under some form of health surveillance, and have practical and feasible vibration control measures implemented to minimize their exposure to the WBV. However, the authors did not try to find correlations between gender, physical condition, age, and posture of work force and probable risk hazards due to workplace vibrations. Also, no investigation was considered to find the effects of fatigue and age of mining vehicles to vibration intensity.

Other mining vehicles which are associated with high levels of vibrations are underground load-haul-dump machines (LHDs). Although the intensity and frequency of vibrations are different from those of surface dump trucks in HISLO, the mechanics and mechanism of shock wave propagation and its transmissibility through the operator's body are

almost the same. Eger et al. (2008a) conducted a research study to evaluate the health risks associated with the operation of LHD vehicles, based on ISO 2631-1 and ISO 2631-5 criteria. They measured WBV using a tri-axial seat pad accelerometer based on the procedures established in ISO 2631-1 for seven LHDs. In this research, the authors provided a comparison of predicted health risks based on ISO 2631-1 and ISO 2631-5.

In order to prevent negative health outcomes associated with WBV exposure, a risk assessment, based on published standards, can be conducted. The most widely accepted standard for measuring and evaluating human exposure to WBV and subsequent prediction of health risks is the ISO report entitled, "ISO 2631-1: Mechanical vibration and shock—Evaluation of human exposure to whole-body vibration, Part 1—General requirements."

ISO (2004) introduced a new standard for evaluating human exposure to WBV that contains multiple shocks. This standard is outlined in the ISO 2631-5 entitled, "Mechanical vibration and shock—Evaluation of human exposure to whole-body vibration, Part 5—Method for evaluation of vibration containing multiple shocks." Given the short period of time since the conception of ISO 2631-5, very few studies have been reported in peer-reviewed publications or published conference proceedings. Based on the limited sample in this study, general health guidance provided in ISO 2631-1 (which considers negative health effects on the whole body) appears to be more stringent than the health guidance based on ISO 2631-5 (which only considers negative health effects on the lumbar spine (Eger et al., 2008b).

2.2. VIBRATIONS AND SUSPENSION SYSTEM MODELING

A comprehensive knowledge of the mechanics of vibration and suspension systems performance, under different working conditions, is required to evaluate the vibration effects and to be able to offer efficient and reliable solutions to the problem. Different researchers have addressed the issue by proposing different mathematical models and numerical solutions to solve the equations of motions, and to investigate the state of the system under different conditions.

Since the vibration mechanics is very complicated, especially for real situations with numerous variables, most researchers have evaluated the problem in some level of simplification. Among these works is a study by Abdeen and Abbas (2011), who proposed a 4-degree-of-freedom (DOF) analytic biomechanical model of the human body in a sitting posture, without backrest and in vertical vibration direction to investigate the biodynamic responses of different masses and stiffness.

They applied artificial neural network (ANN) technique to simulate and predict the response of seated human body for different masses and stiffness. The results of their numerical study showed that the ANN method was capable of simulating and predicting the response behaviors of seated human body that is subjected to WBV exposure. The human body in a sitting posture can be modeled as a mechanical system that is composed of several rigid bodies interconnected by springs and dampers (Boileau and Rakheja, 1990).

The biodynamic response of a seated human body exposed to WBV can be broadly categorized into two types. The first category is termed "to-the-body" force motion, which is defined as a function of the frequency at the human-seat interface, expressed as the driving-point mechanical impedance (DPMI) or the apparent mass (APMS). The second category is termed as the "through-the-body" response function also defined as seat-to-head transmissibility (STHT) for the seated occupant (Abdeen and Abbas, 2011). They concluded that the change in human body mass, pelvic stiffness, and pelvic damping coefficient results in a remarkable change in biodynamic response behaviors of seated human body (directly proportional to the human body mass and pelvic stiffness coefficient, and inversely proportional to the pelvic damping coefficient). The developed ANN models were successful in simulating the effect of the human body mass and stiffness on the biodynamic response behaviors under WBV. The ANN models were also successful in predicting the response behaviors at different masses and stiffness levels, beyond the range of those that were used in the analytic solution.

Rodríguez et al. (2011) designed an adjustable-stiffness spring system, and proposed a mathematical model to solve displacements of the springs. They validated their prototype and mathematical model through experimental results. The authors fabricated a prototype model by four-leaf springs, which were fixed at one end and connected to a series of rollers at the other end. This model provided a horizontal movement of springs by an electrical motor to change length and, consequently, the stiffness of springs. In the mathematical models, they assumed each one of the springs as a beam element which was clamped at its inner extreme, with horizontal displacement-free at its outer extreme. The differential equations were solved numerically, and were compared with the experimental results. The authors considered non-linearities in the proposed system. In other words, it was a new model of an adjustable-stiffness spring employing leaf springs with non-linear elastic deformations. However, the experimental results showed different values than the mathematical model when the springs were working close to the limits of their maximum load and stiffness. This is due to the fact that the protection system modifies the boundary conditions of the problem. A finite element computational model is recommended to obtain more accurate values of the stiffness in these situations.

Walsh and Lamancusa (1992) designed and investigated an adaptable vibration absorber. Their research objectives included: (a) to minimize transient vibrations of rotating machines during startup and shut-down conditions, and (b) to adapt to changes in steady state operating speeds, such as might occur in engines and pumps when load conditions vary. The model was a single DOF with main system consisting of constant mass, stiffness and damping coefficient and an absorber consisting of constant mass and damping coefficient. The optimization of the time-varying-stiffness yielded improvements of 66% and 67% in rms (root mean square) and peak displacements, respectively. In addition, the effects of damping, mass ratio and acceleration of the unbalanced mass were examined. It was shown that, for maximum reduction of vibration amplitude of the main mass, low absorber damping coefficients, high mass ratios and low acceleration rates are desired. However, the authors considered a simple one-DOF system, which

may not be a representative of the actual complicated motions. They also assumed a constant damping coefficient for the proposed absorber for simplification purposes.

The importance of the suspension system of a vehicle is that, it is responsible for the comfort of the driver and the safety of the vehicle. A suspension system is the part, which carries the body mass of the vehicle and also transmits all the forces between this body and the road. Nouri et al. (2011) proposed a three-DOF model of a quarter vehicle suspension system, including the seat and driver masses. The modal parameters of the system, which indicate the comfort and the safety of the suspension, were identified using Wavelet analysis. The authors concluded that wavelets are a powerful tool for the modal analysis in vibration applications, especially for suspension systems. However, their experiment was limited to a simplified three-DOF model, under specified conditions, which cannot cover a wide range of different vibrating scenarios for real complex systems.

Bouazara et al. (2006) formulated a generalized nonlinear model for the dynamic analysis of suspension seats with passive, semi-active and active dampers. The semi-active and active dampers were characterized by force generators in accordance with the control laws based upon suspension mass velocity. The comfort and safety performance characteristics of the optimal suspension seat with semi-active and active dampers were evaluated, under both the sinusoidal and random excitations, based on the guidelines provided by ISO-2631. The authors concluded that, the comfort performance of a suspension seat with semi-active and active dampers can be considerably enhanced.

Passive suspension seats are widely used to reduce the magnitude of low frequency vehicular vibrations that are transmitted to the driver's body. A suspension seat is designed not only for attenuating the vibrations, but also to provide adequate postural support for the driver with adequate seated height. Considering that the vibrations magnitude and dominant frequencies of different vehicles vary considerably, it is essential to fine tune the suspension seat properties for both optimal vibration isolation and ergonomic factors, such as seated height, fore-aft

adjustments and postural support. Theoretically, a suspension seat must be optimally adjusted to provide the driver with adequate vision, while maintaining the suspension ride height near its mid-position. Since the suspension seats are components that are adapted to a wide range of vehicles, they are often inadequately adjusted by the drivers. An inadequately tuned suspension seat can cause high magnitude shocks and vibrations due to the impacts against the motion limiting bump stops. Such impacts may occur more frequently in road vehicles, where the natural frequency of suspension seats is close to that of the bounce mode frequency of the vehicle (Bouazara et al., 2006).

McManus et al. (2002) examined the performance of a semi-active magnetorheological (MR) damper in reducing the incidence and severity of end-stop impacts of a low natural frequency suspension seat. The MR damper was a commercially developed product, referred to as "*Motion Master semi-active damping system*". A lightly damped and soft suspension is considered desirable for elective attenuation of continuous vibration of low-to-medium levels, provided that the excitation occurs at frequencies well above the seat's natural frequency. The attenuation of high-magnitude vibration and shock, on the other hand, requires suspension designs with higher damping and stiffness to prevent end-stop impacts from occurring.

In environments involving combinations of low, medium and high levels of continuous vibration and shocks, means of achieving variable damping are thus desirable to adapt the seat attenuation performance accordingly. This can be achieved through the incorporation of active or semi-active damping within the suspension. The *Motion Master* damping system consists of a controllable damper filled with MR fluid, a controller with an integrated sensor arm, a three-position ride mode switch offering light, medium and firm damping, and a microprocessor. The MR damper algorithm is formulated to provide light damping under low magnitudes of relative deflections. While operating on relatively smooth roads, the suspension damper operates in a passive mode with either little or no current transmitted to the coil.

When the suspension encounters relatively large motions, the algorithm detects the relative position of the seat suspension and its time rate of change, and generates an appropriate command current signal for the magnetic coils to increase the damping force to prevent collision with the end-stops. A three-position ride mode switch is also integrated within the design that allows the driver to adjust the firmness of the overall ride by setting the damping to one of three settings: soft, medium, and firm. The results from McManus et al. (2002) study indicated that significantly higher levels of transient excitation are necessary to induce end-stop impacts for a seat that is equipped with an MR damper. Particularly, the difference with the conventional damper is more pronounced for seat positions, which are closer to the end-stops. They concluded that, the use of the MR damper can result in considerably less severe impacts and correspondingly lower vibration exposure levels.

Goh et al. (2005) evaluated the uncertainties in modeling an automotive suspension system. They presented a case study of a MacPherson strut automotive suspension analysis, and evaluated the uncertainties in modeling using both a simplified analytical model and a complex computational model. In both cases, the variability in design variables was characterized using probabilistic design methods. Dynamic simulation of mechanical subsystems, instead of a full vehicle simulation results in a less complicated model and minimizes the errors and the required time to identify them. Even so, the quarter- or half-vehicle suspension model consists of many independent parts, and the equations of motion describing its dynamics are very complex.

Goh et al. (2005) employed a half-vehicle model in MSC.ADAMS, while a quarter-car model was used as the simplified model to describe the front suspension dynamics in their case study. MSC.ADAMS is general-purpose multi-body system (MBS) simulation software that allows the simulation, understanding, and quantification of the performance of mechanical systems. The ADAMS half-car suspension model, used in this case study, consisted of 37 DOFs, with 32 moving parts. The top mounts were fixed, and the connections between parts were described by joints of various types. The model consisted of a database of all parts definitions

(geometry, inertial properties, characteristics, and variations). The non-linear relationships describing the characteristics of the components were entered as splines in ADAMS, and instantaneous values were interpolated from spline data.

Since the data variability information was not available Goh et al. (2005) estimated the variability for design variables from several sources, such as: tolerances specified in drawings, experts opinions, and published data. They demonstrated that both the simplified and ADAMS models could predict the pattern of top mount force well, with the simplified model having a greater systematic shift from the experimental measurement. The authors concluded that, for optimization purposes, a simplified model could be used in initial design iterations for faster evaluations to obtain sensitivity measures to assess the impact of design changes and guidance for data collection effort. At later design stages, more complex models with probabilistic methods could be used to obtain more accurate results. However, the authors did not address how to measure the level of confidence, and what level was appropriate and optimal for decision making on application of simulation. Their experiment was restricted to a specific suspension system, with several assumptions for simplifications. They also did not address the time-varying characteristics and their effects on future performance of a typical suspension system.

Demir et al. (2012) developed an analytical nonlinear half-vehicle model, which included quadratic tire stiffness, cubic suspension stiffness, and coulomb friction. They designed a hybrid fuzzy logic approach, which combined fuzzy logic and PID controllers for reducing the vibration levels of passenger seat and vehicle body. The authors introduced the process of mathematical modeling as an important step on vehicle vibration control. They mentioned that despite the fact that real suspension system behavior is nonlinear, automotive suspension systems are often modeled as ideal linear characteristics for mathematical simplicity. They assumed both quadratic and cubic stiffness, as well as Coulomb friction as the main nonlinearities in their model of a real suspension system.

Their model included five DOFs and considered only vertical and pitch motions and neglected roll and yaw motions. The DOFs of the half-car model were the bounce motion of passenger seat, the bounce motion of the vehicle body, the pitch motion of the vehicle body, the vertical motion of the front wheel, and the vertical motion of the rear wheel. The authors proposed a control approach for this non-linear half-vehicle model in order to control or minimize the vibration level of passenger seat and vehicle body. The aim of designing fuzzy logic controllers in their study was not only reducing the vibration level of a vehicle but also being able to cope with nonlinearities in the system. The simulation results showed that the controller approach was effective in vibration reduction performance in the nonlinear half-vehicle model so that ride comfort could be guaranteed. Although the authors attempted to include non-linear behaviors in the proposed model, they ignored roll and yaw motions of the vehicle body, but only the vertical and pitch motions of the body were considered.

2.3. ERGONOMIC SEATS

Engineered and ergonomic suspension seats have been effective in shock wave and vibration attenuation and vibration transmissibility characteristics through the human body. Thus, one of the key elements in the dump truck vibration problem is evaluation of different available suspension seats and their performance. Beside the vibration control, a suspension system determines the ride comfort of the vehicle. Therefore, seat characteristics should be properly evaluated to design a proper driver seat under various operating conditions. It also improves the vehicle control, safety, and stability without changing the ride quality, road holding, load carrying, and passenger comfort while providing directional control during maneuvers. A properly designed driver seat can reduce driver fatigue, while maintaining the same vibration levels against different external disturbances, to provide improved performance in riding (Rajapakse et al. 2007).

Boileau and Rakheja (1990) examined four different types of vertical suspension seats, both in laboratory field conditions, in order to measure their adaptability for attenuating WBV in off-road forestry vehicles. The authors found the kinematics of the linkage system and damping mechanism as the most effective factors on vibration transmission characteristics of the seats. They tested four different kinds of seats namely A, B, C, and D to evaluate their performance. All four seats consisted of either elastic or rigid motion-limiting stops, with fore-aft and height adjustments. All except seat D had backrest and seat cushion angle adjustments. Seats A, B, and C were equipped with hydraulic shock absorbers while seat D used a gas shock absorber. A cross-linkage mechanism was used in the experiments on seats B, C and D, while seat A used a behind-the-seat suspension mechanism. The authors developed a set of laboratory and field tests to investigate the static characteristics of seat suspension components and their vibration transmission performance.

Seats B and C exhibited a considerable hysteresis and progressively hardening behavior, in the lab tests. Seat A's cushion exhibited the highest stiffness which failed during testing. The acceleration transmissibility of seat B was improved, considerably, by using soft cushion when increasing the peak-peak displacement excitation. Boileau and Rakheja (1990) concluded that the static testing, under laboratory conditions, was instrumental in determining the parameters that distinguish the seats from one another. The vibration transmission performance of the various seats, although similar under laboratory and field testing, showed certain differences which might be attributed to the different types of excitation used, to their different excitation amplitudes, frequencies and type of seat loadings.

Rajapakse et al. (2007) presented a control method that combined sliding-mode control (SMC) and quantitative feedback theory (QFT) for designing a driver seat of a heavy vehicle to reduce driver fatigue. A mathematical model was considered to analyze tracking control characteristics through computer simulation in order to demonstrate the effectiveness of the proposed control methodology. The simulation results showed that the adaptive driver-seat

controller had a high potential to provide a superior driver comfort over a wide range of road disturbances. However, parameter uncertainties, the presence of un-modeled dynamics, such as structural resonant modes, neglected time-delays, and finite sampling rate can largely change the dynamics of such systems which were not considered in this study.

2.4. VIBRATION TRANSMISSIBILITY THROUGH HUMAN BODY

A good understanding of vibration transmissibility through different parts of the human body provides a platform for more efficient evaluation and understanding of vibration effects on operators' health. Determination of key elements on vibration waves behavior and human body interaction, such as operator's posture is of high importance in understanding of the issue. Wang et al. (2008) measured and analyzed the "to-the-body" and "through-the-body" biodynamic response functions of the seated human body exposed to vertical vibrations (0.25,0.5,1.0 m/s^2 rms acceleration) in an attempt to identify the relationships between the apparent mass and seat-to-head transmissibility measures. They examined three back support conditions (none, vertical and inclined), and two different hands positions (hands in lap, and hands on the steering wheel). The vertical apparent mass and seat-to-head transmissibility responses were acquired during the experiments, where the head acceleration was measured using a light and adjustable helmet-strap mounted accelerometer. Relatively stronger effects of hands position were observed on the seat-to-head transmissibility responses compared with the apparent mass responses under back supported conditions.

Apparent mass (APMS), driving-point mechanical impedance (DPMI), seat-to-head vibration transmissibility (STHT) and absorbed power have been widely used to characterize the response characteristics of the seated subjects who are exposed to vibration. These functions describe "to-the-body" force–motion relationship at the human–seat interface, while the transmissibility function describes "through-the-body" vibration transmission properties. The types and level of vibrations, and sitting posture and muscles tension have important influences

on both types of responses to WBV. Wang et al. (2008) performed measurements to establish the influences of back support condition, hands position and vibration magnitude on the acquired measures. Relationships between the measured vertical apparent mass and seat-to-head transmissibility biodynamic responses of the seated occupants, under vertical vibrations, were investigated as functions of sitting posture and excitation conditions. Their results revealed considerable effects of back support conditions on the magnitudes of acceleration transmitted to the head. The authors found that the back support condition, strongly, affects both the seat-to-head transmissibility and apparent mass responses. Furthermore, the hands position may also influence both responses.

Wang et al. (2008) concluded that there were relatively stronger effects of hands position on the seat-to-head transmissibility compared with the apparent mass magnitude responses under back supported postures. The results further showed strong influences of three back support conditions on both the vertical apparent mass and the seat-to-head transmissibility responses. The vertical apparent mass and the seat-to-head transmissibility magnitudes in the vicinity of the secondary resonance (7–11 Hz) tended to be higher for the back supported postures. Smith et al. (2008) studied the transmission characteristics of selected suspension seats in multi-axes vibration environments. Tri-axial accelerations were measured at the floor of the vibration table and at the interfaces between the subject and mounted seat (seat pan and seat back). The transmission ratios between the overall seat pan and seat back accelerations and floor accelerations provided an effective tool for evaluating the effects of measurement site, vibration direction, and posture among the selected seating systems.

The experimental set up included the following:

(i) Two seating postures.

(ii) Four seating configurations.

(iii) The seat back angle for the locomotive seats was adjusted.

In setup (i), for the back-on posture, subjects were instructed to sit upright with their back in contact with the seat back. For the back-off posture, subjects were instructed to sit upright but lean slightly forward so as not to contact the seat back. In setup (ii), three of the configurations used locomotive seats, two of these seats were suspension seats, the third seat was a freight seat (FS) without any suspension mechanism, and the fourth seat was a rigid metal seat. In setup (iii), the angle was adjusted to six degrees to coincide with the seat back angle of the rigid seat.

The highest weighted seat pan accelerations (between 1 and 10 Hz) occurred in the z direction for all three locomotive seats. Both the transmissibility and transmission ratios, calculated in this study, demonstrated the strong influence of coupling between the seat back and human in the horizontal directions, particularly in the fore-and-aft (x) direction when using non-rigid seating systems in multi-axis environments. The transmission ratio was calculated as the ratio between the overall seat acceleration and overall floor acceleration in each direction. This ratio was similar to the Seat Effective Amplitude Transmissibility (SEAT) defined in Griffin (1990) and ISO 10326-1: (1992) but does not include weighting of the input and output acceleration spectra.

The results of this study suggest that using passive suspension seats in vibration environments, where the major frequency components coincide with the resonance characteristics of the seating system, may not be the best approach to mitigating large occupant motions. In addition, where there is substantial vibration in the x- or y-axis of the body, horizontal suspension systems may be useful additions. The results also showed that the system transfer matrix, estimated using a multiple-input/single-output model, would be less than ideal for predicting low frequency operational seat vibration when using suspension seats. The seat effective amplitude transmissibility (SEAT), estimated for the tested locomotive seats, was used to predict the weighted seat pan accelerations and vibration total values for assessing a 1-hour operational exposure in accordance with ISO 2631-1 (ISO, 2004).

Patil and Palanichamy (1988) modeled a tractor-occupant system as a lumped parameter system. The composite model was analyzed by computer simulation for vertical vibration responses for a new type of seat suspension. They showed that the new tractor seat suspension system (by proper selection of parameters) improved the tolerance to high-intensity vibrations, in the 0.5-11-Hz range, experienced by tractor occupants. This is achieved by reducing (i) the maximum amplitude ratios and relative displacements of the body parts to 0.029 and 0.19 mm, respectively, and (ii) body parts "acceleration levels" to below the ISO specified 7-hour "exposure limit" curve.

Vibration intensity is characterized by the amplitude ratio, acceleration level, and the relative amplitude between the adjacent body parts and pitch of the tractor. Any isolation of vibration, by providing a suspension, should reduce all these characteristics. Measurement of vibration on the suspended seat alone does not truly reflect the vibration level to which the human body parts are exposed. Hence, designing the seat suspension alone without taking into account the combined effect of the vehicle and the occupant does not yield satisfactory results. Patil and Palanichamy (1988) found that the new type of seat suspension of the tractor was able to reduce the amplitude ratio of head by 99.25%, at lower frequencies, and by 99.4%, at higher frequencies. The body parts were subjected to higher responses in lower frequencies, and lower responses at higher frequencies when compared with seat responses.

The transient vibration responses of the body parts, when the trapezoidal type of pulse input is applied at the tires, are lower than that of the seat. The above conclusions show the necessity of designing the suspension parameters based on the principle of minimizing the amplitude ratios of body parts rather than minimizing the response of only the tractor seat. It was found that the maximum relative displacements between the adjacent body parts were of the order of 0.19 mm (representing low strain of 0.112% between abdomen and pelvis). This demonstrates an effective vibration isolation characteristics of the new tractor seat suspension. Among vibration isolation criteria, the acceleration intensity criterion is the most important than other

criteria, since all other criteria are satisfied automatically when acceleration criterion of exposure limit is satisfied.

2.5. AGEING SUSPENSIONS PERFORMANCE

One of the important determinants of the truck vibration research is the estimation of its performance in vibration and shock wave propagation with time. Truck suspension system, linkages, seat and other effective parts in vibration transmission to the operator's body will experience fatigue, tear and wear with time. Therefore, their performance in energy attenuation will decrease with time. Thus, even an optimal suspension system with minimum vibration exposure today, will not guarantee a safe environment after some years of operation. So it is essential to find a correlation between ageing and vibration attenuation characteristics of the whole system.

A technical report by Lardner (2002), who considered a time-varying stiffness coefficient, is among the few published studies conducted in this field. Lardner (2002) evaluated the time-performance of a spring through investigation of the steady-state response of the classic mass-spring-dashpot model when the spring stiffness decays exponentially with time (an ageing spring). The system was excited by a force function whose frequency was equal to the natural frequency of the system with the constant initial stiffness. The classical mass-spring-dashpot model, used to describe the vibration characteristics of a simple mechanical system under time-dependent loading, is well known. When the force function is harmonic with a frequency equal to the natural frequency of the un-damped system, the system is said to be in resonance.

The steady-state response is harmonic with an amplitude dependent on the amount of damping in the system. The amplitude of the response of the system at other values of the force frequency is less than that at resonance and often is of less concern. The spring in this case is called an ageing spring. This model has a simple interpretation of a physical system becoming less stiff in time while excited by a loading that would lead to resonance if the stiffness remained

constant. Lardner (2002) defined the stiffness-time behavior in terms of an exponential function that considered both the primary and long term values of the spring stiffness.

Puff et al. (2010) conducted a study in order to evaluate fatigue behavior of the helical suspension spring system in hermetic compressors. The objective of the study was to present a methodology, based on numerical and experimental analysis, to evaluate the fatigue life of the spring suspension system. They found that the finite element method (FEM) brings improvements to the suspension spring analysis. With FEM, it was possible to include the interaction between springs and stoppers, and to apply the real loads on the springs.

Colquhoun and Draper (2000) used local strain fatigue analysis as a software system for fatigue analysis of finite element model of a suspension component. They showed that fatigue and durability analysis from finite element models is a subject of continuing development, and there is much to be learned from the application of existing methods. In particular, the mesh density and perhaps the types of elements may influence the validity of the fatigue analysis. The authors applied the Miner's rule for predicting fatigue life when a part is subjected to repetitive loads with different amplitudes. However, the Miner's rule does not account for the effect of the sequence of the applied loads, and only considers the magnitudes and number of cycles, which leads to errors in fatigue life predictions.

2.6. OTHER EFFECTIVE PARAMETERS IN VIBRATION EXPOSURE

Several studies have shown that there are secondary factors that affect the relationship between vibrations and health risks. Costa and Arezes (2009) conducted a study to evaluate the influence of operator driving characteristics in WBV exposure from electrical fork-lift trucks. This study provided some understanding of how certain characteristics, such as weight, age, experience, training and dexterity, can affect the stacker's operator vibration exposure levels. Some individual characteristics can play an important role on the risk of vibration exposure. The

results indicated that more experienced and faster workers were exposed to a higher risk of WBV exposure than those with minor experience and less driving skills.

Another issue in under this category is the uncertainty in simulation. Due to the pressure to reduce product development time and costs, there is an increasing need to replace time consuming and expensive prototype testing with computational simulations. However, until the uncertainty in the simulation can be characterized, effectively, in a systematic manner, a complete virtual modeling cannot be achieved. The uncertainty characterization, in both the data and model representation, is crucial to improve confidence in analytical and computational models **(**Goh et al., 2005).

2.7. SUMMARY

Extensive literature survey has been carried out by reviewing the relevant literature to evaluate the contributions and limitations of the previous and current body of knowledge on suspension systems and their effects on dissipating shock waves and vibrations in large mining dump trucks. The large truck loading operation exposes truck's operator to extreme WBV which exceeds the ISO 2631-1 standards, and consequently contributes to both short and long term injuries. In order to address this problem using engineered solutions, a comprehensive evaluation of different parts of the problem is needed**.** Through this report, different aspects of dump truck vibrations in HISLO condition were evaluated, including Operators' Health Risks, Vibration and Suspension System Modeling, Ergonomic Seats, Vibration Transmissibility, and Ageing Suspension Systems Performance. Contributions by different researchers to the body of knowledge in this field have been highlighted, as well as the limitations of each study. The performance deterioration of suspension trucks, in attenuating vibrations, with truck/suspension age has not been addressed in the literature.

This PhD dissertation fills the gap in the knowledge in the area of ageing suspension through an original development of our understanding of the mechanisms underlying and

governing the ageing process of the suspension systems in very large mining dump trucks. The ageing suspensions performance versus time is mathematically modeled. Thus the major contributions of this research study are: (i) providing greater understanding into the performance of truck suspension system under coupled random-time constraints, and (ii) providing recommendations for planning PMs, component replacements and rebuilds.

3. SUSPENSION MECHANISM IN LARGE MINING TRUCKS

The dominant suspension mechanism in today's high-tech mining dump trucks is a hydro-pneumatic type. This mechanism, also called oleo-pneumatic, is composed of a gas medium and a liquid one that play the role of a spring and damper, respectively (also called gas spring and oil damper, respectively). The gas spring sub-system is composed of a gas accumulator, which holds a specific amount of inert nitrogen gas with an initial pressure. This gas accumulator is connected to a cylinder-piston assembly via some hydraulic links.

The impulse force from a shovel dumping process releases a high amount of energy from truck vibrations that is supposed to be dissipated primarily in both the front and rear suspensions. If not dissipated effectively, a component of this energy propagates into the operator's cabin and exposes the operator to extreme shocks from vibrations that could be harmful. The impulse force pushes the rod side of the cylinder-piston assembly that is attached to the chassis via upper mounting, and compresses the hydraulic oil which is entrapped inside the cylinder. The piston forces the oil to pass through a series of orifices and hydraulic links toward the gas chamber. At the orifices the sectional area changes sharply, and causes part of the stored energy in the hydraulic oil to dissipate mainly due to friction. When a component of the energy reaches the nitrogen gas accumulator, it compresses the flexible gas chamber.

This mechanism converts the kinetic energy in the oil to potential energy in the air spring. When the gas accumulator (spring) expands, the potential energy is converted to kinetic energy. This phenomenon causes the hydraulic oil to move through the reverse direction through the orifices, while moving the rod side in the reverse direction until it reaches the bump stop elements at the final suspension stroke. The piston moves fore and aft for several times until all the stored energy is dissipated. This section focuses on both the mechanics and thermodynamics of the hydro-pneumatic mechanism. The literature survey showed that Baeur (2011) is the only available publication that addresses different issues of a typical hydro-pneumatic suspension

comprehensively. Therefore, in this chapter, most of the relevant theories in the subsequent paragraphs are taken from this source.

3.1. HYDRO-PNEUMATIC SUSPENSIONS

Basically there are two other systems that compete with hydro-pneumatics in the area of suspension systems. These two systems include the pneumatic and the mechanical suspension. The first essential difference between the systems becomes obvious when looking at the force versus displacement curves in Figure 3.1. While the spring stiffness rate of the mechanical spring is constant throughout the whole stroke, both systems with gas suspension are more or less progressive, which is caused by the physical laws for a poly-tropic change of state of a gas. When oscillating around the normal position with small amplitudes, this has no significant impact, yet at greater amplitudes, this is important, especially close to the end stops. In particular, the hydraulically preloaded hydro-pneumatic spring, as well as the air spring with a defined contour of the rolling piston can provide the advantage of increased spring stiffness rates near the mechanical end stops thus preventing the suspension from reaching these.

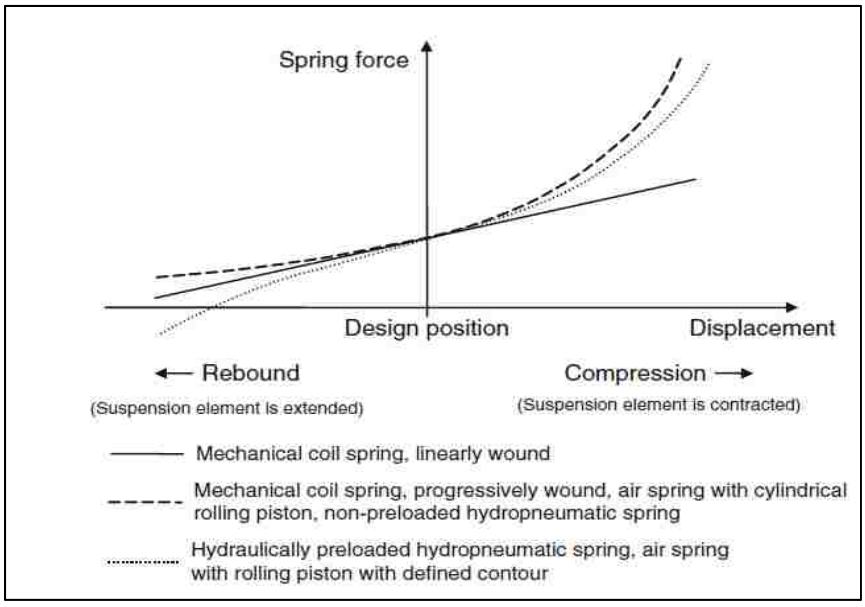

Figure 3.1 Force-displacement-curves for mechanical and gas-sprung systems (Bauer, 2010).

An even more significant difference can be found with changing suspension load by varying the suspended mass. A suspension system without level control is compressed by increasing static load until the spring force is again equal to the static load. In Figure 3.1, it becomes obvious that this causes an increasing spring stiffness rate for the air spring and the hydro-pneumatic spring, whilst the spring stiffness rate of a mechanical spring remains constant. This is a general problem for mechanical suspension systems with large load variations and with no level control.

In purely pneumatic springs, the gas (usually air) is filled up or released. So the suspending gas *volume* of the pneumatic spring remains constant after the load change and subsequent level adjustment. The pressure of this gas volume changes linearly with the load. Therefore, in purely pneumatic springs, the gas mass and hence the spring stiffness rate changes in a linear correlation with the sprung mass. For a hydro-pneumatic suspension system, it is the oil volume which is changed during the leveling process. Thus, it is the gas *mass* which remains constant at all times. Yet this gas mass changes its volume after a load change; a higher load means a smaller gas volume and therefore a higher spring stiffness rate. This is the reason why this system shows progressive behavior of the spring stiffness rate versus the sprung mass.

Figure 3.2 shows a comparison for all three systems, with the condition that they all have the same spring stiffness rate at the design load. In order to provide a constant natural frequency of the oscillating system, it is preferable to have a spring stiffness rate increasing linearly with the spring load. Yet in some cases, depending on the reason for the load changes or the needs of the particular application, it can be favorable to change to a disproportionately higher spring stiffness rate. A spring stiffness rate that is constant at all loads, as with a linearly wound coil spring, is usually only a compromise and only recommended for suspension systems with small relative load changes.

For good protection of the isolated side from the input side, the lowest possible natural frequency (obeying the motion sickness limit of 0.5 Hz), and also the lowest possible spring

stiffness rate needs to be targeted, always considering the limited suspension stroke. A pneumatic suspension provides a constant low level of natural frequency for all load conditions, while the natural frequency of a hydro-pneumatic system will more or less increase with increasing loads, depending on the system layout. On the other hand a mechanical spring will have a high natural frequency at low loads and a low natural frequency at high loads.

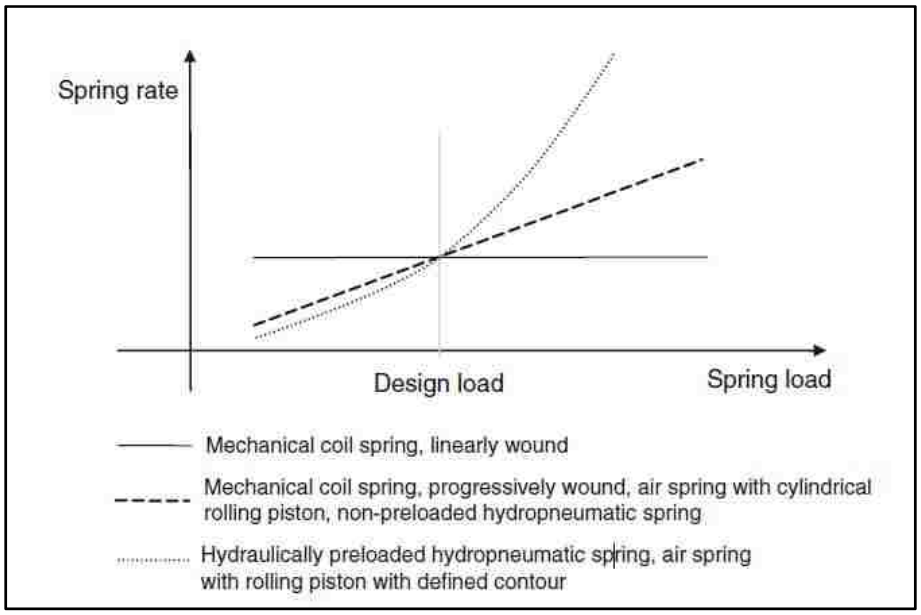

Figure 3.2 Spring stiffness rate as a function of spring load for a mechanical, a pneumatic and a hydro-pneumatic suspension (Bauer, 2010).

The necessary damping for the decay of the oscillations is in most cases provided by viscous friction of a damping fluid –usually oil. The amount of viscous damping can be defined very well for all three types of suspension systems. A negative side effect of the components of suspension systems is the additional damping by boundary friction, in particular in the bushings, dynamic sealing systems and guiding elements. Friction in bushings of mechanical links and control arms has to be minimized. This is similar for all kinds of suspension systems and is therefore also not part of this comparison. The friction in sealing and guiding elements needs to

be avoided as far as possible. There are different causes and therefore different friction levels for different suspension systems. This sub-section explains the reasons.

The mechanical coil spring with a viscous fluid damper scores best when it comes to the friction level. The spring itself has no friction. All deformations are purely reversible, i.e. elastic. Therefore in this suspension element, boundary friction originates only from the friction in the sealing and guiding elements inside the viscous fluid damper. It is a general rule that friction forces from dynamic seals increase with the differential pressures at the seal and the length of the sealing edge. This explains why a mono-tube damper with its internal gas pressure and the rather large rod diameter has a much higher boundary friction than a dual-tube damper (with low or even without internal gas pressure). For the mono-tube damper, there is additional seals friction from the floating internal piston which separates gas and oil. It is essential to avoid lateral forces and bending moments in the sliding components for friction in the guiding elements – this is actually valid for all types of suspension elements.

The standard oil damper technology is also used for pneumatic suspension systems. Thus, it has similar boundary friction for the coil spring suspension on the damper side. Yet for a pneumatic system, there is additional friction from the rolling bellow. This friction causes an additional degradation under harsh conditions and is on a level of about 20 N for the most commonly known cross ply bellow for a passenger car air suspension. The newer technology of axial ply bellows enables a reduction of bellow friction forces below 10 N and finds more applications especially in the field of high comfort passenger car suspensions. A disadvantage of this technology is that the bellow needs additional guidance on the outer diameter to pick up the radial forces from the air pressure. The baseline is that the boundary friction in a pneumatic suspension system will always be slightly higher than in a coil spring suspension system.

Although the suspension cylinder is the only component between input and isolated sides, the seals must cope with very high differential pressures. Therefore, the friction level would be much higher compared to the latter two suspension systems if it does not incorporate additional

countermeasures. The friction is caused on one hand by the rod seal (for single-acting cylinders) and additionally by the piston seal if a hydraulically preloaded system is used with a double-acting cylinder. The hydro-pneumatic suspension friction can be minimized by a suitable components layout, as well as by implementing a high-grade, low friction seal system.

Hydro-pneumatic suspension is integrated into one component. Thus, it is difficult to use additional soft spring-damper-elements to decouple the direct transfer path of static damper friction. The reason behind it is that this additional element would have to carry the complete suspended mass and not only the damping forces as in the case of the decoupled top mounts for passenger cars' suspension elements. High loads and very soft rubber elements are goals that can hardly be achieved at the same time. The use of a rubber bushing is possible though and it can improve the noise transfer properties. It is obvious that the boundary friction is a considerable and challenging issue when designing a hydro-pneumatic suspension. For suspension systems with a coil spring/mechanical spring, level controls are rather seldom due to the high effort of automatic systems and their limited effect. Manual level adjustments are commonly used in motorbikes and for some passenger car sports suspensions. In the last years several new ideas have been developed for level control of mechanical springs. However, overall they currently play a minor role in mechanical springs.

For a hydro-pneumatic and a pneumatic suspension system, level adjustment is quite easily feasible by increasing/decreasing the amount of oil or gas in the system. Both systems have about the same leveling quality, maybe with slight advantages for the hydro-pneumatic system. There is a major advantage for the hydro-pneumatic system in terms of leveling speed. The suspension system can be brought back to the normal position very quickly after a load increase with the necessary power since it has a higher energy density and an incompressible medium. If the same leveling speed had to be achieved with a pneumatic suspension system, a much higher volumetric flow rate and a higher power output would be necessary. This aspect is especially

important for suspension systems that are often subjected to high load changes with required fast readjustment of the desired normal position.

The simplest hydro-pneumatic suspension system consists of only three components: a hydraulic cylinder, a hydro-pneumatic accumulator (directly mounted on the cylinder) and the hydraulic fluid. In case the cylinder and accumulator must be separated, additional oil lines and fittings are required to provide the hydraulic connection. After adjusting the hydraulic pressure (by adding or releasing hydraulic fluid), this system would be ready to serve the suspension function. The fluid volume in the accumulator and the pressure ($p_1 \rightarrow p_2$) are changed when displacing the piston rod. This causes a change in the piston rod force, which in combination with the change of the position, defines the spring stiffness rate c. The external spring force FF which acts upon the piston rod is always in balance with the forces from the pressures on the piston, neglecting inertial and friction forces (See Figure 3.3a).

When the force F_F is increased (see Figure 3.3b), the piston position changes (Δs) and therefore some hydraulic fluid is displaced into the accumulator. This change proceeds until the pressure in the accumulator has reached a level which again provides a system balance. This balance of forces is the basis for understanding and the functioning of the suspension system. A flow resistor between cylinder and accumulator allows for additional damping. It converts part of the kinetic energy of the hydraulic fluid into heat (viscous friction). This provides the desired damping in combination with the (undesirable) boundary friction caused by the cylinder sealing and guiding elements. This so called “suspension unit” consisting of cylinder, accumulator, flow resistor and hydraulic fluid already provides the suspension function and could replace the typical combination of mechanical spring and damper.

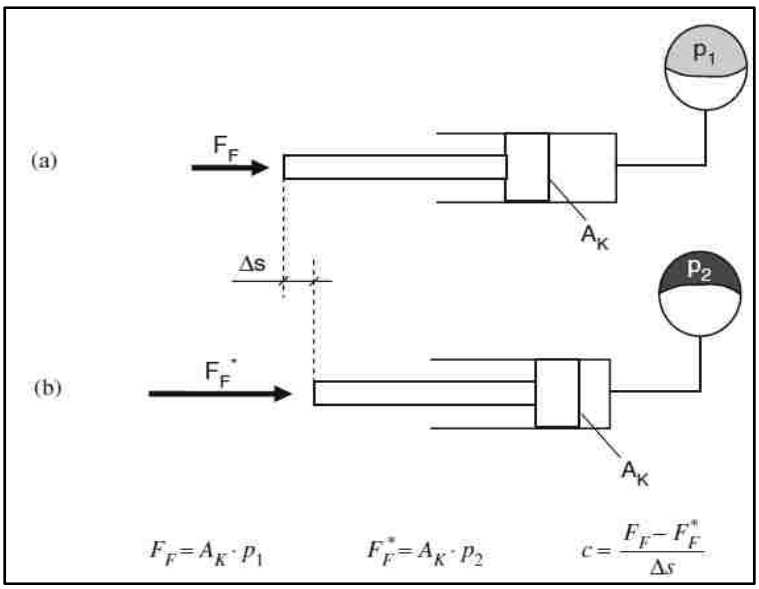

Figure 3.3 Balance of forces at the piston of a single-acting cylinder (Bauer, 2010).

An additional level control unit provides a constant normal position of the suspension independent from the static spring load F_F. The level control unit consists of a position sensor, which directly or via an electronic control unit, sends signals to a hydraulic control valve. This changes the amount of hydraulic fluid in the suspension unit in order to bring the suspension back to the design position if necessary. The system level is increased by increasing the amount of hydraulic fluid, and thus, reducing the amount of hydraulic fluid decreases the level of the system. Pressurized hydraulic fluid, as well as the possibility to dispose of excessive fluid (to a hydraulic reservoir), is required to achieve that adjustment in the system.

3.2. SPRING CHARACTERISTICS

The spring stiffness rate of a hydro-pneumatic suspension system can be determined from the pure spring force–displacement curve measured at the suspension cylinder by removing the hydraulic flow resistor. An increase of force on the cylinder leads to an increase in hydraulic pressure, and therefore, a change in the piston rod position. This is due to the following reasons: (i) compression of the gas in the accumulators; (ii) widening of the (elastic) fluid lines and

fittings; and (iii) compression of the hydraulic fluid. Each of these three effects causes an individual spring stiffness rate. So what is measured at the suspension cylinder is the spring stiffness rate of a spring which is made up of a sequential combination of these three individual springs. Using general laws of physics, Equation (3.1) is obtained as:

$$C_S = \frac{C_G C_L C_F}{C_G K_L + C_G \ C_F + C_F C_L} \tag{3.1}$$

The stiffness of the lines and fittings, as well as the compression modulus of the hydraulic fluid are usually very high, so their impact on the overall spring stiffness rate C_S is low. This means that the characteristic properties of a hydro-pneumatic spring are mainly influenced by the properties of the gas which is enclosed in the hydraulic accumulators.

3.2.1 Calculation of the Spring Stiffness Rate. Two types of hydro-pneumatic cylinders are illustrated in Figure 3.4. The suspension cylinder can be designed as a single-acting cylinder (for example, a plunger cylinder) or as a double-acting cylinder with interconnected piston-side and rod-side of the cylinder. The latter system is able to provide higher amounts of rebound damping.

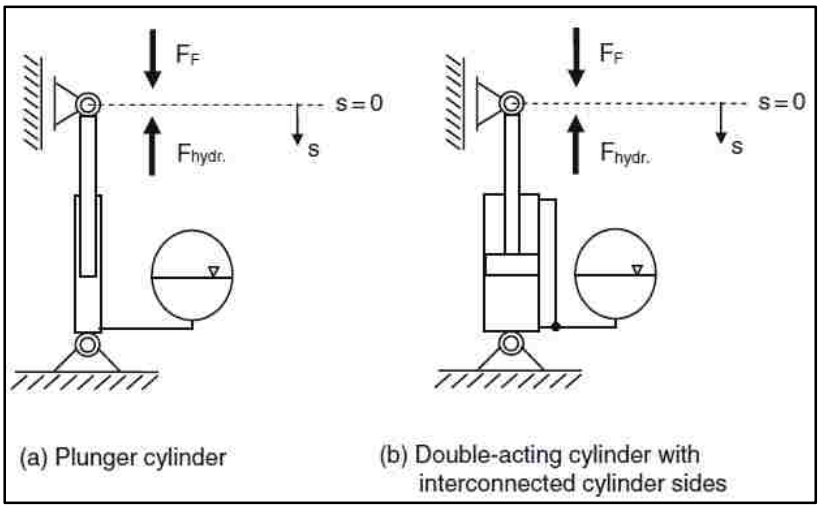

Figure 3.4 Schematic of non-preloaded hydro-pneumatic suspensions (Bauer, 2010).

The externally effective active area is only the cross-sectional area of the piston rod. This is due to the interconnection of the piston and rod chambers that allows only the fluid volume displaced by the piston rod to flow into the accumulator while the other portion of the fluid displaced by the piston flows back into the rod-side. The spring behavior is described as the force–displacement curve for compression and rebound. This curve is basically linear for a regular mechanical coil spring; other curves are possible by special winding techniques, as well as parallel connection of multiple springs. The hydro-pneumatic spring always has a disproportionately progressive shape of the force–displacement curve.

Before calculating the hydro-pneumatic suspension it is necessary to define some of the various states that a suspension system can be in:

State 0: Spring force, $F_{F0} = 0$: The pressure in the accumulator is the pre-charge pressure P_0, which is defined during the production process. The gas fills out the complete internal volume, V_0, of the accumulator.

State 1: Now the static suspension force, F_{F1}, is loading the suspension system (while $F_{F1} > F_{F0}$). The force is sufficient to compress the gas volume in the accumulator isothermally to the volume V_1 and the pressure, P_1.

State 2: F_{F2} is the dynamic suspension force and oscillates around, F_{F1}. Therefore the gas volume is compressed (compression) and expanded (rebound) by a poly-tropic change of state to the volume, V_2, and the pressure, P_2.

The starting point for the calculation is the correlation of the force acting onto the surface of the piston, F_K, and the pressure in the piston chamber, P_K.

$$F_K(s) = P_K(s)A_K \tag{3.2}$$

Using the state equation for poly-tropic changes of state

$$P_1 V_1^n = P_2 V_2^n \tag{3.3}$$

and the definition that an increase of the displacement *s* causes a compression of the gas

$$V_2 = V_1 - A_K s \tag{3.4}$$

It can be deduced that:

$$P_2 = \frac{P_2 V_1^n}{V_2^n} = \frac{P_1 V_1^n}{(V_1 - A_K s)^n} \tag{3.5}$$

On the basis of the isothermal change of state from 0 to 1, it is stated that

$$P_1 V_1 = P_0 V_0 \tag{3.6}$$

and therefore:

$$V_1 = \frac{P_0 V_0}{P_1} \tag{3.7}$$

As well as on the basis of the balance of forces at the piston

$$F_{F1} = P_1 A_K \tag{3.8}$$

and thus

$$P_1 = \frac{F_{F1}}{A_K} \tag{3.9}$$

For the following calculation it can be applied that

$$P_K(s) = P_2 \tag{3.10}$$

Combining all above equations brings us to

$$F_K(s) = \frac{\frac{F_{F1}}{A_K} \times \left(\frac{P_0 V_0}{\frac{F_{F1}}{A_k}} \right)^n}{\left(\frac{P_0 V_0}{\frac{F_{F1}}{A_k}} - A_K s \right)^n} A_k \tag{3.11}$$

After canceling A_K

$$\mathrm{F_K(s) = F_{F1} \times \frac{\left(\frac{P_0 V_0}{F_{F1}}\right)^n}{\left(\frac{P_0 V_0}{F_{F1}} - s\right)^n}} \tag{3.12}$$

By the substitution

$$\mathrm{\frac{P_0 V_0}{F_{F1}} = h_{0F}} \tag{3.13}$$

The following simple relationship is obtained:

$$\mathrm{F_K(s) = F_{F1} \times \frac{h_{0F}^n}{(h_{0F} - s)^n}} \tag{3.14}$$

The dimension, h_{0F}, can be interpreted easily by a virtual image. It is equivalent to the height of a column of gas with the pressure, P_0 (the pre-charge pressure) and the volume, V_0,

which has exactly the right base area so that it supports the force, F_{F1}. Figure 3.5 illustrates this condition for several different static spring loads, F_{F1}.

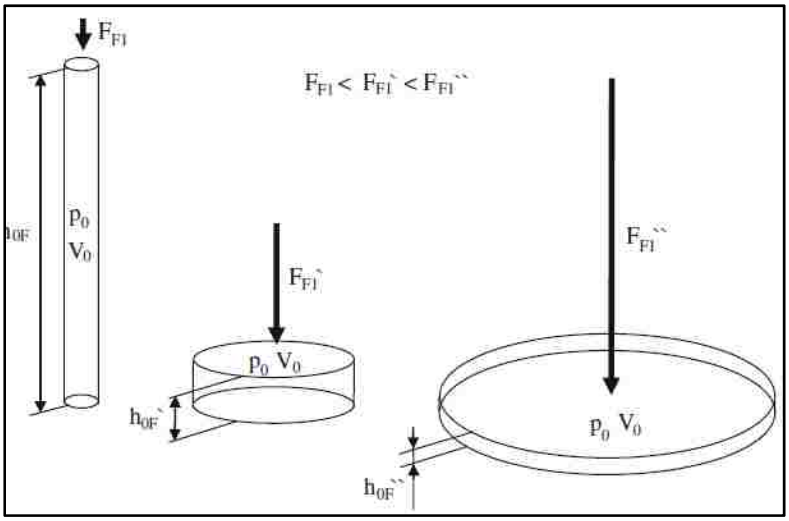

Figure 3.5 h_{0F} for various static spring loads, F_{F1}.

Figure 3.5 shows one of the most important features of a hydro-pneumatic suspension: the higher the static spring load, the smaller the height of the gas column, h_{0F}. Therefore, the more significant the change in the gas pressure forces on the piston at a given displacement, *s,* the higher the spring stiffness rate. The simple background to this is the relative change of the column height $(h_{0F} - s)/h_{0F}$. It becomes more meaningful with smaller h_{0F} and therefore the relative volume decrease and the relative pressure increase are more significant. Another important characteristic curve has to be considered in case a hydro-pneumatic suspension is subjected to a wide range of static spring loads. The dependency of the spring stiffness rate on this very static spring load is deduced by Equation (3.15).

$$c = \frac{dF}{ds} = \frac{d(PA_K)}{ds} = A_K \frac{dP}{ds} \tag{3.15}$$

Differentiating Equation (3.5) and applying the chain rule results in Equation (3.16).

$$\frac{dP}{ds} = P_1 V_1^n (-n)(V_1 - A_K s)^{-n-1}(-A_K) \tag{3.16}$$

The application of isothermal change of state from 0 to 1 and the balance of forces at the piston, according to Equations (3.9) and (3.7), results in Equation (3.17).

$$c = A_K \frac{dP}{ds} = A_K \frac{F_{F1}}{A_K}\left(\frac{P_0 A_K V_0}{F_{F1}}\right)^n (-n)\left(\frac{P_0 A_K V_0}{F_{F1}} - A_K s\right)^{-n-1}(-A_K) \tag{3.17}$$

Dissolving and again using the dimension h_{0F} in Equation (3.13) results in Equation (3.18).

$$c(s) = F_{F1} n \frac{h_{0F}^n}{(h_{0F} - s)^{n+1}} \tag{3.18}$$

It is obvious that h_{0F} is also important for the spring stiffness rate. It should be noted that h_{0F} is a variable, which depends on F_{F1}. For s = 0 and dissolving h_{0F}, the spring stiffness rate in normal (design) position becomes Equation (3.19).

$$c = n \frac{F_{F1}^2}{P_0 V_0} \tag{3.19}$$

One interesting consequence is that the geometry of the suspension cylinder(s) plays no role in these equations. The gas in the accumulator and the suspended load determine the contour of the force–displacement curve and therefore the spring stiffness rate. On one hand the gas in the accumulator can be described by the product of the accumulator pre-charge pressure, P_0, and the accumulator volume, V_0. On the other hand it can, according to the equation of state for the

ideal gas, be given as $mGRT$. This clearly points out that, apart from the static spring load and the mass of the gas fill m_G, the spring stiffness rate also depends on the temperature of the gas/the accumulator. The use of a hydro-pneumatic suspension system must consider that the pre-charge pressure during the production process is 20° C. The actual operating temperature can vary due to influences from the environment but can also be increased due to heat in the hydraulic fluid that arises from the viscous damping. The general rule is that higher temperatures soften the spring, and lower temperatures make it stiffer.

3.3. DAMPING CHARACTERISTICS

The energy transferred to the suspension by an external excitation must be dissipated to achieve decay in the resulting oscillation amplitude and to avoid increasing amplitudes due to resonance. Therefore additional elements in the suspension system are necessary to transform the kinetic and/or potential energy of the suspension. In most cases kinetic energy is transformed into heat by applying a retarding force during operation of the suspension elements. This retarding damping force usually is based on the principle of friction. In general two different fundamental principles create the damping in a suspension system as follows.

(1) Boundary, dry or solid body friction: Two bodies against each other with a normal force slide along their interface with a resistant force caused by surface roughness and adhesion. The resistant force is called friction force and acts as a damping force.

(2) Fluid, viscous or hydrodynamic friction: A flow resistor is placed in the flow path of a fluid and causes internal fluid friction which therefore causes a pressure increase upstream of the resistor. This additional pressure is acting upon the active areas of the cylinder thus creating a retarding force, a damping force.

In addition to the above principles, there are other principles which are rarely used in suspension technology. For example, the eddy-current principle is often used in vehicles as a wear-free retarder to reduce vehicle speed on downhill slopes. It is based on the principle of

induction of current in an electric conductor when it is moved through a magnetic field. Furthermore, there are the so-called gas-spring-damper-elements, which serve the function of a spring as well as a damper only by their internal gas fill.

In general the damping forces are kept as low as possible to get the best possible decoupling of the suspended mass on the isolated side from the excitation on the input side. If damping is changed to provide optimal results under normal operating conditions, it becomes be too low under extreme operating conditions. This will result in high amplitude oscillations and, as a consequence, bottoming out of the suspension. To avoid heavy accelerations when the suspension hits the mechanical end, another type of damping is integrated into many suspension systems. This damping is only active when the suspension reaches the end of its stroke. Additional damping elements dissipate the excessive kinetic energy before the suspension reaches the end stop. Therefore this energy is prevented from being transferred into the isolated side by a short term but very high force peak.

3.3.1 Fluid Friction Damping. The hydraulic fluid in a hydro-pneumatic suspension system is used as a medium to transfer the pressure on the active areas of the piston to the accumulator(s). Due to the suspension movement, and therefore, the displacement of the piston, the hydraulic fluid steadily flows between cylinder and accumulator with frequent flow direction changes. The kinetic energy of the hydraulic fluid is transformed into heat due to shear flows inside the fluid if a flow resistor is present in the fluid flow. The flow resistor creates a pressure loss, which creates a force to counteract the piston motion via the active piston areas. This force removes energy out of the oscillation and hence it is a damping force (see Figure 3.6). In Equation 3.20, $F_{D,hyd}$ is the rod side force inserted from the upper suspension mount, which is connected to truck's chassis. The major drivers of this force are either HISLO (if the truck is idle) or surface bumps (if the truck is moving). $F_{D,hyd}$ is equivalent to the resulting pressure drop in the

piston side by the effective cross sectional area of the piston. Equivalently, Equation 3.20 can be rewritten in terms of the hydraulic oil velocity as in Equation 3.21.

$$F_{D,hyd} = \Delta P A_K \tag{3.20}$$

$$P_{D,hyd} = F_{D,hyd}\, v = \Delta p \dot{V} \tag{3.21}$$

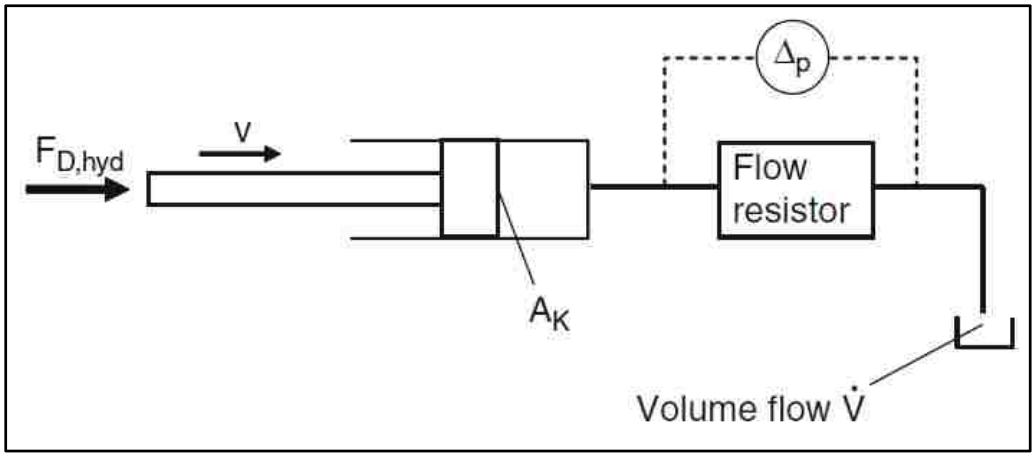

Figure 3.6 Active principle of fluid friction damping (Bauer, 2010).

It is typical for fluid friction that the pressure loss depends very much on the volume flow through the flow resistor. This is why the fluid friction damping force depends significantly on the speed of the suspension motion instead of the boundary friction. This means that a fluid friction damper adapts to the amount of energy stored in an oscillation: first by the amplitude of the oscillation and secondly (for same oscillation frequency) by the velocity of the oscillation. Simple flow resistors can be divided into two different types based on their dependency on pressure loss and volume flow. These resistor types include:

(a) Throttle: The flow is decelerated by a slow transition of the flow cross-section from wide to narrow and back to wide (see Figure 3.7). The cross-section of the throttle for a defined additional damping usually has a circular shape and is provided by a small bore in a component in the fluid path between cylinder and accumulator. The small cross-section

causes high flow velocities of the hydraulic fluid. Due to the high-gradient flow velocity from the flow center to the inner wall of the bore, the system generates high shear forces and pressure losses. Another important characteristic of the throttle therefore also is the direct dependency of pressure losses on the viscosity of the hydraulic fluid. The pressure loss across a throttle bore with laminar flow can be calculated by:

$$\Delta P = \dot{V}\, v\rho K_D \tag{3.22}$$

K_D is a constant related to the geometry and dimensions of the throttle bore while ρ is the density of the hydraulic fluid. K_D can be calculated for the throttle geometry below using Equation (3.23).

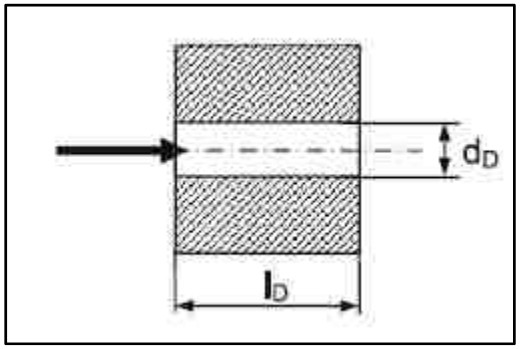

Figure 3.7 Active principle of fluid friction damping (Bauer, 2010).

$$K_D = \frac{128 l_D}{\pi d_D^4} \tag{3.23}$$

Typical hydraulic components with the character of a throttle include tubes, hoses and hose fittings without tight bends, bores with constant diameter in control blocks or straight pipe fittings with constant inner diameter.

(b) Orifice: The fluid flow is subjected to one or more sudden transitions from a wide to a narrow or a narrow to a wide flow path (see Figure 3.8). This causes high turbulence in the hydraulic fluid, which is the reason for internal fluid friction and the transformation of fluid flow energy into heat energy. Ideally, this flow resistor is characterized by a quadratic dependency of the pressure loss on volume flow. Only a minor amount of additional surface is in contact with the fluid flow in regions with high flow velocities.

$$\Delta P = \dot{V}^2 K_B \tag{3.24}$$

K_B is a constant that is related to the geometry and dimension of the throttle, as well as the density of the hydraulic fluid. K_B can be calculated for an orifice using Equation (3.25).

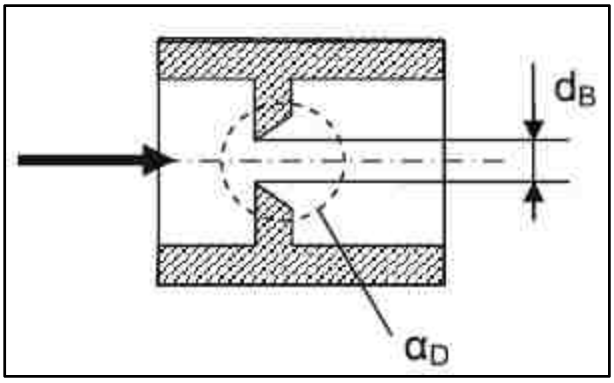

Figure 3.8 A typical orifice-type fluid resistor.

$$K_B = \frac{8\rho}{\alpha_D^2 \pi^2 d_B^4} \tag{3.25}$$

The parameter α_D is called the flow coefficient and depends mainly on the geometry of the inlet edge and the Reynolds number. Typical hydraulic components with the character of an orifice are components, which changes in flow direction especially with a low turning radius (for example elbow fittings or crossdrills in control blocks). Other orifices may include components

with sudden changes in cross-section, for example the bore in the cylinder wall for the hydraulic connection of piston/rod and fittings with a wide jump in sizes on their connectors.

3.3.2. End-of-Stroke Damping. Every suspension system has a limited stroke available to isolate the excitations from the input side. The softer a suspension system is, the more the acceleration reductions on the isolated side and the longer is the displacement between input and isolated sides for certain excitations. If excitations exceed a certain limit, the necessary displacement becomes greater than the available suspension stroke and therefore the suspension bottoms out. This causes short-term high forces and accelerations, which reduce comfort. This situation can overload suspension system components, as well as components on the input or isolated side.

One way to avoid this problem is to tune up spring and damper to a harder level. This makes available sufficient suspension stroke even for the worst conditions and most extreme excitations. This results in reduced comfort level in all other operating conditions. Thus, it is important to consider the expected frequency and amplitude distribution of the various excitations to find an optimum level for spring stiffness rate and damping. It is quite acceptable to have the suspension bottoming out slightly sometimes, if the overall comfort level in all other operating conditions is improved by a softer setting. A suspension system can be tuned to be softer than that if an additional end-of-stroke damping is used and the (rare) cases of bottoming out are softened by an additional damper or an additional spring.

To reduce the harshness of a bottoming out event at the end of the stroke, it is necessary to reduce the velocity of the piston relative to the cylinder. Additional decelerating force must be activated if the piston gets close to the end positions. Most suitably this additional force creates a constant or slightly progressive gradient of velocity over displacement. This means the deceleration is constant or increases slightly as the piston gets closer to the cylinder bottom. Ideally, the end-of-stroke damping system recognizes the excessive kinetic energy, which has to be dissipated until the end of the stroke.

Many suspension systems use *elastomer elements for end-of-stroke damping.* Just before hitting the end stops, the suspension motion is decelerated by an additional elastomer spring with a minor amount of damping. Strictly speaking, this is more of an end-of-stroke spring than an end-of-stroke damping. The spring force and the piston deceleration increases from the first contact to the elastomer up to the mechanical end stop. The characteristic curve of deceleration force versus displacement is at least a linear increase. In most cases, even a disproportionately higher increase can be shaped by the outer contour of the elastomer element, internal bores or by collars supporting the elastomer circumference.

This layout allows soft cushioning of minor impacts with small spring forces and in other cases it can take extreme bumps without the bottoming out of steel parts. In passenger cars this type of end-of-stroke damping is clearly noticeable for passengers, and it fulfills the requirement to protect the components from overload. During the rebound motion out of the end stop, the elastomer extends back to its original shape and reintroduces most of the absorbed energy back into the suspension system. Due to a slight damping effect, a minor amount of energy remains as heat inside the elastomer. This behavior is characterized by the loss angle of the elastomeric material.

A major disadvantage of the elastomer elements is the fact that the material is subjected to strong ageing and settlement depending on the extent of use and the stresses induced therewith as well as the environmental conditions (UV-radiation, ozone, chemicals). This makes an exchange of the elements necessary in some applications. In order to prevent overloading of the elastomer elements, an additional mechanical end stop is designed into the system. This design limits the stroke and therefore reduces the maximum deformation of the elastomer to a level which is acceptable for the material in long term.

In hydro-pneumatic suspension systems, another type of end-of-stroke damping is popular since it can be designed into the suspension cylinder. Theoretically, the use of elastomer elements is possible, but mostly it is the *hydraulic end-of-stroke damping* that is used for these

cylinders. In this case, an additional damping force is introduced to decelerate the piston velocity unlike the additional spring force with minor damping in the elastomer elements. The effect of the hydraulic end-of-stroke damping is achieved by reducing the cross-section of the oil path out of the cylinder when the piston reaches a freely selectable distance to the end stop. During a compression stroke the piston-side chamber is active while during a rebound stroke the rod-side chamber is active for end-of-stroke damping.

A pressure drop across the flow resistor is generated, which then causes a pressure increase inside the respective cylinder chamber. The active area of the respective cylinder chamber is subjected to this additional pressure and therefore causes the damping force. If the cross-sectional area of the additional flow resistor is designed to be variable with cylinder stroke, a system is created to define the effect of the flow resistor depending on piston position. A more constant end-of-stroke damping force level and a lower maximum force can be achieved compared to a flow resistor with constant cross-section area.

3.4. SUMMARY

There are two other systems that compete with hydro-pneumatics in the area of suspension systems. These include (i) the pneumatic; and (ii) the mechanical suspension. However, the dominant system in large mining trucks is the hydro-pneumatic type. In conventional mechanical springs, the spring stiffness rate is constant throughout the whole suspension stroke. In contrast, the force versus displacement curve is progressive in both the gas springs and hydro-pneumatic suspensions. This phenomenon is caused by the physical laws for a poly-tropic change of state of a gaseous medium. In particular, the hydraulically preloaded hydro-pneumatic spring can provide the advantage of increased spring stiffness rates near the mechanical end stops, thus preventing the suspension from reaching these.

For a hydro-pneumatic suspension system, it is the oil volume which is changed during the leveling process. This gas mass changes volume after a load change; a higher load means a

smaller gas volume and therefore a higher spring stiffness rate. This is the reason why this system shows progressive behavior of the spring stiffness rate versus the sprung mass. For a hydro-pneumatic suspension system, a level adjustment is quite easily feasible by increasing/decreasing the amount of oil in the system. The geometry of the suspension cylinder(s) plays no role in spring stiffness rate equations. The gas in the accumulator and the suspended load determine the contour of the force–displacement curve and the spring stiffness rate.

4. MODELING AGEING SUSPENSIONS

4.1 RESEARCH METHODOLOGY

The time-performance behavior of a typical hydro-pneumatic suspension system in large surface mining haul trucks is conceptually illustrated in Figure 1. The performance index (PI) is assumed to be 1 for a brand new suspension, which deteriorates with time until reaching a minimum threshold of PIT. The age of the suspension at PIT (i.e., t (PIT)) is the suspension's life time. The suspension age (t) is measured in terms of actual working hours (or cycles), that is always equal or less than its actual (chronological) age. The PI deterioration takes place under the effects of two governing power functions f(t) and g(t). Power functions have been used extensively in the literature in reliability engineering analysis. For instance it is a common practice to assume a system/component hazard rate in form of a power function.

The PI decreases, in between the scheduled maintenance (SM), according to the function f(t). On the other hand, the PI decreases at random times (e.g., due to sporadic shocks) according to the function g(t). Loosely speaking, the function f(t) causes a gradual slow degradation (ageing) in PI, while function g(t) causes instantaneous sharp decreases (e.g., due to shocks) at random times. The cumulative PI degradation between the scheduled maintenance times is compensated by minor routine maintenance and repair actions (e.g., nitrogen gas recharging, oil leakage compensation, repairing malfunctioning valves, and links). In contrasts, the sudden sharp decreases in PI that are mainly due to shocks or failure accumulation in sub-systems until reaching a threshold are compensated by major repair actions. Thus, the first kind of maintenance/repair is scheduled (SM), and the second type is corrective (CM).

The major mechanisms that cause PI drop between SMs are due to gas diffusion (thermodynamically) and oil leakage (hydro-mechanically). The effects of these processes (Type I) are taken into account in the form of the small non-linear and rate-increasing curves that are illustrated in Figure 1 (see $f_i(t)$ functions). On the other hand, the effects of major deteriorating

mechanisms (Type II), such as metal fatigue, elastomer degradation, corrosion, and oil contamination are taken into account in the form of the large non-linear and sharply decreasing curves in Figure 4.1 (see $g_i(t)$ functions). The major differences between the two types of deteriorating phenomena are as follow: i) the former mechanisms are more rapid but reversible through SMs, while the latter mechanisms are very slow and non-reversible; (ii) in the latter case some part(s) should be either repaired or replaced to bring the suspension functionality to a better state; and iii) the effect of the former mechanisms in PI reduction is gradual, while that of the latter mechanisms is almost (instantaneous).

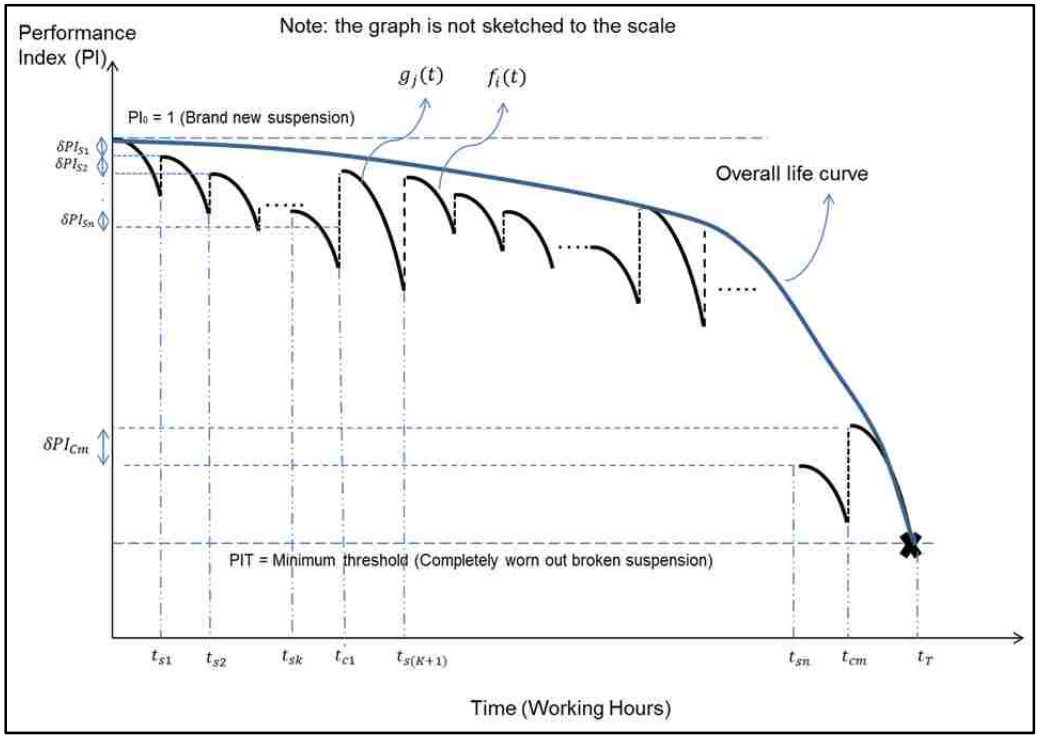

Figure 4.1 – Dump truck suspension performance deterioration with time.

The i^{th} SM and j^{th} CM compensate for part (or all) of the PI drops that have happened, respectively, during the i^{th} ageing and j^{th} shock events. These parameters are labeled with CSM and CPC for the SM and CM repairs/maintenance, respectively. The goal is to find parameters of

both functions f(t) and g(t), as well as, values of CCM and CSM, using several PI observations at different suspension ages. Both the f(t) and g(t) functions are assumed to be a power shape. A power function can have different deterioration rates depending on the ranges of its two parameters (i.e., the multiplier and the power parameters). Thus, the problem of suspension ageing modeling reduces to finding three parameters (i.e., multiplier, power, and compensation variables) per function (6 variables) to minimize the square of errors (observation vs. model).

There are three alternatives in defining the nature of the parameters: (i) all parameters are deterministic; (ii) all parameters are random variables; and (iii) a mixture of deterministic and random variables. In case (i), all the f(t) and g(t) functions, for all deteriorating cycles, are equal with constant parameters as defined in Equations (4.1) to (4.4).

$$f_1(t) = f_2(t) = \cdots f_n(t) = \quad at^b \tag{4.1}$$

$$a \quad < 0;\ b \quad > 1; \forall i = 1..n \tag{4.2}$$

$$g_1(t) = g_2(t) = \cdots g_m(t) = \quad ct^d \tag{4.3}$$

$$c \quad < 0;\ d \quad > 1; \forall j = 1..m \tag{4.4}$$

Equations (4.2) and (4.4) constraint the parameter values so that both functions become decreasing (see Figure 4.1), and the rate of PI drop, gradually, increases with time during both the ageing and shock cycles. Moreover, in case (i), both the CSM and CCM variables are constant, and defined in Equations (4.5) and (4.6).

$$CSM = a(TS)^b - \delta PI_S \tag{4.5}$$

$$CCM = c(TC)^d - \delta PI_c \tag{4.6}$$

The effects of thermodynamically and hydro-mechanically deteriorating mechanisms are incorporated in Equation (4.5), whereas the effects of fatigue, material degradation, and oil contamination are incorporated in Equation (4.6). TS and TC are also assumed to take on constant values. Thus, δPI_S and δPI_c will also be constant parameters. In other words, it is assumed that the effectiveness of all SM and CM maintenance schedules are the same (constant). Though the deterministic approach has several restricting assumptions, it is possible to solve the problem with only a few data.

In contrast in case (ii), all the six parameters can take on random values. Due to many uncertainties associated with different modes of failures in a typical hydro-pneumatic suspension strut an assumption of constant parameters will be simplistic. These uncertainties may characterize metal fatigue, oil leakage, diaphragm rupture, bushing and sealing degradation, thermal fatigue, corrosion, wear, and oil degradation. Furthermore, the effectiveness of the SMs and CMs as well as the rate of occurrence of shocks are all stochastic variables in nature. Thus, to compensate for the lack of knowledge (uncertainty) in the physics of the failure modes, their likelihood, frequency, interrelations and interaction with each other, as well as, SM and CM qualities, the stochastic approach is applied to address this variability.

In the probabilistic approach (case ii), the f(t) and g(t) functions, CSMs and CCMs are not necessarily the same for different cycles as shown in Equations (4.7) – (4.10).

$$f_1(t) \neq f_2(t) \neq \cdots f_n(t) \tag{4.7}$$

$$g_1(t) \neq g_2(t) \neq \cdots g_m(t) \tag{4.8}$$

$$CSM_1 \neq CSM_2 \neq \cdots CSM_n \tag{4.9}$$

$$CCM_1 \neq CCM_2 \neq \cdots CCM_m \tag{4.10}$$

Equations (4.7) and (4.8) show the randomness in deteriorating mechanisms due to type I and II mechanisms, respectively. For instance, the initial pressure of the gas accumulator decreases randomly between SM maintenance points. After each SM maintenance, the drop in the initial pressure due to the immediately preceding deterioration interval (i.e., $t_{sk} - t_{s(k-1)}$) is compensated through CPS_k. Furthermore, the maintenance efficiency uncertainties are considered in Equations (4.9) and (4.10).

In the probabilistic approach, the shapes of (f, g, CSM, and CCM) are different for all cycles. Each of these curves is considered as a "realization" of a random process. The randomness in the six parameters (*a, b, c, d*, CSM, and CCM) are defined with stochastic models. Parameters (*a* and *c)* are the multipliers of the type I and II deteriorating mechanisms, respectively. The powers of the type I and II deteriorating mechanisms are *b* and *d*, respectively. CSM and CCM are SM and CM maintenance qualities, respectively.

For every single variable, a specific probability distribution function (PDF) should be defined, as illustrated in see Equation (4.11).

$$X_k = pdf_k(\theta_k | x_k) \tag{4.11}$$

$$k = a, b, c, d, CPS, \text{and } CPS$$

X_k is the random model describing (a, b, c, d, CSM, and CCM); θ_k is a 1-D vector of PDF parameters of the kth random variable; x_k is a 1-D vector of observations of the kth random variable. Two major approaches in statistical data analysis are considered including "frequency" and "Bayesian" approaches. In the "frequency" approach, a large number of observations are required to identify the vector of parameters for each of the six random processes. To

compensate for the lack of sufficient data, the Bayesian inference can be used. In this approach, a prior knowledge of the probability distribution functions (PDF) from experience or expert judgment is updated with a few numbers of observations, within the Bayes theory, to render an updated PDF.

4.1.1. The Physical Counterpart of the PI Model. The mathematical model for suspension performance deterioration (PI model) is translated into suspension parameters via the time-varying spring stiffness rates and damping coefficients. Illustrated in Figure 4.2 is a free body diagram (FBD) of a virtual prototype model of CAT 793 D truck in the MSC ADAMS environment. The role of the PI model is to identify both the rear and front stiffness and damping characteristics, which are depicted in Figure 4.2. After proposing the PI model in this Chapter and validating the model via a numerical example in Sections 5.1-5.2, the link between the PI model and the illustrated suspension parameters in Figure 4.2, is manifested in Sections 6.1-6.4 with further discussions in Sections 7.1-7.4.

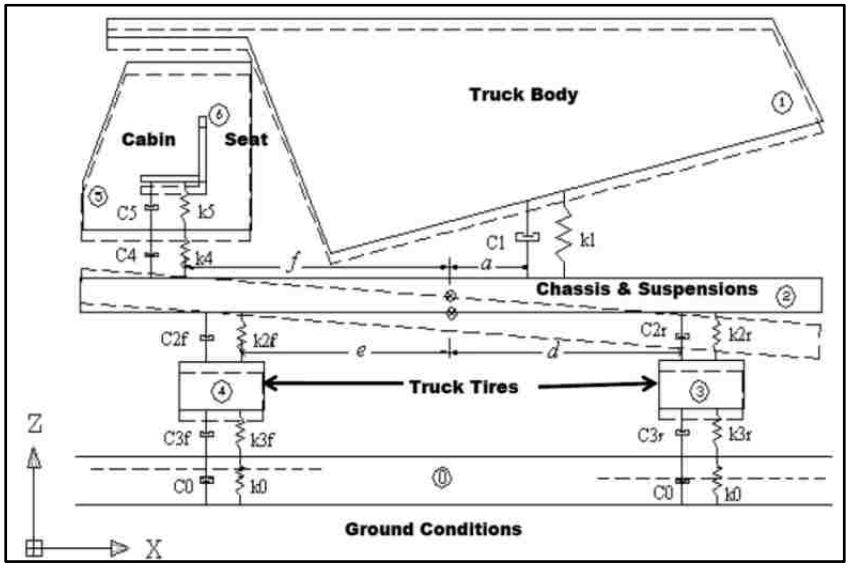

Figure 4.2. FBD of a virtual prototype model of CAT 793 D truck in the MSC ADAMS environment, which shows the interest area of the PI model in the whole truck model (i.e., suspension struts).

The PI parameters of influence are identified as K2f and K2r for the front and rear spring stiffness rates, and C2f and C2r for the front and rear damping coefficients, respectively. The PI model determines the temporal behavior of these parameters with ageing, which will be discussed further in Chapters 6 and 7.

4.1.2. Assumptions.

1. There are only two distinct types of maintenance, namely: (i) scheduled minor maintenance (SM), and (ii) major corrective maintenance (CM)
2. The suspension performance in energy dissipation (i.e., PI (t)) decreases, gradually, from an index value of 1 until reaching a minimum quality threshold at the end of its service life (T). The system is completely overhauled or replaced after this point.
3. In the deterministic approach, the gradual decrease of PI takes place monotonically, while in the probabilistic approach (See Figure 4.3) it takes place randomly.

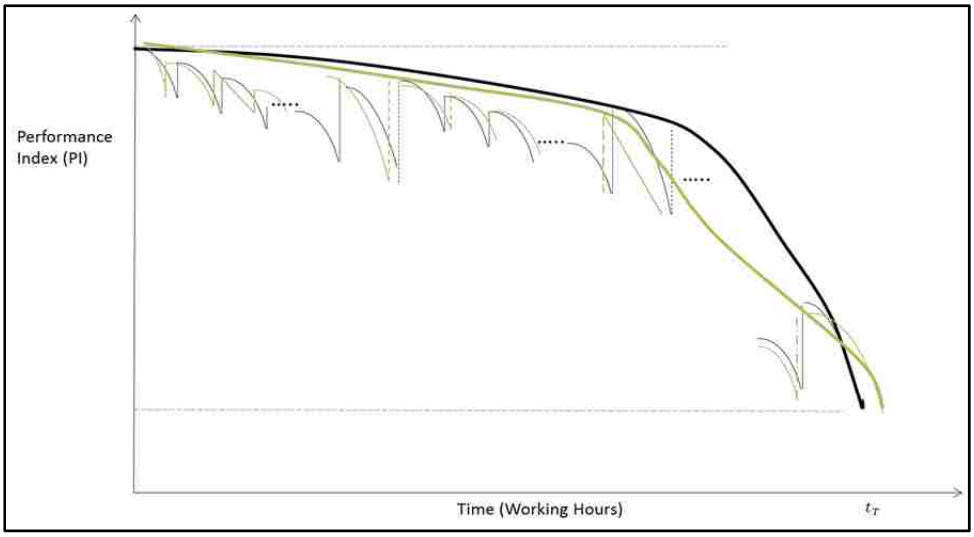

Figure 4.3 – Dump truck suspension performance with time (probabilistic approach).

4. Both $f_i(t)$ *and* $g_j(t)$ are power functions of the type $X(t)^Y$

5. The impacts of all the environmental, operational, and maintenance variables, that are effective in the ageing of a suspension unit, are taken into the account through $f_i(t)\ and\ g_j(t)$ parameters.
6. The CMs occurrence is modeled as a homogenous Poisson process, i.e., the inter-arrival times of the major failures are independent and exponentially distributed random variables with a constant scale (mean) parameter.
7. Within the context of maintenance quality, the following cases can happen after each maintenance (either SM or CM).
    (i) The component/system state becomes the same as a brand new system after each maintenance. The renewal processes are the dominant modeling scheme in reliability engineering that considers this assumption (Whitaker and Samaniego, 1989). This is called "the-as-good-as-new" in reliability engineering. This case is mathematically represented as in Equations (4.12) and (4.13) for the SM and CM maintenance/repairs, respectively. $a(TS)^b$ and $c(TC)^d$ are the amount of cumulative PI degradation during one cycle of type I and type II ageing mechanisms, respectively. Thus, if the system is supposed to be restored to a "the-as-good-as-new" state, the amount of compensation in PI drop due to SM and CM actions (e.g., CPS and CPC) should be higher than their corresponding per-cycle deteriorations.

$$CSM > a(TS)^b \tag{4.12}$$

$$CCM > c(TC)^d \tag{4.13}$$

(ii) The component/system state becomes the same as the old, i.e., the same as the system's state just after the previous repair/maintenance action. Non-homogeneous Poisson processes (NHPP) are the major mathematical framework for modeling this assumption (van Noortwijk, 2009). This is called "the-as-bad-as-old" in reliability engineering. In the "the-as-bad-as-old" scenario, every SM or CM repair should result in an increase of PI that are equivalent to on-cycle deterioration due to Type I and II mechanisms, respectively, as shown in Equations (4.14) and (4.15).

$$CSM = a(TS)^b \tag{4.14}$$

$$CCM = c(TC)^d \tag{4.15}$$

(iii) The component/system state becomes better than the old, but not as-good-as-new. The Kijima virtual age models are the dominant framework for modeling the systems with this assumption (Kijima, 1989). Both the first and second assumptions are extreme cases. The Kijima's concept of virtual age is between the two extreme cases, and thus, is a better representative for the real conditions. This scenario is defined by Equations (4.16) and (4.17). The left hand sides of the inequalities in (4.16) and (4.17) are set to take the maximum achievable PI value, that is PI =1 for a brand new suspension unit.

$$a(TS)^b < CSM < 1 \tag{4.16}$$

$$c(TC)^d < CCM < 1 \tag{4.17}$$

Both the first and second assumptions are extreme cases. The Kijima's concept of virtual age is between the two extreme cases, and thus, is a better representative for the real conditions.

(iv) The component/system state improves, but it doesn't reach its state just after the previous maintenance. This is associated with poor or insufficient maintenance or repair actions. In other words, the SM and CM actions compensate (i.e., CPS and CPC) for only a portion of the per-cycle PI reductions (i.e., $a(TS)^b$ and $c(TC)^d$ for type I and II mechanisms, respectively). This concept is defined by Equations (4.18) and (4.19).

$$0 < CSM < a(TS)^b \tag{4.18}$$

$$0 < CCM < c(TC)^d \tag{4.19}$$

(v) The component/system becomes better than a brand new one. This extreme case is associated with technological improvements between the maintenance actions, which result in replacing an obsolete component with a high-tech one.

In this study, CSM/CCM functions are not restricted (to the above five scenarios) in the deterministic approach. Thus, each of the above 5 cases may happen, depending on the observations. After estimating the values of CCM and CSM, discussions will focus on which assumption is more likely to happen for the given observations.

4.2. SOLUTION

Assuming there are four data points (i.e., for pairs of (t, PI(t))), the goal is to estimate (a, b, c, d, CSM, and CCM) to minimize the estimation error associated with PI (t). This process

identifies the shape of the curves in Figure 1. Without of loss of generality, it is assumed that the first observation is from a point before the nth SM, which has a PI = F (see Equation (4.22)).

$$X_1 = PI\ (t_{Sn}) = F \tag{4.20}$$

The second data is from the point before the 1st CM, which has a PI = S. It is also assumed that the 1st CM takes place after the nth SM, i.e. $t_{C1>}\ t_{sn}$.

$$X_2 = PI\ (t_{C1}) = S \tag{4.21}$$

The third data is from the point before the 2nd CM with a value of T.

$$X_3 = PI\ (t_{C2}) = T \tag{4.22}$$

The fourth data is from an arbitrary point with value A.

$$X_4 = PI\ (t_a) = A \tag{4.23}$$

The parameters of the deterministic model will be estimated using the first three points, reserving the fourth point for model validation. From X_1:

$$1 - na(TS)^b + (n-1) \times CSM = F \tag{4.24}$$

From X_2: The number of SMs between $X_1$and X_2 is obtained from equation (4.25).

$$n_{1-2} = \frac{t_{c1} - t_{sn}}{TS} \tag{4.25}$$

$$1 + (n + n_{1-2})\left(-a(TS)^b + CSM\right) - c(TC)^d = S \tag{4.26}$$

From X_3: The number of SMs between $X_2$and X_3 is obtained from equation (4.27).

$$n_{2-3} = \frac{t_{c2} - t_{c1}}{TS} \tag{4.27}$$

$$S + CCM + n_{2-3}\left(-a(TS)^b + CSM\right) - C(TC)^d = T \tag{4.28}$$

There are three equations (4.24), (4.26), and (4.28), and six unknowns (a, b, c, d, CSM, and CCM). This system of equations cannot be solved analytically. The heuristic search methods are used to find the best estimates of the 6 unknowns. A multi-objective genetic algorithm model is used to solve the numerical example. The three objectives of the algorithm are to minimize equations (4.26), (4.28), and (4.30). After estimating the parameters from the first three data points, the model will be examined in estimating the value of the fourth point.

4.2.1 Genetic Algorithm Optimization. Proposed by Deb et al. (2002), NSGA-II is a non-dominated sorting-based multi-objective optimization technique, which is based on a genetic algorithm. NSGA-II is a development of a non-dominated sorting genetic algorithm (NSGA), which was originally proposed in a seminal publication by Srinivas and Deb (1995). The original algorithm had several limitations that are resolved in the modified version NSGA II. These limitations include: high computational complexity, and the need for specifying some model parameters (Deb et al., 2002).

The major difference between NSGA and the ordinary genetic algorithm is in the way the selection parameters work. Other important genetic algorithm functions, such as the crossover

and mutation operators remain the same in the NSGA. In NSGA, first the population is ranked on the basis of an individual's "non-domination" property, and then the selection operation is performed. Subsequently, the same fitness value is assigned to all individuals in order to give an equal "reproductive" potential to them. In the next step, in order to maintain diversity in the population, all individuals are *shared* with their respective dummy fitness values.

After sharing, the non-dominated individuals are ignored temporarily to process the rest of the population in the same way. This is performed for identifying the appropriate individuals for the second "non-dominated front". Later, these new individuals are given new (smaller) dummy fitness values, and the process continues until the whole population is classified into several fronts. The population is then reproduced according to the dummy fitness values. Figure 4.4 is a flowchart of the NSGA algorithm, which is adopted from Srinivas and Deb (1995). For more information about the NSGA II algorithm, which is an improved version of the NSGA, see Deb et al. (2002).

Savic et al. (2011) developed a decision support system for multi-objective optimization called GANetXL. GANetXL is a spreadsheet-based environment, which employs the NSGA II algorithm. This tool is used in Chapter 5 for concurrent optimization of the three minimization functions in equations (4.24), (4.26), and (4.28). There are six unknowns (a, b, c, d, CSM, and CCM) that will be estimated in GANetXL with the aim of minimizing the three objective functions (Savic et al, 2011).

In Figure 4.4, a non-dominated solution is the one for which it is not possible to improve one objective without exacerbating at least one other objective. For instance, changing the parameters of a non-dominated solution may result in decreasing the error in equation (4.24), but at the cost of increasing the error in equation (4.26) and/or equation (4.28). Therefore, all non-dominated solutions can be considered as the best achievable solutions to a given problem. This is also called Pareto optimal front in the multi-objective optimization terminology. Also, the "population" in the genetic algorithm terminology refers to all available solutions at each

generation. At generation zero, all of the solutions (population) are randomly selected. A generation includes all solutions that are obtained from each iteration of the algorithm.

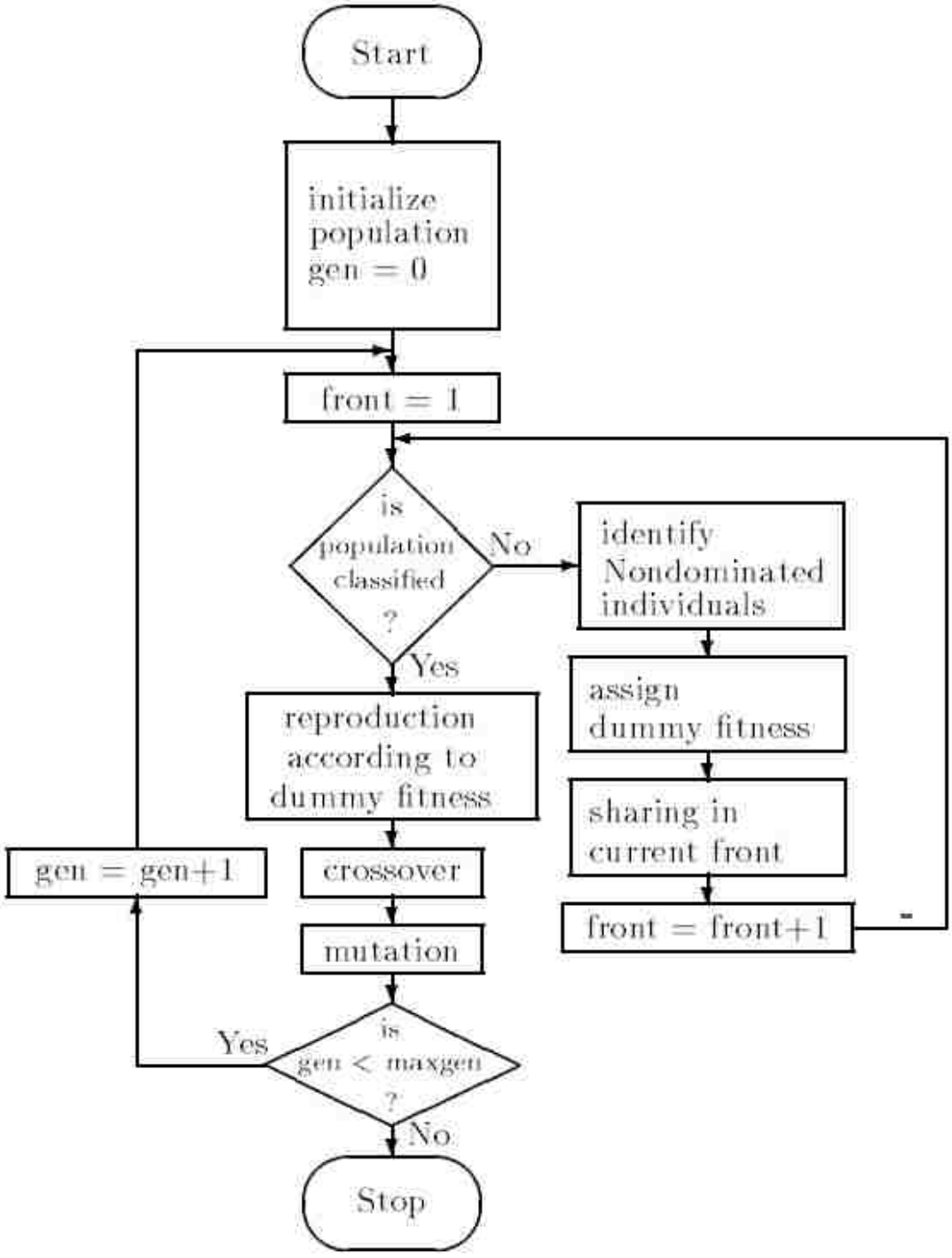

Figure 4.4. Flowchart of NSGA algorithm (adopted from Srinivas and Deb, 1995).

A non-dominated front includes all non-dominated (best) solutions. In Figure 4.4, crossover and mutation are typical genetic algorithm operators. Mutation changes randomly the new offspring. In a binary encoding, a few bits are randomly selected and switched. The purpose of mutation is to prevent the algorithm from converging to a "local minimum" by discarding the solutions that are too close to each other. In a crossover, more than one "parent" solution (from the previous population) are selected and a "children" solution is produced and transferred to the next generation. Dummy fitness functions are temporary fitness functions in each generation (algorithm iteration) that are used for measuring the quality of the population.

In this problem, the squares of equations (4.24), (4.26), and (4.28), are defined as the error (objective) functions, which are inputs to the NSGA II algorithm. These error functions should be minimized simultaneously in order to fit the best model to the measured points (i.e., points with PI values of F, S, and T, respectively). Therefore, the multi-objective minimization task is to tune (optimize) the 6 model parameters (i.e., a, b, c, d, CSM, and CCM). Hence, the model outputs are the 6 unknowns, which together define the shapes of the aging, shock, and maintenance effect curves in Figure 4.1.

In other words, the model error is defined as the difference between the available PI measurements at different truck ages and the model estimates. Since the error can be either positive or negative (a 0 error is obtained from an ideal model) the squares of the equations (4.24), (4.26), and (4.28) are the objective function inputs to the algorithm. The optimization constraints are defined in equations (4.2) and (4.3) for a/b and c/d parameters, respectively. As discussed in Section 4.1.2., the other two maintenance parameters (CSM and CCM) are not constrained and will be identified from the available historical data. Constraining these maintenance unknowns means that a priori assumption from the five assumptions in Section 4.1.2 should be selected. Here, in order to propose a more generalizable model these parameters are not constrained.

NSGA II is an evolutionary algorithm, which is based on its ancestor genetic algorithm. Genetic algorithm is inspired by the Darwin's theory of evolution. In the theory of (biological) evolution only the best species and organisms survive and evolve in time. Similarly, in NSGA II several thousand solutions are initially generated randomly. First, the fitness of these solutions to the problem objective(s) is checked. Then, through some genetic operators (i.e., selection, crossover, and mutation) the "offspring" solutions are generated from the parents. Then, the fitness of the new offspring is checked against the same metrics as the parents. Finally, the best fits will "breed" for the next generation, and the algorithm repeats until the optimization objectives (or stop criteria) are attained. In the genetic algorithm terminology "solution breeding" is defined as creating/transferring the best (offspring) solutions from (parent solutions) in a generation to the next generation.

In this problem, the values of the 6 unknown variables are tuned through the same evolutionary algorithm. Therefore, initially some completely random values are selected and assigned to each of the unknowns. Then the errors (squares of equations (4.24), (4.26), and (4.28)) are measured. If the results are not satisfactory, new offspring solutions will be generated through the genetic operators. The criteria for satisfactory results are defined within the fitness function. Depending on the problem at hand a tolerable error value is considered as the error cu-off. Whenever the algorithm reaches this cut-off it will be terminated and the solutions in the last generation will be rendered as the best achievable solutions for the problem. Also, the algorithm termination criteria can be set in the form of the number of iterations. The quality of the new offspring (new values for the 6 unknowns) are checked (against the errors). In the next step, only those values that result in minimum errors are allowed (bred) for the next generation. The threshold for selecting the minimum error is defined via the dummy fitness functions for each generation (see Figure 4.4.) After several thousands of iterations, all the unknowns are tuned in such a way to minimize the three error (objective) functions concurrently. These values will be

selected as the model parameters, and subsequently the curves in Figure 4.1 will be depicted until the desired time.

A confidence interval can also be defined for each of the 6 unknowns. Usually, a 95% confidence interval is selected in the literature. A 95 % confidence interval in this case means that if the NSGAA II algorithm is executed several times, each time with a new random number seed, there is a 95% chance that the solutions will fall in specific ranges. For instance, assume that the best value for parameter b is found to be 2.415. This value is obtained from a single execution of the NSGA II, which includes several thousand genetic iterations. If one changes the random number seed and executes the algorithm again, the new value of b may be slightly different (say, 2.433). In order to identify the 95% interval confidence for parameter b, first the model should be executed several (hundred) times, each with several thousand iterations. Then a range will be identified in which the parameter falls with a probability of 95%. For this example, the 95% confidence interval for parameter b can be [2.385 and 2.445]. The confidence intervals for a numerical example will be produced in Section 5.2.

4.3 SUMMARY

The suspension performance (PI) decreases in between the scheduled maintenance (SM) according to a gradual slow degradation (ageing) process. The PI can also decrease randomly (e.g., sporadic shocks) due to instantaneous sharp decreases (e.g., due to shocks) at random times. The cumulative PI degradation between the scheduled maintenance points is compensated by minor routine maintenance and repair actions (e.g., nitrogen gas recharging, oil leakage compensation, repairing malfunctioning valves, and links). In contrasts, the sudden sharp decreases in PI that are mainly due to shocks or failure accumulation in sub-systems until reaching a threshold are compensated by major repair actions. Thus, the first kind of maintenance/repair is scheduled (SM), and the second type is corrective (CM).

The major mechanisms that cause PI drop between SMs are due to gas diffusion (thermodynamically) and oil leakage (hydro-mechanically). The effects of major deteriorating mechanisms, such as metal fatigue, elastomer degradation, corrosion, and oil contamination are considered in the form of large non-linear and sharply decreasing curves.

5. MODEL VALIDATION AND NUMERICAL EXAMPLES

5.1 SOLUTION

Assuming there are four data points (i.e., for pairs of (t, PI(t))), the goal is to estimate a, b, c, d, CSM, and CCM to minimize the estimation error associated with PI (t). This process will determine the shape of the curves in Figure 4.1. Without of loss of generality, it is assumed that the first observation is from a point before the nth SM, which has a PI = F (Equation (5.3)).

$$X_1 = PI\ (t_{Sn}) = F \tag{5.1}$$

The second data is from the point before the 1st CM, which has a PI = S. It is also assumed that the 1st CM takes place after the nth SM, i.e. $t_{C1>}\ t_{sn}$.

$$X_2 = PI\ (t_{C1}) = S \tag{5.2}$$

The third data is from the point before the 2nd CM with a value of T.

$$X_3 = PI\ (t_{C2}) = T \tag{5.3}$$

The fourth data is from an arbitrary point with value A.

$$X_4 = PI\ (t_a) = A \tag{5.4}$$

The first three points will be used to estimate the parameters of the deterministic model, reserving the fourth point for model validation.

From X_1:

$$1 - na(TS)^b + (n-1) \times CSM = F \tag{5.5}$$

From X_2: The number of SMs between $X_1$and X_2 is obtained from Equation (5.6).

$$n_{1-2} = \frac{t_{c1} - t_{sn}}{TS} \tag{5.6}$$

$$1 + (n + n_{1-2})\left(-a(TS)^b + CSM\right) - c(TC)^d = S \tag{5.7}$$

From X_3: The number of SMs between $X_2$and X_3 is obtained from Equation (5.8).

$$n_{2-3} = \frac{t_{c2} - t_{c1}}{TS} \tag{5.8}$$

$$S + CCM + n_{2-3}\left(-a(TS)^b + CSM\right) - C(TC)^d = T \tag{5.9}$$

Therefore the problem is defined by three equations, Equations (5.5), (5.7), and (5.9), and six unknowns (a, b, c, d, CSM, and CCM). This system of equations cannot be solved analytically. The heuristic search methods are used to find the best estimates of the 6 unknowns. A multi-objective genetic algorithm model is used to solve the numerical example in Section 5.2. The three objectives of the algorithm are to minimize Equations (5.7), (5.9), and (5.10).

5.2 NUMERICAL EXAMPLE

Table 5.1 summarizes the available data. All values have been selected randomly, using a pseudo random number generator, and there are only 4 measured data points.

Table 5.1 Available database.

Point	Event	Time (hour)	PI
1	Before the 3rd SM	120	0.99859
2	Before the 1st CM	212	0.99722
3	Before the 2nd CM	345	0.99653
4	No specific event	581	0.996946

From point 1:

$$TS = {}^{120}/_{3} = 40 \tag{5.10}$$

$$1 - 3a(40)^b + 2CSM = 0.99859 \tag{5.11}$$

From point 2:

$$n_{1-2} = \frac{212 - 120}{40} \approx 2 \tag{5.12}$$

$$TC = 212 - 120 + 2(40) = 12 \tag{5.13}$$

$$1 + 5\left(CSM - a(40)^b\right) - c(12)^d = 0.99722 \tag{5.14}$$

From point 3:

$$n_{2-3} = \frac{345 - 212}{40} \approx 3 \tag{5.15}$$

$$0.99722 + CCM + 3(CSM - a(40)^b - c(12)^2 = 0.99653 \tag{5.16}$$

As stated above, the three minimization objectives are equations (5.11), (5.14), and (5.16). Since there is more than one objective, the genetic algorithm gives an optimal Pareto

solution, instead of a single point. The results of the best 50 solutions are summarized in Table 5.2.

Table 5.2 Genetic Optimization Results

No.	a	b	c	d	CSM	CCM	Equation (5.11)	Equation (5.14)	Equation (5.16)
1	2.2E-07	2.377519	6.78E-06	2.424405	0.001424	0.002331	8.32103E-19	1.02229E-21	4.55949E-07
2	2.2E-07	2.439903	6.78E-06	2.068702	0.001457	0.006901	1.07335E-06	6.98549E-10	2.29407E-19
3	2.2E-07	2.377519	6.78E-06	2.424405	0.001424	0.002296	2.94294E-23	1.33257E-18	4.5595E-07
4	2.2E-07	2.42488	4.62E-06	2.060725	0.001289	0.002295	1.17579E-06	5.63636E-12	2.6097E-15
5	2.2E-07	2.423439	4.62E-06	2.193152	0.001355	0.002296	8.54697E-07	5.42616E-09	6.91593E-11
6	2.2E-07	2.432605		2.300947	0.001464	0.0068	7.74252E-07	3.25837E-14	5.7054E-09
7	2.2E-07	2.423456	4.62E-06	2.070652	0.001284	0.002331	1.13753E-06	4.19871E-13	1.05067E-10
8	2.2E-07	2.424878	4.62E-06	2.193116	0.001355	0.002296	9.05073E-07	8.40924E-10	1.23037E-09
9	2.2E-07	2.423439	4.62E-06	2.070652	0.001286	0.0068	1.13098E-06	6.49606E-11	1.96233E-11
10	2.2E-07	2.438751	6.78E-06	2.071071	0.001458	0.002296	1.02567E-06	3.56797E-11	2.88364E-10
11	2.2E-07	2.394728	4.86E-06	2.301769	0.001323	0.002322	2.31092E-07	1.25669E-07	1.14657E-09
12	2.2E-07	2.392814	4.86E-06	2.302144	0.001323	0.002322	2.01416E-07	1.65105E-07	1.09769E-11
13	2.2E-07	2.394968	4.86E-06	2.315652	0.001352	0.002322	1.8331E-07	1.9125E-07	5.44889E-10
14	2.2E-07	2.398556	4.86E-06	2.423447	0.001424	0.004581	1.18089E-07	5.21764E-08	4.7404E-08
15	2.2E-07	2.402384	4.62E-06	2.308603	0.001286	0.002331	4.7128E-07	5.42642E-12	7.08295E-08
16	2.2E-07	2.426795	4.62E-06	2.301775	0.001429	0.002331	7.04879E-07	3.10918E-11	1.17491E-08
17	2.2E-07	2.423456	4.62E-06	2.301703	0.001424	0.002322	6.1842E-07	7.51171E-09	4.13511E-09
18	2.2E-07	2.382122	6.78E-06	2.300947	0.001317	0.0023	8.30952E-08	6.53655E-09	1.91936E-07
19	2.2E-07	2.377519	6.78E-06	2.315323	0.001306	0.002322	5.63144E-08	5.24668E-09	2.34403E-07
20	2.2E-07	2.42488	4.62E-06	2.307996	0.001426	0.002296	6.55578E-07	8.0931E-10	1.1333E-08
21	2.2E-07	2.400725	4.74E-06	2.308604	0.001286	0.002322	4.32988E-07	6.09284E-11	7.56192E-08
22	2.2E-07	2.377519	6.78E-06	2.313509	0.001424	0.002322	2.94294E-23	4.56048E-07	5.47988E-15
23	2.2E-07	2.423693	4.62E-06	2.362953	0.001464	0.0023	5.05742E-07	2.23103E-09	1.97759E-08
24	2.2E-07	2.425427	4.62E-06	2.192802	0.001352	0.0023	9.37482E-07	1.44065E-11	3.33092E-09
25	2.2E-07	2.402459	4.74E-06	2.308605	0.001317	0.002301	3.91516E-07	1.28535E-08	3.26213E-08
26	2.2E-07	2.400725	4.74E-06	2.285018	0.001306	0.009151	3.81823E-07	3.67212E-08	1.23693E-08
27	2.2E-07	2.400727	5.7E-06	2.376902	0.001425	0.0023	1.44471E-07	5.96508E-09	1.18693E-07
28	2.2E-07	2.402384	4.62E-06	2.308603	0.001306	0.009151	4.1783E-07	9.58863E-09	3.45727E-08
29	2.2E-07	2.379655	6.78E-06	2.315592	0.001354	0.0068	3.0388E-08	6.58155E-08	1.06222E-07

Table 5.2. Genetic Optimization Results Cont.

No.	a	b	c	d	CSM	CCM	Equation (5.11)	Equation (5.14)	Equation (5.16)
30	2.2E-07	2.393609	4.86E-06	2.307996	0.001352	0.002322	1.6349E-07	2.56836E-07	5.94778E-09
31	2.2E-07	2.398573	4.86E-06	2.315413	0.001306	0.002322	3.37846E-07	1.12706E-08	4.88988E-08
32	2.2E-07	2.382122	6.78E-06	2.308604	0.001424	0.002331	5.32038E-09	3.35858E-07	2.21647E-09
33	2.2E-07	2.394255	4.86E-06	2.315652	0.001352	0.002322	1.73248E-07	2.09014E-07	1.24317E-09
34	2.2E-07	2.438751	6.78E-06	2.070652	0.001459	0.002296	1.01901E-06	2.37926E-10	6.14292E-10
35	2.2E-07	2.393609	4.86E-06	2.307996	0.001357	0.002322	1.56459E-07	2.7959E-07	8.96812E-09
36	2.2E-07	2.398571	4.86E-06	2.315652	0.001323	0.004571	2.97564E-07	3.78659E-08	2.26758E-08
37	2.2E-07	2.42488	4.62E-06	2.307996	0.001464	0.002296	5.38568E-07	4.75083E-08	2.03906E-09
38	2.2E-07	2.432069	4.62E-06	2.300947	0.001464	0.0068	7.56229E-07	2.88618E-10	4.25529E-09
39	2.2E-07	2.377758	6.78E-06	2.301769	0.001323	0.002322	4.21731E-08	5.11853E-08	1.19502E-07
40	2.2E-07	2.394728	4.86E-06	2.315322	0.001306	0.002322	2.66696E-07	4.60273E-08	2.43256E-08
41	2.2E-07	2.42537	4.62E-06	2.313509	0.001424	0.002322	6.75921E-07	2.1857E-10	2.01434E-08
42	2.2E-07	2.426791	4.62E-06	2.307996	0.001465	0.0023	5.87431E-07	2.76985E-08	2.52258E-10
43	2.2E-07	2.42488	4.62E-06	2.060725	0.001289	0.002295	1.17341E-06	1.38757E-13	5.05516E-12
44	2.2E-07	2.398573	4.86E-06	2.303928	0.001317	0.0023	3.12786E-07	4.16865E-08	1.79848E-08
45	2.2E-07	2.378054	6.78E-06	2.315562	0.001355	0.004571	2.15657E-08	9.26088E-08	8.76706E-08
46	2.2E-07	2.423439	4.62E-06	2.193152	0.001352	0.002322	8.66931E-07	3.26967E-09	4.62293E-10
47	2.2E-07	2.439903	6.78E-06	2.068702	0.001461	0.006901	1.05973E-06	9.90117E-11	1.73797E-10
48	2.2E-07	2.382122	6.78E-06	2.308604	0.001323	0.004571	7.53731E-08	5.70496E-09	2.02753E-07
49	2.2E-07	2.382122	4.86E-06	2.315413	0.001306	0.002331	9.62535E-08	3.1117E-07	2.48673E-09
50	2.2E-07	2.398573	6.78E-06	2.308604	0.001424	0.002322	1.18294E-07	1.63507E-08	1.01173E-07

The (single) optimal solution is the one that results in 0 values in the last three columns of Table 5.2 (i.e., zero error). However, as it can be seen the last three columns, there is no solution to minimize all the three functions at the same time. In other words, the optimal solution of one function may be sub-optimal solution for other function(s). However, not all the solutions in Table 5.2 are physically logical. For instance, solution number 36 is illustrated in Figure 5.1.

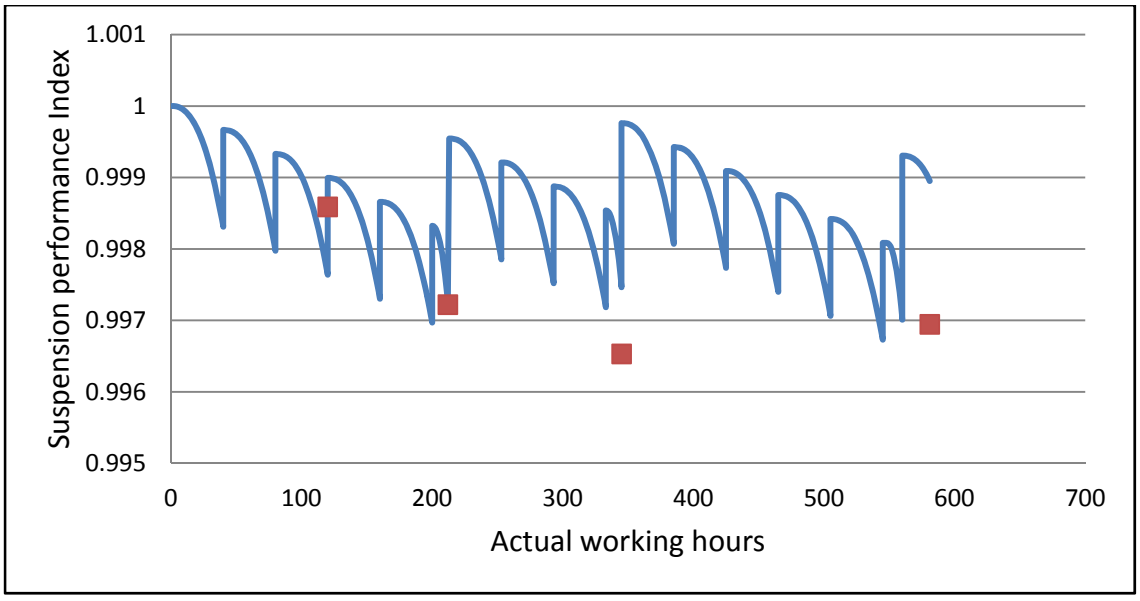

Figure 5.1 Results from Solution No. 36.

The parameter values are summarized in Table 5.3. Using the parameters in Table 5.3, the cyclic ageing curves for both Types I and II mechanisms are illustrated in Figure 5.2. Moreover, the effects of both the SM and CM maintenance/repairs, on improving the systems sate (i.e., increasing the PI value), are illustrated in Figure 5. 2. The red squares are actual measurements of PI at different operating ages according to Table 5.1. Figure 5.2 shows that after using the first 3 data points to train the model, the value of the 4th data point can be predicted with a negligible error as summarized in Table 5.4. This error is less than 0.2 percent. To test the model solution, and without loss of generalizability, all PI values in Tables 5.1 and 4, were selected randomly. Model estimates are compared with actual data in Table 5.4.

Table 5.3 Parameters from Solution No. 36

a	b	c	d	CSM	CCM
2.20401E-07	2.425427407	4.61505E-06	2.192802	0.001352	0.0023

Table 5.4 Model vs. Measurements (Solution No. 36)

Point	Time	PI	PI Model	Absolute error (%)
1	120	0.99859	0.998974	-0.04
2	212	0.99722	0.997216	0.00
3	345	0.99653	0.999717	-0.32
4	581	0.996946	0.998879	-0.19

The absolute errors are less than 0.5%. The fourth point (validation) was not used in parameter estimation. Nevertheless, the model error at this point is less than 0.2%. It should be noted that solution No. 36 is one of several "close enough" estimations. Figure 5.2 shows the model results from solution No. 22. The six parameters were selected based on Table 5.2, and the diagram is depicted until the time of the 4th data point in Figure 5.2.

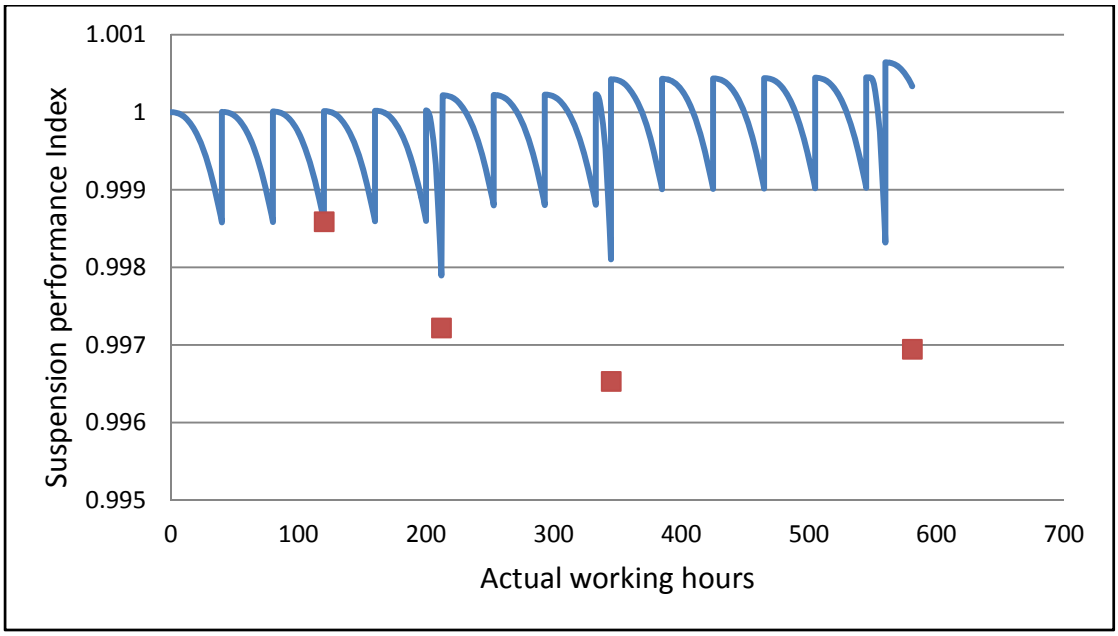

Figure 5.2 Results from Solution No. 22.

Although, No. 22 is mathematically a valid solution to the problem (with very small errors), from a mechanical point of view, it is invalid. The reason is that the overall life curve is

increasing with time, which contradicts the ageing assumption. Figure 5.3 and Table 5.5 shows solution No. 8.

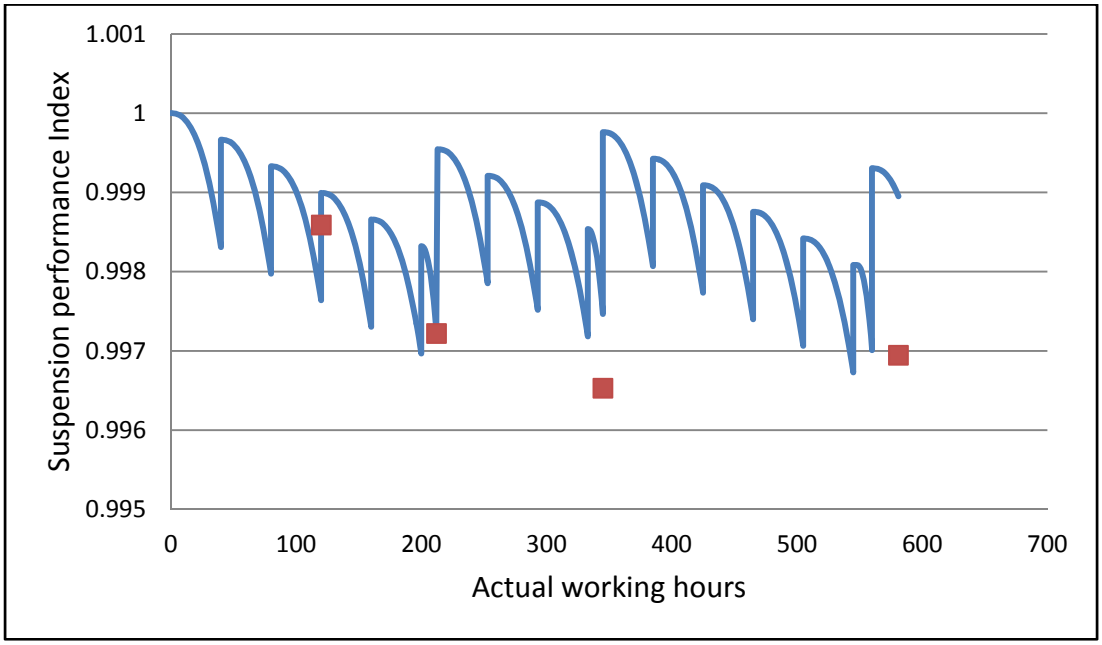

Figure 5.3 Results from Solution No. 8.

Solutions No. 8 (Figure 5.3) and No. 36 (Figure 5.1) are mathematically (in terms of prediction errors) nearly the same. However, both the ageing and shock curves are different.

Table 5.5 Model vs. Measurements (Solution No. 8)

Point	Time	PI	PI Model	Absolute error (%)
1	120	0.99859	0.997904	0.07
2	212	0.99722	0.997218	0.00
3	345	0.99653	0.997307	-0.08
4	581	0.996946	0.998951	-0.20

In conclusion, all solutions from the Pareto optimal front should be examined to find the best one which is a better representative for an actual suspension unit. The 95% confidence intervals, per Section 4.2.1, are summarized in Table 5.6.

Table 5.6. The 95% confidence intervals for the numerical model parameters

Parameter	95% Confidence Interval
a	[0.00000021 , 0.00000023]
b	[2.377515 , 2.439908]
c	[0.00000457 , 0.00000682]
d	[2.308597 , 2.424415]
CSM	[0.001281 , 0.001467]
CCM	[0.002292 , 0.009156]

5.3. SUMMARY

In this chapter, numerical examples were introduced to examine the validity of the proposed models. The model precision was demonstrated by predicting future suspension performance under both ageing and shock phenomena that are typical in surface mining operations. The effects of thermodynamically and hydro-mechanically deteriorating mechanisms, as well as the effects of fatigue, material degradation, and oil contamination are mathematically modeled and incorporated into the formula for the temporal functional relationship for the suspension performance. The proposed mathematical framework was solved using a minimum number of experimental data points. Using only four data points (i.e., for pairs of (t, PI(t))), all model constants and parameters such as a, b, c, d, CSM, and CCM are estimated and used to characterize the process.

6. EXPERIMENTAL DESIGN AND EXPERIMENTATION

A detailed experimental design is followed to analyze the impact of truck ageing on the operator exposures to WBV levels. The experimentation is twofold. The first set of experiments is designed to analyze the response and sensitivity of a virtual model of a CAT 793D dump truck to suspension input parameters, including the spring stiffness rate and damping coefficient. The second set of experiments is designed to analyze the impact of ageing hydro-pneumatic suspension parameters in the truck operator's exposure to WBV levels. The experimentation is performed using computer simulations in the MSC ADAMS environment. To achieve the above objectives, several hundred virtual experiments are designed and simulated in MSC ADAMS using the CAT 793D dump truck to illustrate the impact of ageing on the WBV levels and exposures. The model in Chapter 4.0 and the numerical example in Chapter 5.0 are used as the basis for the virtual experiments. The impact of truck age and HISLO conditions on WBV levels and exposures are outlined in the following sections.

6.1 EXPERIMENT ENVIRONMENT

The virtual experiments for the ageing suspensions model are performed using MSC ADAMS, which is a highly used multibody dynamics analysis platform. The virtual model of a CAT 793D dump truck in ADAMS/View is employed as the basis for the virtual experimentations. This model is built and simulated using the model from Aouad (2008).

The virtual prototype truck model is built and simulated in the MSC ADAMS environment. After creating the CAD geometry of the truck, using the shape and dimensions of different components, the whole geometry is imported into MSC ADAMS and each component is assigned a mass and a corresponding density in order to retain its material properties. The dump truck comprises rigid-body components linked together to form one entity. This virtual prototype model is created by connecting different parts or rigid bodies together via joints.

In the MSC ADAMS environment, the applied forces are input into the model. These forces are the external excitations of the truck system under HISLO conditions, and thus they correspond to the load dumped by a shovel under gravity. After assigning the input forces, MSC ADAMS/View evaluates the reactive forces on the structure that corresponds to the spring-damper systems. It also evaluates the reactions in the joints connecting different components due to the dynamic motion of the structure under the input force. Once the virtual model is built and validated, a static simulation is performed to configure the model under equilibrium conditions. This is then followed by a dynamic simulation, which reduces some of the initial, transient system responses. During the simulation process, ADAMS/View is used to complete the following: (i) sets the initial conditions for all model objects; (ii) formulates appropriate equations of motions (EOM) based on the second law of Newton (the EOMs control the object motions given the set of forces and constraints acting on them); and (iii) solves the EOMs for displacements, velocities and accelerations. Finally, ADAMS/Post Processor displays and manipulates the results for further investigations.

6.2. CONSTRAINTS AND CONTROL ENVIRONMENT

All model simulations are based on an available virtual prototype of a CAT 793D truck in the MSC ADAMS environment. The model comprises the major truck parts (called bodies in ADAMS), including: bed, cabin, chassis, tires, seat, and human body, which are interconnected through different joints (called connectors in ADAMS), which represents a complete rigid multibody truck model. The whole model oscillates in reaction to the impulse force due to HISLO conditions. HISLO introduces shock waves to the truck bed, which propagate through different components of the dump truck. A component of these shock waves reaches the operator seat and exposes the operator to WBVs. The main mechanism for attenuating these shock waves and vibration is the hydro-pneumatic suspension unit.

The HISLO working condition in a typical surface mining operation is considered for these simulation experiments. The effects of ambient conditions and constraints such as dust, temperature, and humidity on suspension performance are neglected.

The control environment for the virtual model consists of maintaining the static equilibrium by connecting all parts to each other with one part connected to a fixed reference. This fixed reference is essential for successful simulation and to avoid free falling parts due to gravity. Thus, the connections between the parts are achieved by adding spring and damping controls to the model. Also, the impulse force generated under HISLO conditions is input as a SPLINE data element function. This force has a single component in the vertical direction and is constrained in the other five directions (Aouad, 2008).

6.3. METHODS AND PROCESSES FOR THE EXPERIMENTAL DESIGN

A CAT 793D has two pairs of rear and front hydro-pneumatic suspension struts. These suspension struts are the core components for providing several critical functionalities, including: (i) ride comfort, (ii) truck handling, and (iii) level adjustment.

Under the HISLO operations the first major functionality (i.e., ride comfort) is effective. The truck handling functionality is effective when a truck is in motion. The level adjustment functionality is performed occasionally by adding/removing hydraulic oil to the suspension struts to adjust the overall truck height. Therefore, the primary functionality of suspension struts, when a truck is stopped for the HISLO operations, is to provide ride comfort. Ride comfort can be measured in terms of operator WBV exposure during the loading operation. Therefore, in order to evaluate the efficiency of ageing suspension struts under HISLO conditions, the temporal behavior of suspension performance is linked to operator's exposure to WBVs. The temporal behavior of an ageing suspension strut is governed by its two major sub-systems. As discussed in Sections 3.2 and 3.3, respectively, these sub-systems are the gas spring and hydraulic damper assemblies. The effectiveness of a whole suspension strut is governed by its spring and damper

elements, which are determined by spring stiffness rate and damping coefficient, respectively. Therefore, for understanding the operator's exposure to WBVs (under HISLO) in ageing trucks, the damping coefficient and spring stiffness rates must be modeled with time.

In Sections 4.1-4.2 and 5.1-5.2, a suspension performance was modeled with time in the form of a time-varying performance index function. In this chapter, the PI model is linked to the spring-damper characteristics via the time-varying spring stiffness rates and damping coefficients. Consequently, for every point on the time vector, a specific damping-spring setup will be defined. In the next step, the CAT793D truck will be simulated in ADAMS/view for all the obtained setups from the previous step. Finally, each single model execution results in an RMS value for accelerations. This step will be repeated for the whole life of the suspension strut until its temporal effect in WBVs is completely modeled. As a result, a time function of WBVs will be obtained, which mathematically describes the effect of ageing suspensions in WBVs.

ADAMS/Vibration environment is a module of MSC ADAMS, which allows frequency-domain analysis in ADAMS/View. ADAMS/Vibration evaluates the frequency response functions for magnitude and phase characteristics and solves for the system modes (Aouad, 2008). The RKF 45 method is used to integrate the differential equations of motions. It is a single-step method, which is primarily designed to solve non-stiff and stiff differential equations when derivative equations are not expensive or time consuming. RFK 45 uses the DDERKF code, which is a driver for a modification of the RKF 45 (Shampine and Watts, 1979).

The different stages for solving the complete vibration problem of the truck model under HISLO conditions are by using ADAMS/View for dynamic analysis; followed by a modal and forced response analysis in ADAMS/Vibration. Finally, ADAMS/Post Processor is used to render the results. Post processing involves animation and plotting (Aouad, 2008).

Six hundred iterations have been completed using the virtual model in ADAMS/View, in order to model the effect of the ageing suspensions in WBVs for the first 600 working hours of the CAT 793 D. However, for full-life modeling the simulations should be iteratively executed

for several thousand times, each time with a new set of both the rear and front suspension configurations. Therefore, it will be very cumbersome to examine the proposed model for the whole life of a typical truck. This is due to the fact that several thousand simulations should be completed, each with a set of specific input parameters.

Different mining truck manufacturers propose different suspension useful lives for different truck models within the range of 5-10 years. It is assumed that a pair of hydro-pneumatic suspension struts in a large mining truck has an approximate useful life of 7 years (under normal surface mining operation conditions). Assuming that the truck works 330 days per year and 15 hours per day (two 8-hour shifts minus 1-hour break and shift change time), the suspensions will work 34,650 hours during their useful lifetime. Therefore, for a full-life simulation, 34,650 iterations should be completed. To address this difficulty, the data obtained from 600 simulations (with different input setups) in ADAMS/view for the first 600 working hours are initially used to model the RMS accelerations for a brand-new CAT793D's suspension strut. These simulations are carried out for times 0, 1, 2, … 600 suspensions worked hours. Subsequently, several new simulation experiments were designed and carried out to model the effect of suspension ageing in WBVs for truck ages 3, 5 and 7 years.

The model verifications for all 600 iterations are confirmed in ADAMS/View. All models coverage for two passes of material dumping under HISLO. Subsequently, the displacements, velocities, and accelerations of all bodies (rigid parts, such as cabin and seat) are available in the post-processing step of the simulations, which confirms the iterations convergence.

6.4. EXPERIMENTATION

Initially, four different scenarios for understanding the effect of ageing in spring-damper parameters were defined. Each of the four suspension struts has two governing parameters of

spring stiffness rate and damping coefficient, which identifies the effectiveness of the struts in shock wave attenuation. Any deviations from the manufacturers (optimal) nominal values (see Table 6.1) results in sub-optimal suspension performances.

Table 6.1. Nominal suspension parameters for CAT793D.

	Stiffness (N/m)		Damping (Ns/m)	
	Rear	Front	Rear	Front
Nominal Values	1.927E+07	1.327E+07	1.596E+06	1.224E+06

In order to investigate and link the effect of PI drop (ageing) to spring-damper parameters, four scenarios were examined as follows:

(i) both the spring stiffness rate and damping coefficient increase with time.

(ii) both the spring stiffness rate and damping coefficient decrease with time.

(iii) spring stiffness rate decreases and damping coefficient increases with time.

(iv) spring stiffness rate increases and damping coefficient increases with time.

The above four scenarios cover all possible ageing alternatives. The PI model was coupled with the ADAMS model to examine the above scenarios. The third scenario was the only alternative, in which the virtual model showed a meaningful sensitivity to the inputs (spring stiffness rate and damping coefficient) in terms of the resulting WBVs.

In the next step, 600 virtual experiments were conducted to obtain the ageing effect in WBVs (see Table 6.2).

Table 6.2. Characteristics of the experiments (600 iterations).

Experiments Objectives	Component Variations	Rationale of Experiments	Expected Contributions
Simulating ageing suspensions in MSC ADAMS	Deteriorating (time-varying) Damping and stiffness per the PI model parameters	Effect of ageing struts in WBVs is revealed	Molding ageing suspension struts, and simulating the ageing effect in the operator's perceived WBVs under HISLO

Solution No. 36 for the numerical example in Chapter 5.0 which resulted in the best model in terms of the prediction accuracy is selected for conducting the virtual experimentations and determining the effect of ageing in WBV levels. Table 6.3 summarizes the optimized parameters for solution No. 36.

Table 6.3 Parameters from Solution No. 36.

a	b	c	d	CSM	CCM
2.20401E-07	2.425427407	4.61505E-06	2.192802	0.001352	0.0023

Following the discussion in Section 4.1.1 on the nature of the intervening maintenance/repair processes, this solution (No. 36) follows a Kijima framework for the condition-based maintenance. The solution follows a type (iv) process for the scheduled maintenance. In other words, after a condition-based (corrective) maintenance, the component/system state becomes better than the old, but not as-good-as-new. On the other hand, after a scheduled maintenance, the suspension performance improves, but it doesn't reach its performance level just after the previous maintenance. The following inequalities are valid with the data presented in Table 6.3, and TS =40 hr. and TC = 12 per Figure 5.1, which justify the above prepositions.

$$a(TS)^b > CSM \tag{6.1}$$

$$c(TC)^d < CCM \tag{6.2}$$

The above argument validates the flexibility of the proposed methodology in identifying the maintenance qualities. In other words, this study is not limited to a-priori assumption for the maintenance quality as discussed in Section 4.1.1. It identifies the maintenance qualities directly from historical data, which can be different for different trucks that work under different conditions.

In order to link the deteriorating performance of the ageing hydro-pneumatic suspension struts with the WBV levels, a virtual prototype of a CAT 793D dump truck is examined. The model is built in MSC ADAMS, which is both a modeling and simulation platform for multibody dynamic analysis. Figures 6.1 and 6.2 illustrate the 2D and 3D views of the model, respectively

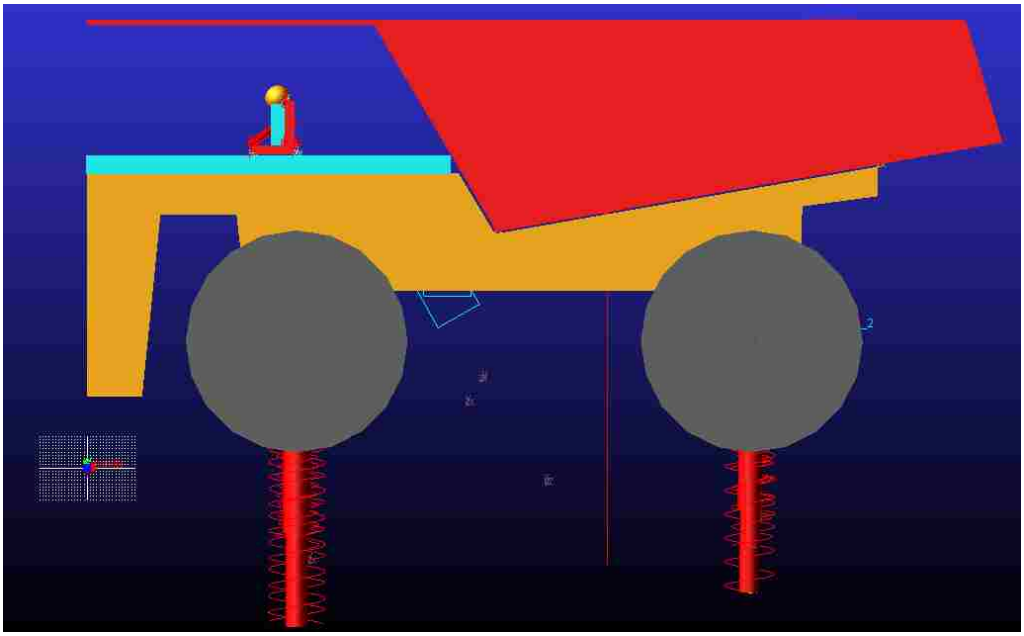

Figure 6.1 A side view of the virtual prototype model of the CAT 793D dump truck in ADAMS/View.

Figure 6.2 A 3D view of the virtual prototype model of the CAT 793D dump truck in ADAMS/View.

The whole model oscillates in reaction to the impulse force due to HISLO. The HISLO introduces shock waves to the truck bed, which propagate through different components of the dump truck. A component of these shock waves reaches the operator seat and exposes the operator to WBVs. The main mechanism for attenuating these shock waves and vibration is the hydro-pneumatic suspension unit.

Using the suspension parameters from Table 6.1., along with a three-step function for a 100 metric ton impulse force on truck bed, the acceleration of the center of mass of the seat in vertical direction for 10 seconds after inserting the impulse force is simulated and illustrated in Figure 6.3. The RMS value of the seat vertical accelerations is calculated as 3.29 m/s^2. In Figure 6.3, a negative acceleration indicates a downward displacement.

In the following sections, a series of virtual experimentations with deteriorating (ageing) rear/front suspension parameters are conducted in order to examine the effect of ageing suspensions on WBV in terms of the RMS values for the vertical acceleration of the center of mass of the seat.

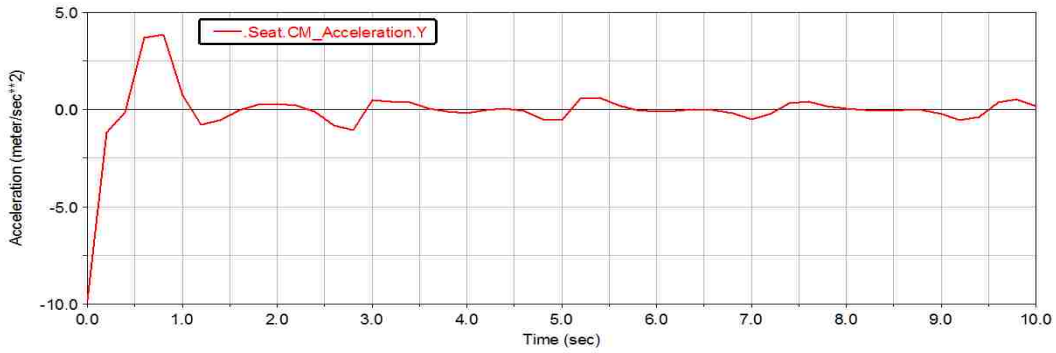

Figure 6.3 Vertical acceleration of the CAT 793D seat C.M. due to HISLO.

In Sections 4.1-4.2, a typical hydro-pneumatic suspension strut performance with ageing was mathematically modeled in the form of a performance index (PI). However, in order to examine the effect of a decreasing PI with time in the WBV, the PI model should be translated into the ADAMS model in the form of suspension parameters. The suspension parameters include both the rear and front suspension damping coefficient and spring stiffness rates. Solution No. 36 is employed for this purpose. A decreasing PI is equivalent to decreasing spring stiffness rates and increasing damping coefficient. As the PI decreases with age, the performance of the air spring component of the hydro-pneumatic suspension decreases. This is demonstrated by a decreasing stiffness rate from the nominal values.

As discussed in Section 3.2, the nominal spring stiffness rate is governed by the pre-pressure and volume of the gas accumulator. The accumulator seals and polymeric membrane performance in entrapping the inert nitrogen gas inside the accumulator decreases with time due to deteriorating polymers as the ageing effect. When nitrogen molecules diffuses into the environment (due to the old and malfunctioning seals and membranes), the pre-pressure state decreases from the nominal values. Therefore, the air spring stiffness rate reduces (spring softening), which results in a more severe and prolonged WBVs. On the other hand, the effect of PI drop with ageing on the damping sub-system is manifested by the time-increasing damping

coefficient. This process again introduces more severe shocks and vibrations to other truck parts than a brand new damper. A brand-new hydraulic damping parameters are summarized in Table 6.1. Thus, the combined effects of the deteriorating hydraulic damping coefficient and spring stiffness rate is translated into more severe and prolonged WBVs.

Using model No. 36, the ADAMS model was executed several times, each time with a different damping-stiffness parameter setting(per the PI model) and for different truck working hours until 600 hours. Therefore, the virtual model was executed 600 times with different suspension parameters in ADAMS (see Figure 6.4). The RMS value of the vertical acceleration of the truck seat C.M. increases from 3.288 m/s^2 to 3.293 m/s^2 after 600 working hours. This is equivalent to 0.24% increase in WBVs. The overall trend in RMS curve in Figure 6.4 is upward. However, there are periodic fluctuations in RMS values, which are due to the temporary ameliorating effects of both the scheduled and corrective maintenance actions.

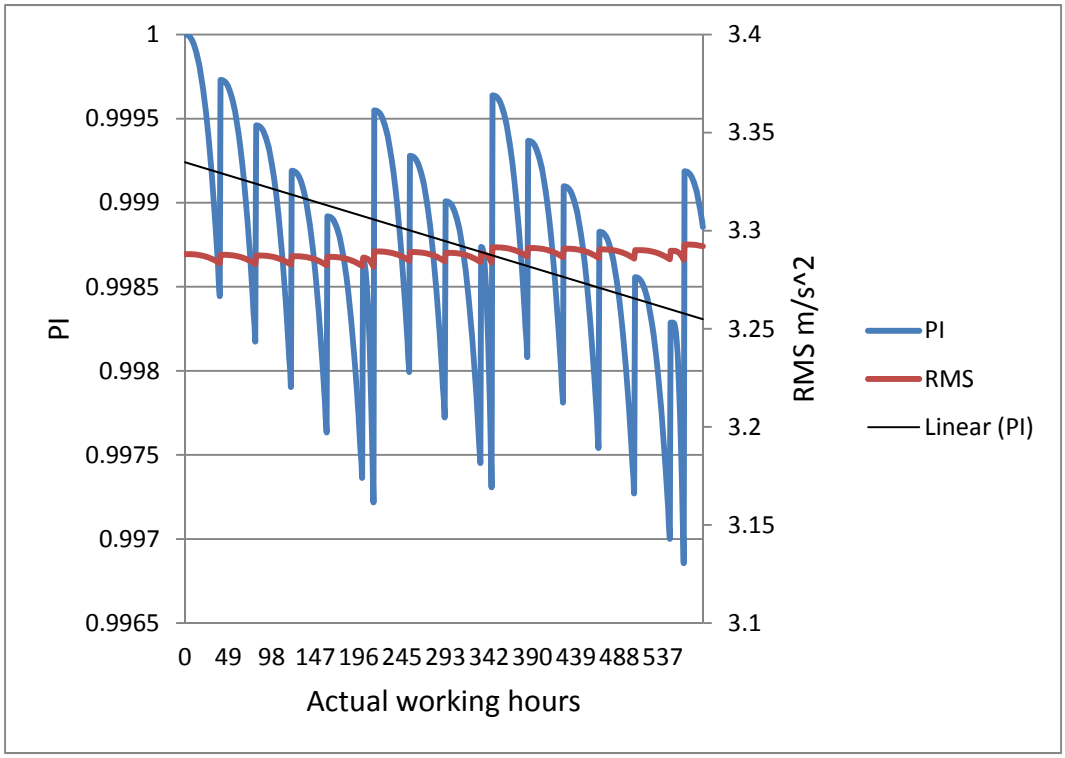

Figure 6.4. The effect of truck ageing on both the suspension's PI and WBVs in terms of the RMS values of the vertical accelerations of the seat C.M., using 600 iterations.

In the following sections, the WBV levels in both the vertical and horizontal directions for ageing suspension struts are obtained. The nominal, 3-year, 5-year, and 7-year suspension configurations are determined in terms of their corresponding stiffness and damping. Table 6.4 summarizes the suspension parameters for different truck ages. The decreasing trend in the PI model (with age) is equivalent to the decreasing stiffness and increasing damping for different truck ages per Table 6.4.

Table 6.4 Suspension characteristics of different age trucks.

Truck age	Stiffness (N/m)		Damping (Ns/M)	
	Rear Struts	Front Struts	Rear Struts	Front Struts
Brand-new	19,270,000	13,270,000	1,596,000	1,224,000
3-year old	17,794,303	12,253,783	1,737,185	1,332,277
5-year old	15,751,876	10,847,296	1,882,227	1,443,512
7-year old	13,140,924	9,049,303	2,056,039	1,576,812

6.4.1 The Rationale for Selecting the Ageing Suspension's Parameters. The ageing suspension parameters are obtained from the PI model that was proposed in Sections 4.1-4.2 It is assumed that solution No. 36 in Section 5.2 captures the ageing processes of a CAT 793 D truck, which is simulated in Section 6.4. In summary, the PI model describes the time-dependent performance behavior of the suspensions. This behavior is governed by the suspension parameters, which are the damping and stiffness characteristics. Therefore, in Table 6.4, solution No. 36 is translated into the damping-stiffness parameters that change with time. As discussed earlier in Section 6.4, a decreasing PI (ageing suspension) translates into the decreasing stiffness rate and increasing damping coefficient. Therefore, with truck ageing the stiffness-damping parameters deteriorate. The effect of this parameter deterioration is manifested in higher levels of

WBVs under the HISLO operations, which will be discussed in the following sections. The values in Table 6.4 were generated from the mathematical ageing function due to the ageing process. Both the decreases (due to ageing and shock processes) and the increases (due to maintenance and repairs) in the PI model are translated into equivalent temporal stiffness-damping characteristics. For instance, it is assumed that a 0.246% decrease in the PI value after 345 hours of truck working (see Table 5.1) is equivalent to 0.246% deterioration in the stiffness-damping characteristics. This is also equivalent to a 0.246% decrease in the both rear and front spring stiffness rates, and a 0.246% increase in the damping coefficients of both the rear and front hydraulic dampers (see Table 6.1 and its following paragraphs). Therefore there is a one-by-one correspondence between the PI values at different ages and the stiffness-damping characteristics at the same ages. Thus, the PI model acts as a medium to translate the suspension ageing process into the suspension inputs (i.e., the time-varying spring stiffness rates and damping coefficients) in the ADAMS model.

6.4.2. Experimentations for the 3-Year Old CAT793. Again it is assumed that a CAT 793D works 15 hours per day for 330 days/year under both the normal surface mining and HISLO conditions. The effect of ageing in WBVs for a 3-year old (14,850 hours) truck is examined through conducting 20 different virtual experiments in the ADAMS environment. The objective of these experiments is to approximately determine the WBV levels, after 3 years, in terms of the RMS values of the vertical accelerations at the center of mass of the operator's seat.

The varying input parameters for each of the 20 experiments are summarized in Table 6.5. All other truck parameters, including inertia, stiffness, and damping of other components (except the suspension struts) are fixed throughout all the experiments in this dissertation. The rationale for selecting the suspension parameters is underpinned by the PI model as discussed in Section 4.1.1.

Table 6.5. Inputs for the 3-year old truck experiments.

Experiment No.	Spring (N/m)		Damping (Ns/m)	
	Rear	Front	Rear	Front
1	17,527,388	12,069,976	1,792,775	1,374,910
2	17,548,947	12,084,822	1,786,930	1,370,428
3	17,150,550	11,810,472	1,806,472	1,385,414
4	17,532,647	12,073,597	1,790,624	1,373,260
5	17,162,708	11,818,844	1,792,826	1,374,949
6	17,221,404	11,859,265	1,788,613	1,371,718
7	16,997,526	11,705,094	1,790,759	1,373,364
8	17,206,596	11,849,067	1,826,574	1,400,831
9	17,418,237	11,994,811	1,822,921	1,398,030
10	17,940,784	12,354,655	1,779,171	1,364,477
11	18,120,192	12,478,201	1,814,755	1,391,766
12	17,819,396	12,271,063	1,820,925	1,396,498
13	17,919,185	12,339,781	1,824,567	1,399,291
14	17,883,347	12,315,102	1,724,215	1,322,330
15	17,901,230	12,327,417	1,649,557	1,265,074
16	18,121,415	12,479,044	1,644,608	1,261,278
17	19,975,961	13,756,149	1,593,132	1,221,800
18	20,035,889	13,797,418	1,558,083	1,194,921
19	19,775,422	13,618,051	1,589,245	1,218,819
20	19,524,274	13,445,102	1,586,066	1,216,381

All the following diagrams must be moved and merged into Chapter 7.0. Use only the 5 worst cases and put the rest in the appendix section.

6.4.3. Experimentations for the 5-Year Old CAT793. Similarly, 20 new virtual experimentations were completed for a 5-year old truck. The ageing suspension parameters for the experimentations are selected per Table 6.6. The rationale for selecting the suspension parameters is underpinned by the PI model as discussed in Section 4.1.1.

Table 6.6. Inputs for the 5-year old truck experiments.

Experiment No.	Spring (N/m)		Damping (Ns/m)	
	Rear	Front	Rear	Front
1	15,751,876	10,847,296	1,882,227	1,443,512
2	15,720,372	10,825,602	1,904,813	1,460,834
3	15,500,287	10,674,043	1,948,624	1,494,433
4	16,166,799	11,133,027	1,989,545	1,525,817
5	15,811,130	10,888,100	1,983,577	1,521,239
6	16,337,641	11,250,674	2,025,232	1,553,185
7	15,811,568	10,888,402	2,067,762	1,585,802
8	15,258,164	10,507,308	2,315,893	1,776,098
9	15,917,316	10,961,224	2,321,219	1,780,183
10	15,053,006	10,366,030	2,169,180	1,663,581
11	14,646,575	10,086,147	2,162,672	1,658,591
12	14,939,506	10,287,870	2,208,088	1,693,421
13	15,283,115	10,524,491	2,181,591	1,673,100
14	15,471,709	10,654,363	2,086,474	1,600,153
15	15,630,015	10,763,378	1,926,785	1,477,685
16	16,130,176	11,107,806	1,864,165	1,429,660
17	15,388,188	10,596,847	1,747,729	1,340,364
18	16,049,880	11,052,512	1,803,657	1,383,255
19	15,302,758	10,538,017	1,861,374	1,427,520
20	14,637,700	10,080,035	1,941,413	1,488,903

6.4.4. Experimentations for the 7-Year Old CAT793. Similarly, 20 new virtual experimentations were completed for a 7-year old truck. The ageing suspension parameters for the experimentations are selected per Table 6.7. The rationale for selecting the suspension parameters is underpinned by the PI model as discussed in Section 4.1.1.

Table 6.7. Inputs for the 7-year old truck experiments.

Experiment No.	Spring (N/m)		Damping (Ns/m)	
	Rear	Front	Rear	Front
1	13,140,924	9,049,303	2,056,039	1,576,812
2	13,114,642	9,031,204	2,080,711	1,595,734
3	12,931,037	8,904,767	2,128,568	1,632,435
4	13,370,692	9,287,672	2,154,111	1,666,717
5	13,076,537	9,083,343	2,147,648	1,661,716
6	13,511,986	9,385,819	2,192,749	1,696,613
7	13,076,900	9,083,595	2,238,797	1,732,241
8	12,619,208	8,765,669	2,507,452	1,940,110
9	13,164,358	9,144,346	2,513,219	1,944,573
10	12,449,533	8,647,808	2,348,603	1,817,203
11	12,113,396	8,414,318	2,341,558	1,811,751
12	12,355,664	8,565,775	2,390,730	1,849,798
13	12,639,844	8,762,788	2,362,042	1,827,601
14	12,795,820	8,870,921	2,259,057	1,747,917
15	12,926,747	8,961,688	2,086,160	1,614,140
16	13,340,403	9,248,462	2,018,360	1,561,681
17	12,726,744	8,823,033	1,892,293	1,464,138
18	13,273,994	9,202,423	1,952,846	1,510,991
19	12,656,090	8,774,050	2,015,337	1,559,342
20	12,106,056	8,392,730	2,101,997	1,626,394

6.4.5. Impact of Major Overhauls and Rebuilds after 7 Years. As discussed in Section 6.4.3, after 7 years of operations (about 35,000 hours) the vertical and horizontal accelerations increase by 29% and 30%, respectively, from a brand-new suspension under HISLO. The ameliorating effects of the regular scheduled and corrective maintenance in temporarily improving the WBVs are manifested in Figure 6.4. However, these effects are temporary and although they decrease the rate of RMS curve (see the fluctuations in the curve), they cannot

prevent the increasing trend in the RMS curve in Figure 6.4. Therefore after 7 years the suspensions struts should be either rebuilt or replaced thoroughly to bring the RMS accelerations to the safe (acceptable) regions.

6.5. LIMITATIONS

The major limitations of the virtual experimentations include:

(i) Uncertainty in input parameters of the virtual model, which are due to data unavailability. There is no published data for the stiffness and damping coefficients for the CAT 793D. These coefficients were approximated based on the literature (Trangsrud, et al., 2004).

(ii) The computation times are considerable for sophisticated and detailed models

(iii) Since the suspension parameters are approximated from the literature the simulation results in ADAMS/Post Processor may not be a reasonable approximate of the real world measurements under the same conditions, which were not available to this study.

6.6. SUMMARY

In Sections 6.1-6-5, using the mathematical ageing model created in Sections 4.1-4.2 and the numerical example provided in Sections 5.1-5.2, appropriate virtual experiments were designed. These experiments were examined in the case of a virtual model of a CAT 793D dump truck in the MSC ADAMS environment. The objective was to illustrate the impact of ageing in the WBV levels and exposures. Initially, 600 virtual experiments were completed in ADAMS/View, and were post processed in ADAMS/ Post Processor. Consequently, the impact of age and HISLO conditions on WBV levels and exposures was outlined. Consequently, appropriate virtual experimentations were designed and carried out in order to capture the WBV levels at different truck ages (i.e., 3, 5, and 7 years). Further, the major limitations of the virtual experimentations were identified as (i) input uncertainty, (ii) long computation/simulation times, and (iii) lack of real measurements for assessing the simulations outputs.

7. ANALYSIS AND DISCUSSION OF RESULTS

This section focuses on analysis and discussions of the results from the experiments conducted in Section 64. The developed mathematical model for the temporal effectiveness of suspension performance in Sections 4.1-4.2 (with the numerical example in Section 5.2) was linked to WBVs for a virtual CAT793D in Section 6.1. In this chapter, the data obtained through the virtual experimentations is processed into useful information for estimating the WBVs with truck ageing. The results have been used to formulate and implement appropriate strategies to prevent WBVs levels from exceeding pre-specified levels. These strategies are in the form of (i) modifying current scheduled maintenance/repair of hydro-pneumatic suspension struts, (ii) enhancing condition based maintenance/repair using sophisticated sensor technologies to be able to gain real time data in the form of deterioration (ageing) symptoms (e.g., vibration, noise, oil quality, etc., measurements), (iii) scheduling appropriate suspension re-build and replacement schedules, when the two previous counteractions are not sufficient to prevent WBVs from exceeding the recommended safe levels.

7.1. SIMULATION RESULTS

The developed mathematical model for the temporal effectiveness of suspension performance in Sections 4.1-4.2 (with numerical example in Section 5.2) was linked to WBVs for a virtual CAT793D in Section 6.1. Subsequently, 600 virtual experiments were conducted in MSC ADAMS, with the objective of investigating the effect of deteriorating suspension parameters (i.e., the damping coefficient and stiffness rate of a virtual CAT 793 D) in operator exposure to WBV levels under HISLO conditions. The mathematical ageing model in Section 4.1 (validated with the numerical example in Section 5.1) was used as the basis for identifying the properties of ageing suspension struts with time. These parameters were used as inputs in the virtual experiments conducted in Section 6.4.

The virtual simulation results in MSC ADAMS include displacements, velocities, and accelerations of the center of mass of different rigid bodies in the truck model. They also include the relative motion of the truck components with respect to each other due to the impulse force (Aouad, 2008). The objective of these experimentations was to investigate the effect of time-deterioration spring-damper parameters in the truck operator perceived WBVs in HISLO. This is identified by the acceleration peaks and their corresponding durations. The available 38-DOF CAT 793D model allows for the inspection of the acceleration fields for the center of mass of the operator seat. The seat is selected as a reference point, because it is in direct and immediate contact with the operator body. Therefore, the magnitudes of the displacements, velocities, and accelerations at seat are experienced by the operator directly.

The operator's head, lumbar region, and legs could also be used as reference points for obtaining the accelerations. However, the parameters of the operator's virtual model (i.e., damping and stiffness of different human body parts) in the available CAT 793D prototype are not obtained from actual measurements. Therefore the displacements, velocities, and accelerations of different human parts (in particular head) are not realistic See Figure 7.1 for a snapshot of the model in simulation (animation) which illustrates the unrealistic position of the operator head and lumbar region under HISLO. The vertical (y-direction) RMS acceleration diagram of the operator's head is illustrated in Figure 7.2. The results show a 4.02 m/s^2 vertical acceleration for the head. The magnitude of this value at the head and neck region is well beyond the real situation, which could be endured by human body. Therefore the center of mass of the seat was set as the reference point for post processing the results.

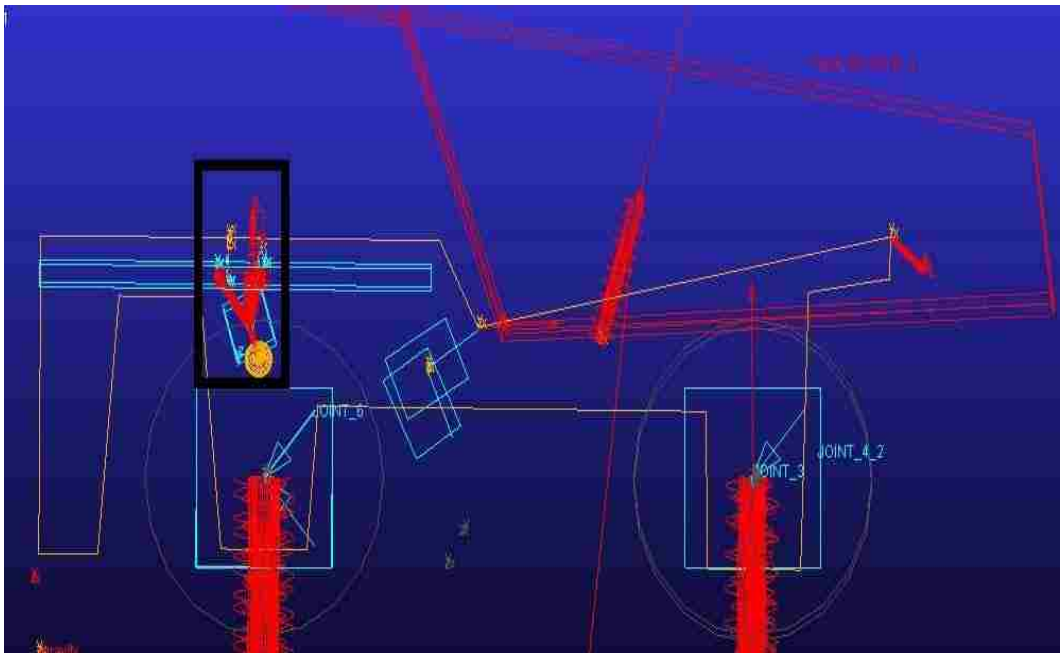

Figure 7.1. A snapshot of the virtual model in animation, depicting the position of the operator body under HISLO.

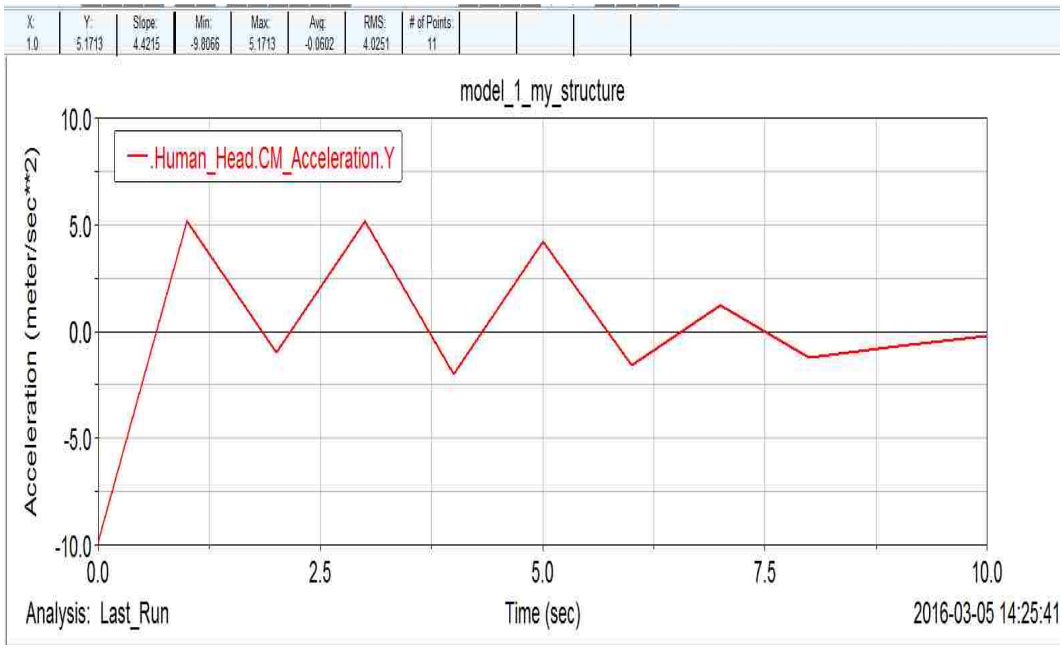

Figure 7.2. Acceleration of operator head under HISLO in the vertical direction.

The vertical acceleration is the major component of the acceleration field; hence the highest RMS value compared to x- and z- RMS accelerations. Expectedly, this is due to fact that the impulse force is downward. Figure 7.3 illustrates the vertical acceleration of the operator seat (center of mass) in the vertical direction. This vertical acceleration has a 3.56 m/s^2 RMS value of for the first 7 seconds after inserting the impulse force due to dumping materials by a shovel.

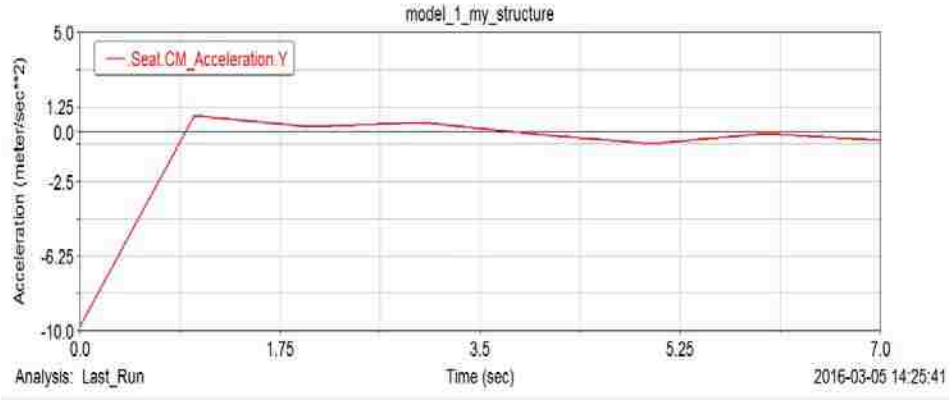

Figure 7.3. Acceleration of the center of mass of the seat under HISLO in the vertical direction.

Figure 7.4 illustrates the RMS acceleration (over ten seconds after the first pass of impulse force) in the x- (horizontal) direction, with an RMS value of 0.304 m/s^2, which is well below the RMS value for the vertical accelerations as well as the ISO recommended dose for WBV exposures relating to an operator's health and comfort.

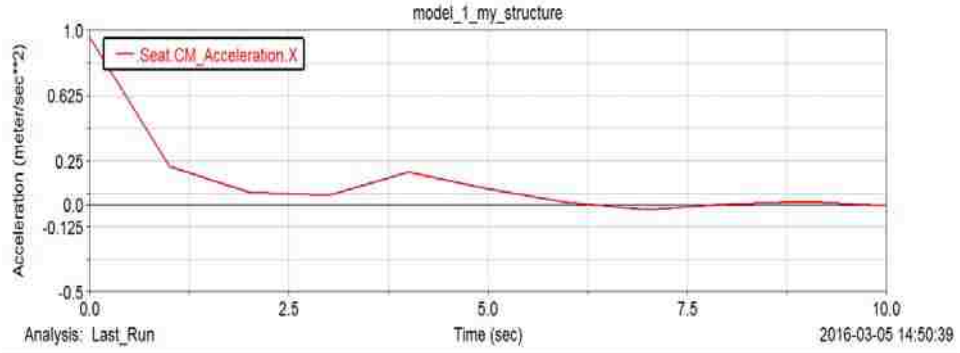

Figure 7.4. Acceleration of the center of mass of the seat under HISLO in the x-direction (horizontal).

7.1.1. Displacements, Velocities, and Accelerations. As discussed in Section 7.1., the center of mass of the seat is set as the reference point for measuring all displacements, velocities, and accelerations. Figure 7.5 illustrates the displacements of the center of mass of the seat for the period 10 seconds after the first pass of the impulse force in vertical direction. The RMS accelerations are different for different time periods after the impulse force. The RMS values decrease with increasing the time period. Therefore the highest RMS values will be due to the operator's exposures to WBVs in the first few seconds after the impulse force. In this dissertation, the RMS values for the first 10 seconds of impulse force have been considered thoroughly for the consistency purposes.

Similarly, Figure 7.6 illustrates the velocity profile of the center of mass of the seat for the period 10 seconds after the first pass of the impulse force in the vertical direction. Figure 7.6 shows the minimum, maximum, and RMS velocity values of 0.064 m/s, 0.2 m/s, and 0.067 m/s in the vertical direction.

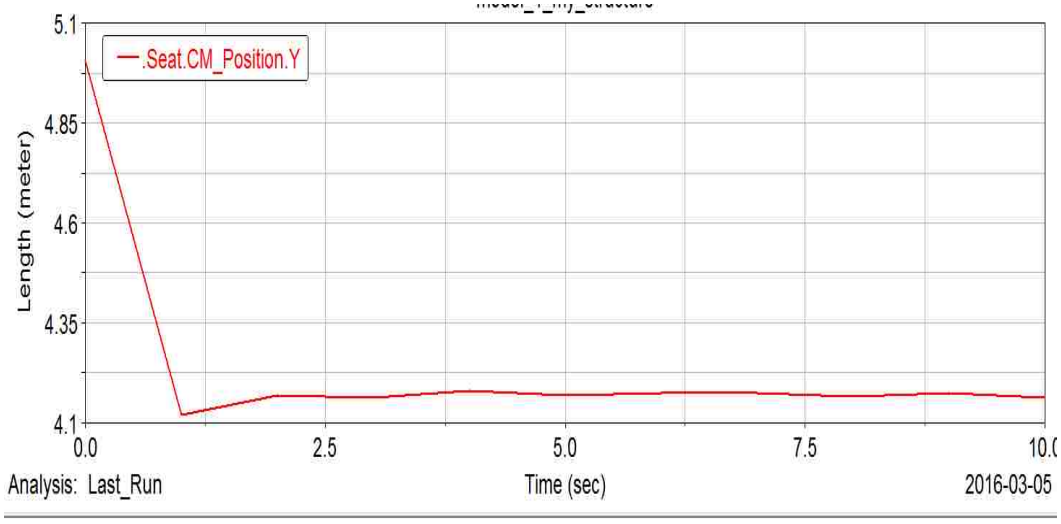

Figure 7.5. Displacement of the center of mass of the seat under HISLO in the vertical direction.

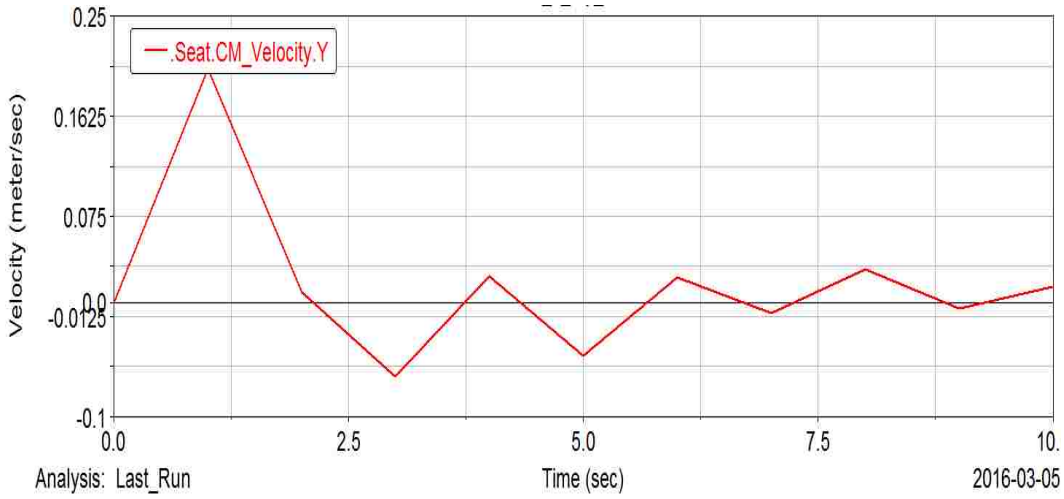

Figure 7.6. Displacement of the center of mass of the seat under HISLO in the vertical direction.

7.1.2. Vertical Acceleration of the Seat. Figure 6.4 illustrates the increasing trend in WBVs for the first 600 hours. However, for the full-life suspension ageing modeling, the MSC ADAMS model should be executed several thousand times. Each model execution corresponds to a new set of both the rear and front suspension configurations. Thus it will be very cumbersome to examine the proposed model for the whole life of a typical truck. Because, as discussed in Chapter 6, for a full-life simulation, 34,650 experimentations should be completed in the ADAMS model. Each experimentation takes approximately 5 minutes for performing the main steps of input adjustment, simulation running, and result interpretations. All the steps are performed by hand, which need a total of 2,888 man-hour of working. To address this difficulty the data obtained for the first 600 working hours were used to extrapolate the RMS values until 35,000 hours as illustrated in Figure 7.7.

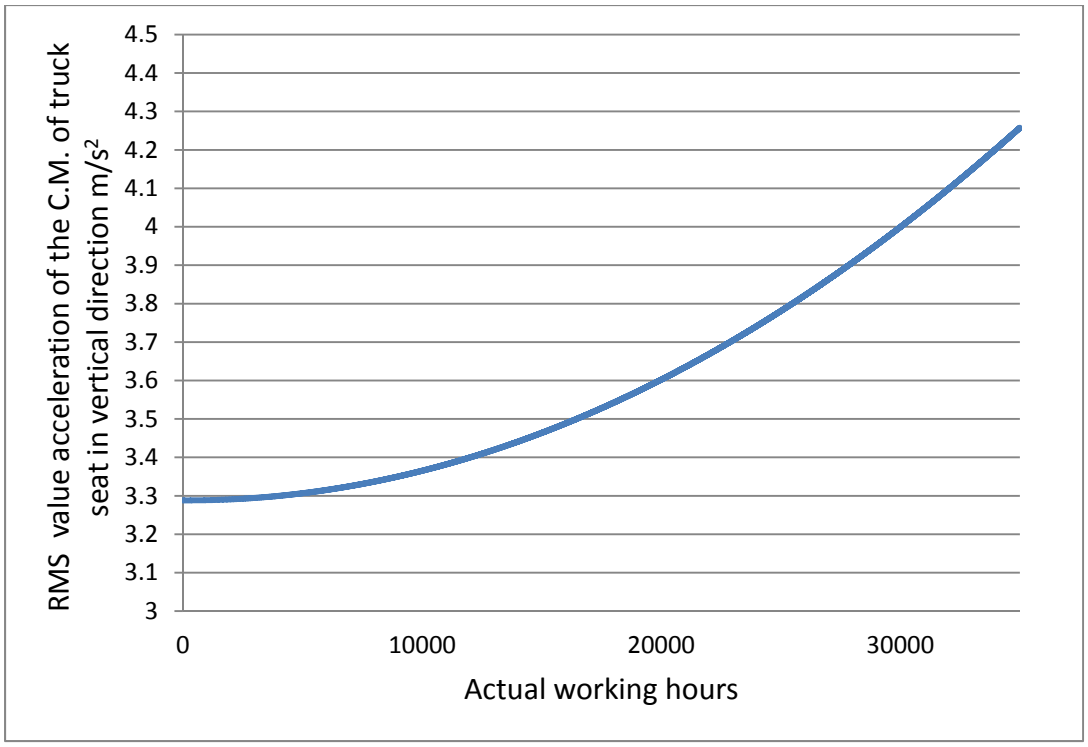

Figure 7.7. WBVs in terms of seat RMS values for a typical ageing suspension strut in a CAT793D for 7 years (35000 working hours).

Figure 7.7 shows that the RMS accelerations increase from a 3.29 m/s^2 nominal value for the two pairs of brand-new CAT793D rear and front suspension struts to 4.2575 m/s^2 after 35,000 hours (nearly 7 years) of continuous operations. Therefore, using Figure 7.7, appropriate interventions in the form of preventive, condition-based maintenance, suspension overhaul and replacement should be scheduled to prevent the WBVs from exceeding pre-specified thresholds.

7.2. EXPERIMENTATIONS RESULTS

7.2.1. The Five Worst Accelerations for the 3-Year Old Truck. Figures 7.8-7.12 illustrate the ADAMS/Post Processor results for the 5 worst accelerations that were obtained in the experiments in the case of a 3-year old truck. The results of the remaining 15 experiments are presented in the Appendix.

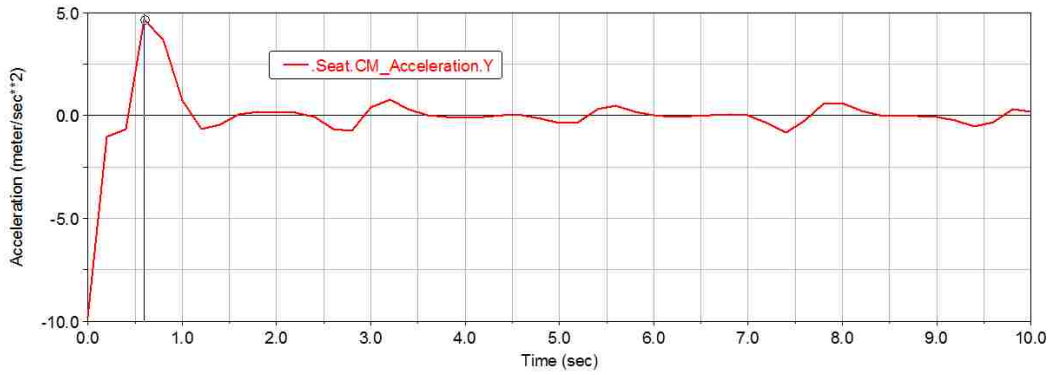

Figure 7.8. The RMS values of vertical accelerations for experiment No. 9 in Table 6.5 (3-year old truck).

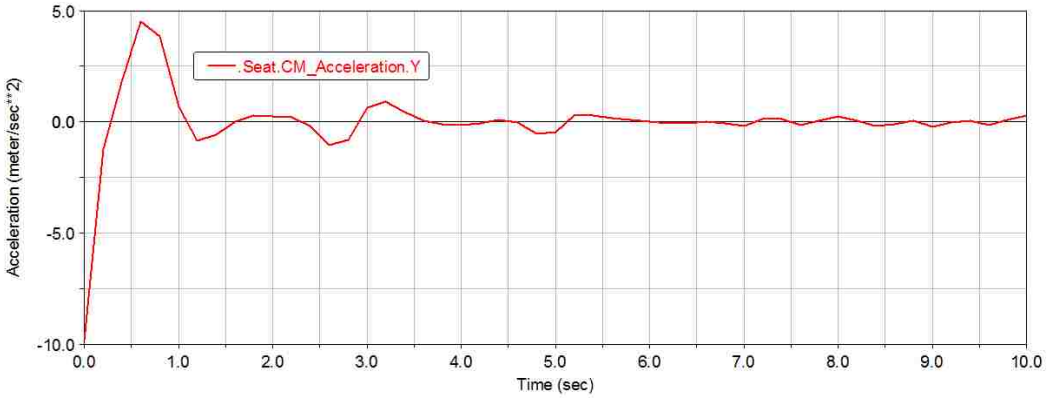

Figure 7.9. The RMS values of vertical accelerations for experiment No. 12 in Table 6.5 (3-year old truck).

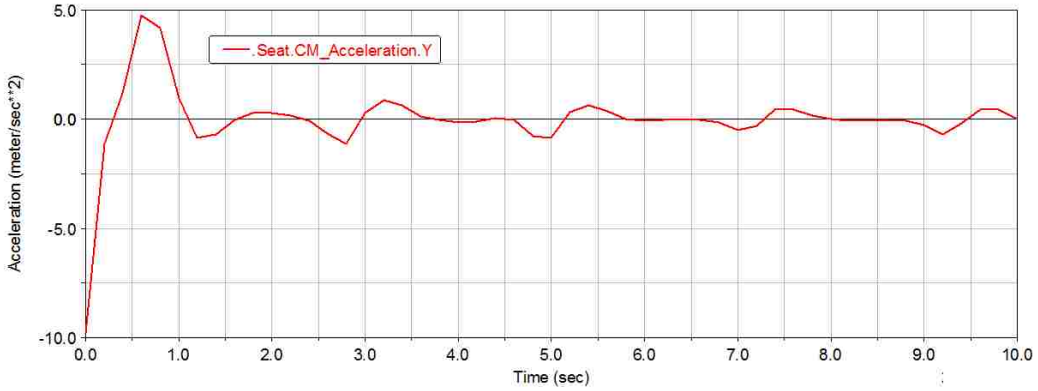

Figure 7.10. The RMS values of vertical accelerations for experiment No. 13 in Table 6.5 (3-year old truck).

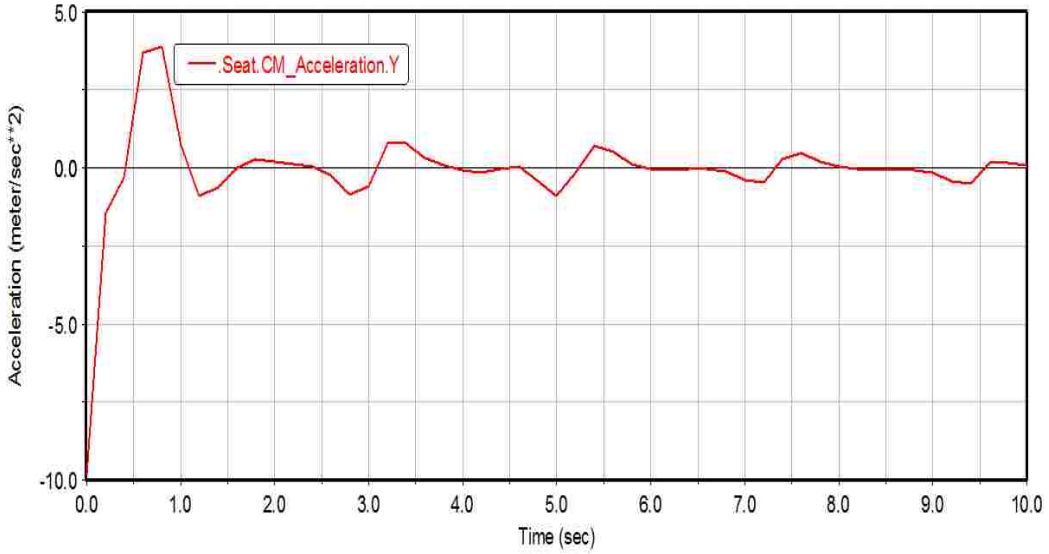

Figure 7.11. The RMS values of vertical accelerations for experiment No. 18 in Table 6.5 (3-year old truck).

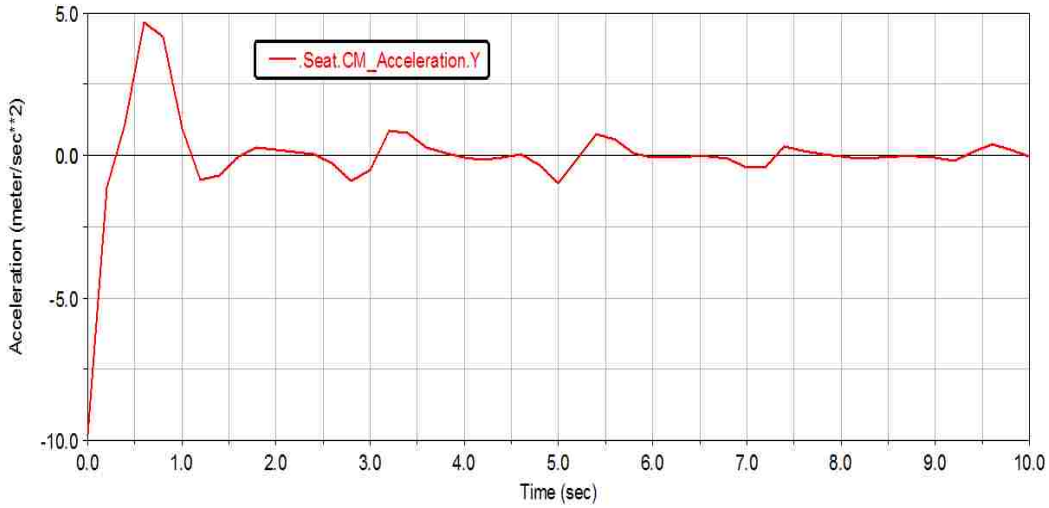

Figure 7.12. The RMS values of vertical accelerations for experiment No. 20 in Table 6.5 (3-year old truck).

The calculated RMS values for the above 20 experiments are summarized in Table 7.1.

Table 7.1. ADAMS/Post Processor results for 20 virtual experiments for a 3-year old truck.

Experiment No.	RMS acceleration values (m/s^2)	
	Vertical direction	Horizontal x-direction
1	3.4586	0.3180
2	3.4571	0.3176
3	3.4613	0.3204
4	3.4580	0.3176
5	3.4627	0.3302
6	3.4527	0.3015
7	3.4593	0.3023
8	3.4615	0.3213
9	3.4731	0.3278
10	3.4602	0.3215
11	3.4698	0.3249
12	3.4719	0.3426
13	3.4743	0.3431
14	3.4566	0.3168
15	3.4555	0.3154
16	3.4546	0.3148
17	3.4578	0.3173
18	3.4703	0.3452
19	3.4676	0.3321
20	3.4751	0.3428

Therefore, a 3-year old truck exposes the operator to a maximum RMS value of 3.4751 m/s^2 in the vertical direction under the HISLO operations, which is 5.6% higher than a brand-new truck. Furthermore, the maximum RMS value for the 20 experiments in the horizontal direction is equivalent to 0.3452 m/s^2, which is 13.2 % higher than the nominal 0.3041 m/s^2 value that is obtained in the x-direction.

7.2.2. The Five Worst Accelerations for the 5-Year Old Truck. Figures 7.13-7.17 illustrate the ADAMS/Post Processor results for the 5 worst accelerations that were obtained in the experiments in the case of a 5-year old truck. The results of the remaining 15 experiments are presented in the Appendix.

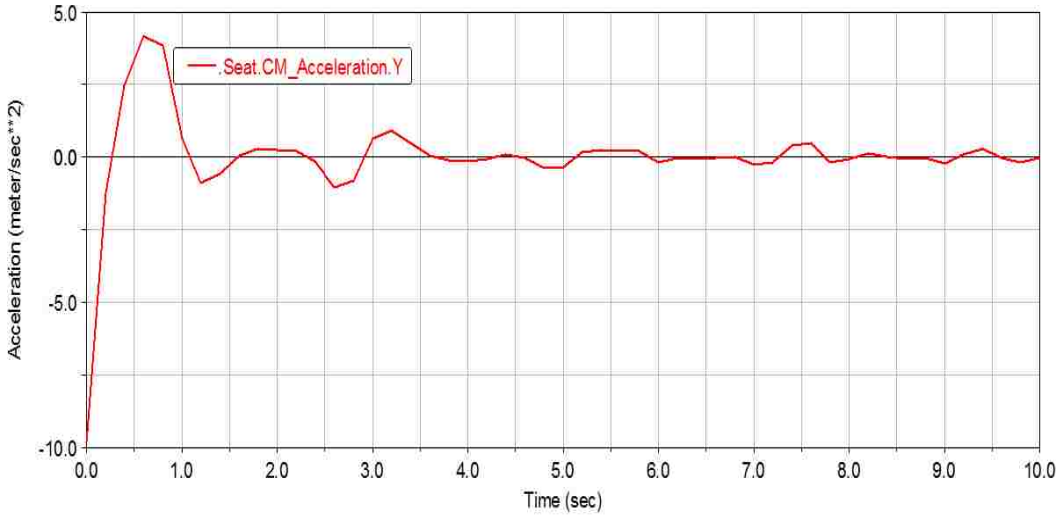

Figure 7.13. The RMS values of vertical accelerations for experiment No. 1 in Table 6.6 (5-year old truck).

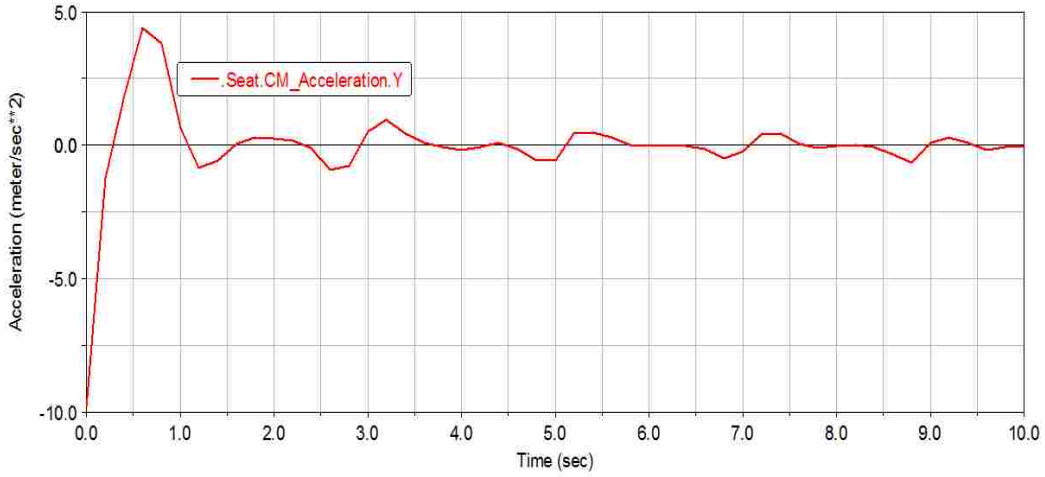

Figure 7.14. The RMS values of vertical accelerations for experiment No. 11 in Table 6.6 (5-year old truck).

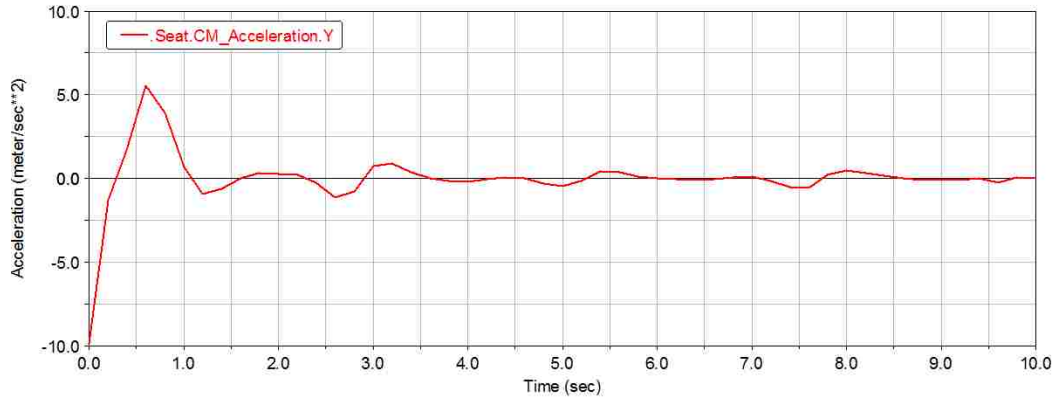

Figure 7.15. The RMS values of vertical accelerations for experiment No. 12 in Table 6.6 (5-year old truck).

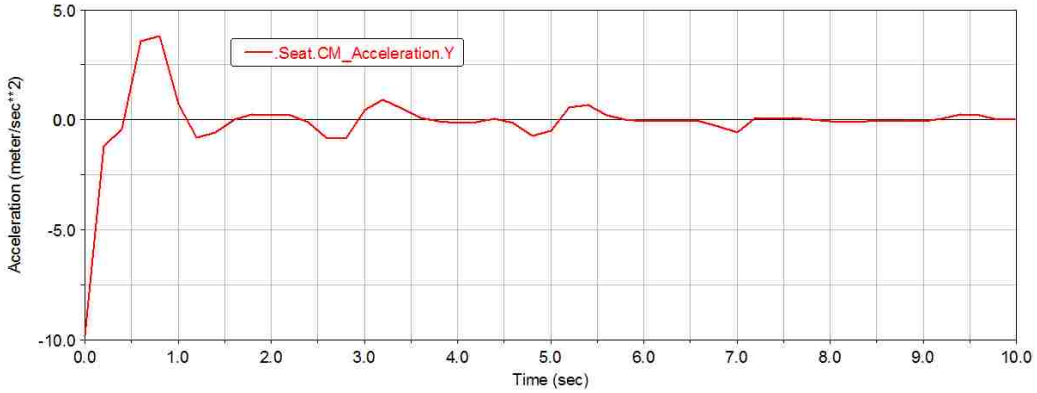

Figure 7.16. The RMS values of vertical accelerations for experiment No. 14 in Table 6.6 (5-year old truck).

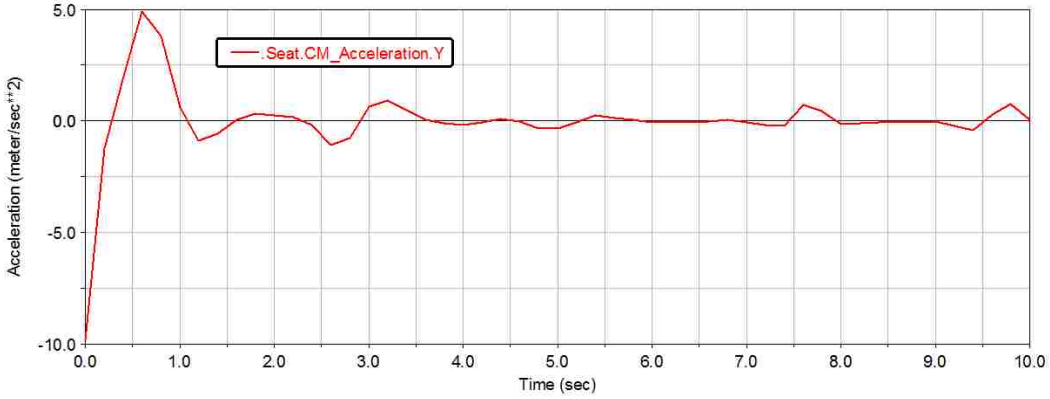

Figure 7.17. The RMS values of vertical accelerations for experiment No. 20 in Table 6.6 (5-year old truck).

The vibration analysis results are summarized in Table 7.2.

Table 7.2 ADAMS/Post Processor results for 20 virtual experiments for a 5-year old truck.

Experiment No.	RMS Values of accelerations (m/s^2)	
	Vertical direction	Horizontal x-direction
1	3.7643	0.3488
2	3.7773	0.3503
3	3.7903	0.3511
4	3.7905	0.3510
5	3.7747	0.3493
6	3.7866	0.3510
7	3.7670	0.3494
8	3.7809	0.3498
9	3.7676	0.3495
10	3.7893	0.3475
11	3.7581	0.3491
12	3.7567	0.3497
13	3.7757	0.3504
14	3.7637	0.3501
15	3.7829	0.3519
16	3.7769	0.3515
17	3.7669	0.3504
18	3.7910	0.3508
19	3.7733	0.3494
20	3.7869	0.3508

Therefore, a 5-year old truck exposes the operator to the maximum RMS value of 3.7910 m/s^2 in the vertical direction under the HISLO operations, which is 15.2% higher than a brand-new truck. Furthermore, the maximum RMS value for the 20 experiments in the horizontal direction is equivalent to 0.3519 m/s^2, which is 15.7 % higher than the nominal 0.3041 m/s^2 value the is obtained in the x-direction.

7.2.3. The Five Worst Accelerations for the 7-Year Old Truck. Figures 7.18-7.22 illustrate the ADAMS/Post Processor results for the 5 worst accelerations that were obtained in

the experiments in the case of a 7-year old truck. The results of the remaining 15 experiments are presented in the Appendix.

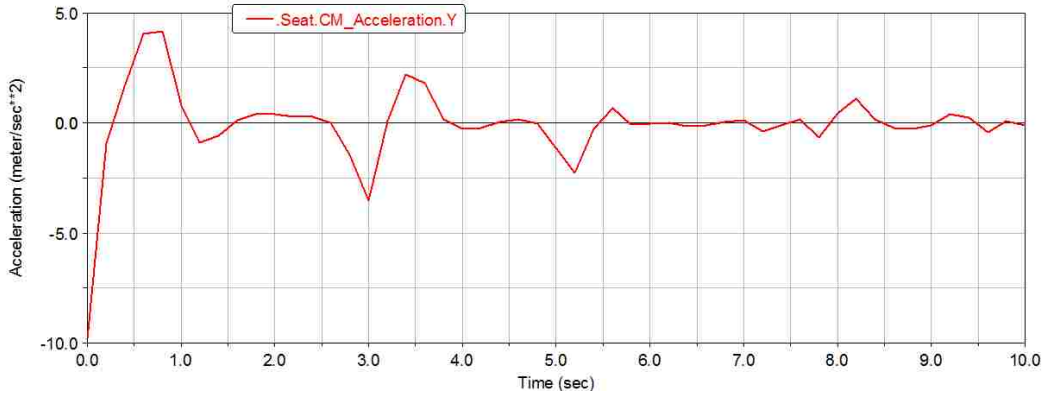

Figure 7.18. The RMS values of vertical accelerations for experiment No. 1 in Table 6.7 (7-year old truck).

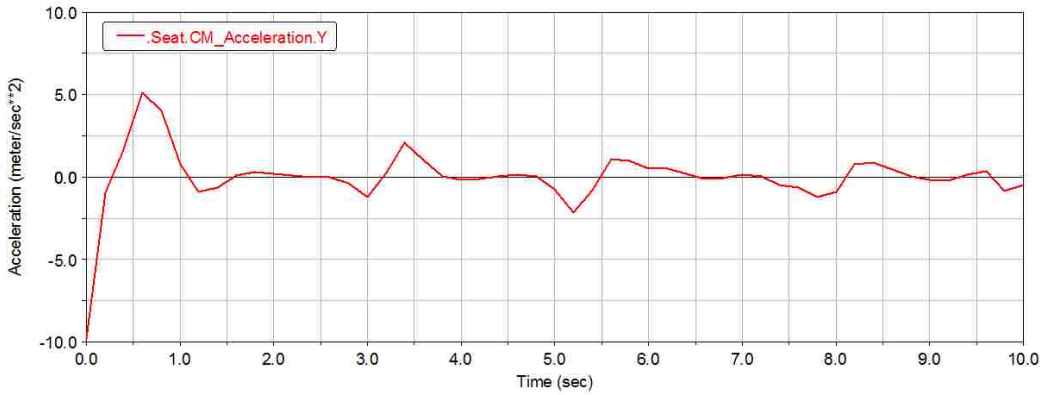

Figure 7.19. The RMS values of vertical accelerations for experiment No. 3 in Table 6.7 (7-year old truck).

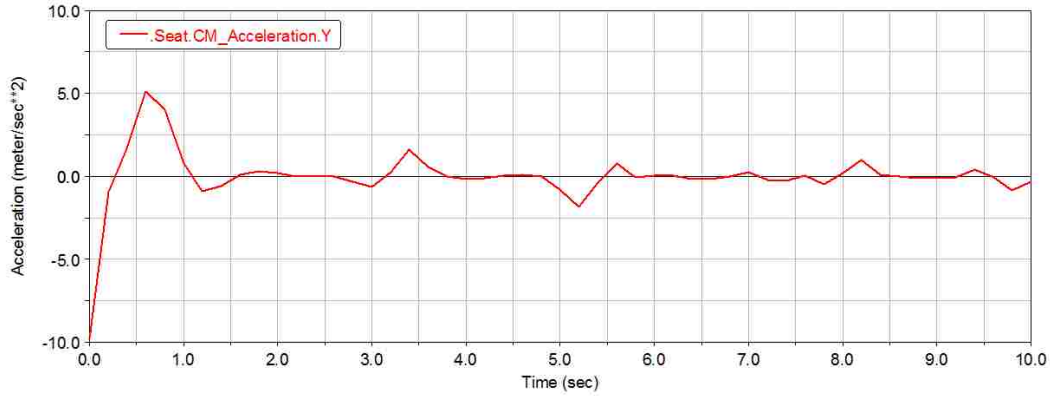

Figure 7.20. The RMS values of vertical accelerations for experiment No. 13 in Table 6.7 (7-year old truck).

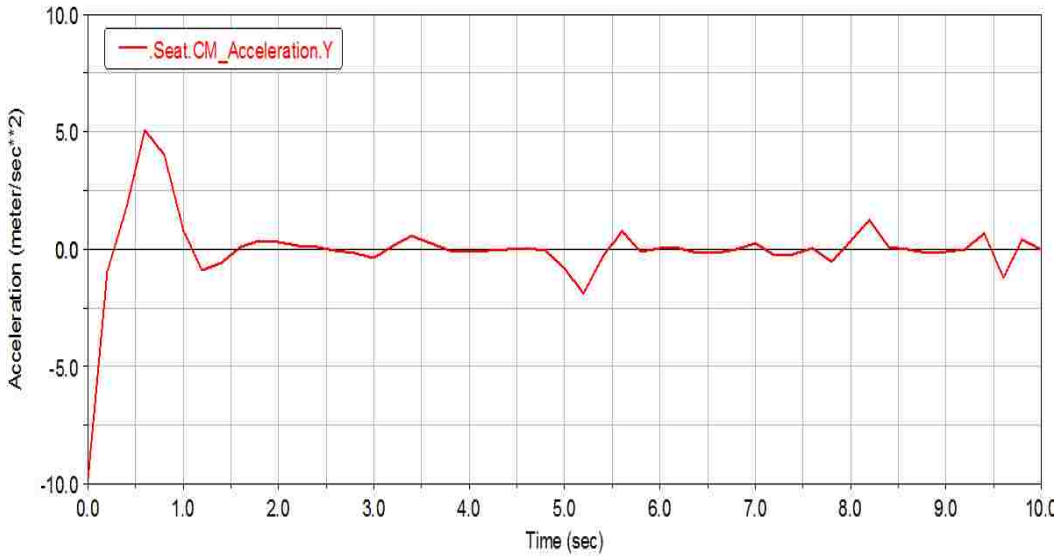

Figure 7.21. The RMS values of vertical accelerations for experiment No. 17 in Table 6.7 (7-year old truck).

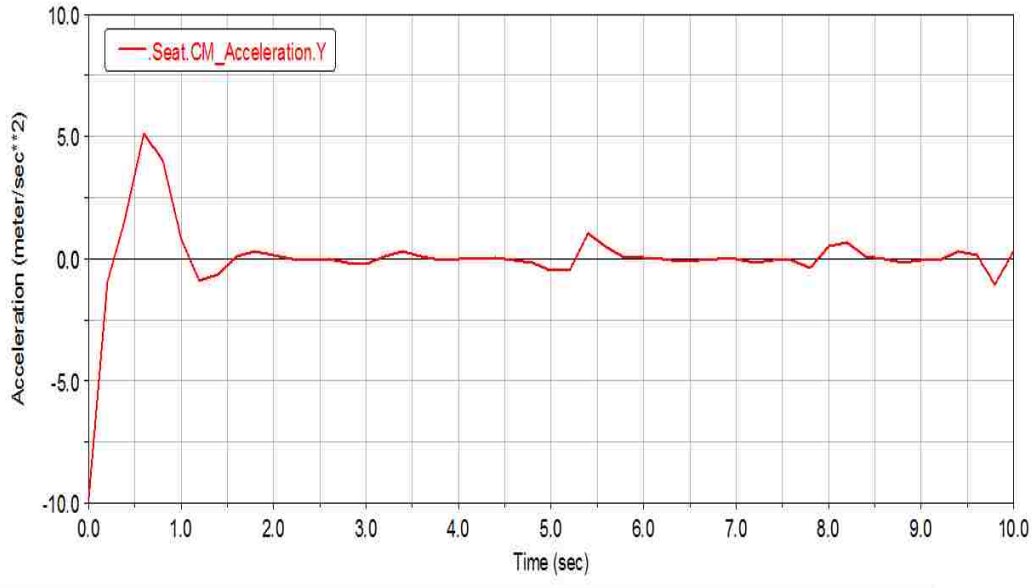

Figure 7.22. The RMS values of vertical accelerations for experiment No. 20 in Table 6.7 (7-year old truck).

The results are summarized in Table 7.3.

Table 7.3.ADAMS/Post Processor results for 20 virtual experiments for a 7-year old truck.

Experiment No.	RMS Values of accelerations (m/s^2)	
	Vertical direction	Horizontal x-direction
1	4.2423	0.3963
2	4.2365	0.3967
3	4.2373	0.3966
4	4.2240	0.3945
5	4.2309	0.3964
6	4.2166	0.3898
7	4.2367	0.4024
8	4.2289	0.3964
9	4.2094	0.3959
10	4.2158	0.3980
11	4.2331	0.3997
12	4.2351	0.4054
13	4.2535	0.4125
14	4.2174	0.3934
15	4.2272	0.3059
16	4.2187	0.3976
17	4.2453	0.4006
18	4.2368	0.3985
19	4.2226	0.3960
20	4.2533	0.4146

Therefore, a 7-year old truck exposes the operator to the maximum RMS value of 4.22535 m/s^2 in the vertical direction under the HISLO operations, which is 29.2% higher than a brand-new truck. Furthermore, the maximum RMS value for the 20 experiments in the horizontal direction is equivalent to 0.4146 m/s^2, which is 36.4 % higher than the nominal 0.3041 m/s^2 value the is obtained in the x-direction.

7.2.4. Comparing the RMS Accelerations. In this section the obtained RMS values from the experiments in the sections 6.4.1-6.4.3 are compared with nominal RMS accelerations in Figures 7.23-7.26.

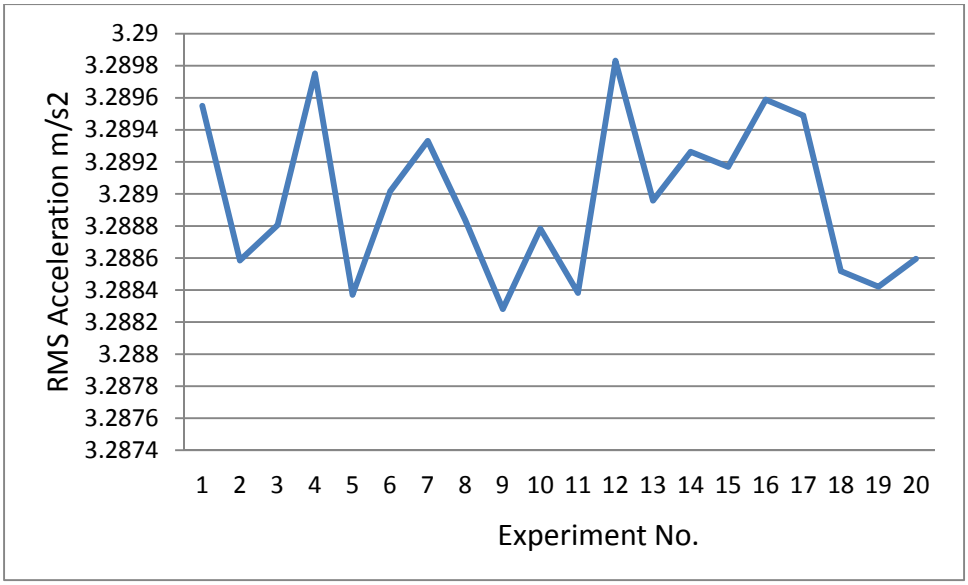

Figure 7.23. The vertical RMS accelerations for brand-new suspensions.

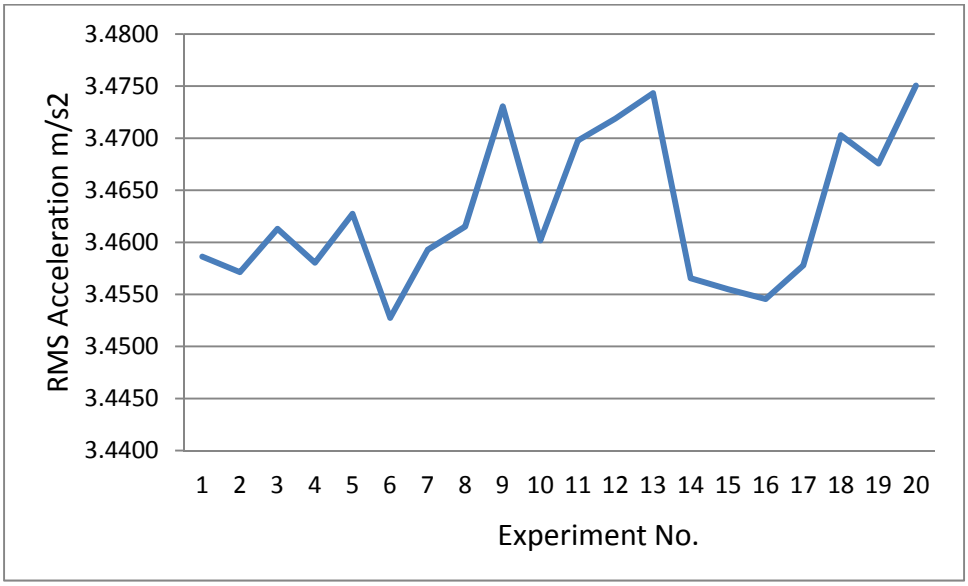

Figure 7.24. The vertical RMS accelerations for 3-year old suspensions.

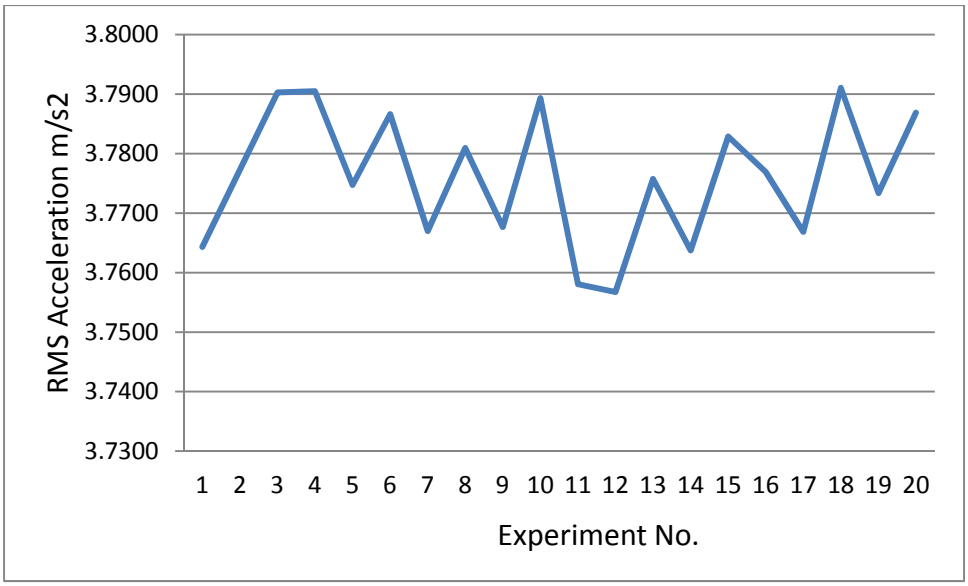

Figure 7.25. The vertical RMS accelerations for 5-year old suspensions.

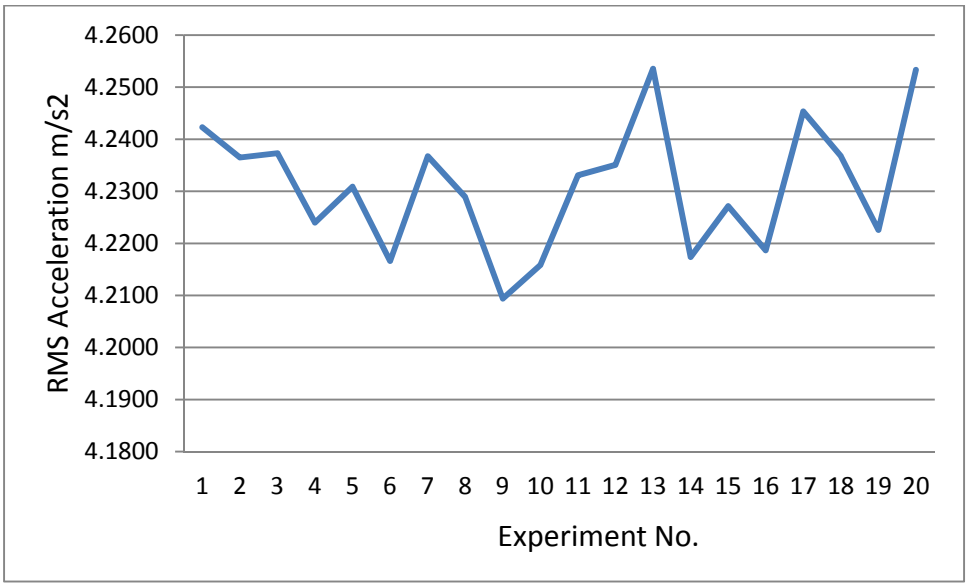

Figure 7.26. The vertical RMS accelerations for 7-year old suspensions.

Furthermore, the five worst charts (the highest accelerations) from each of the 20 experiments for truck ages 3, 5, and 7 years are compared with the nominal brand-new results in Figures 7.27 to 7.29, respectively.

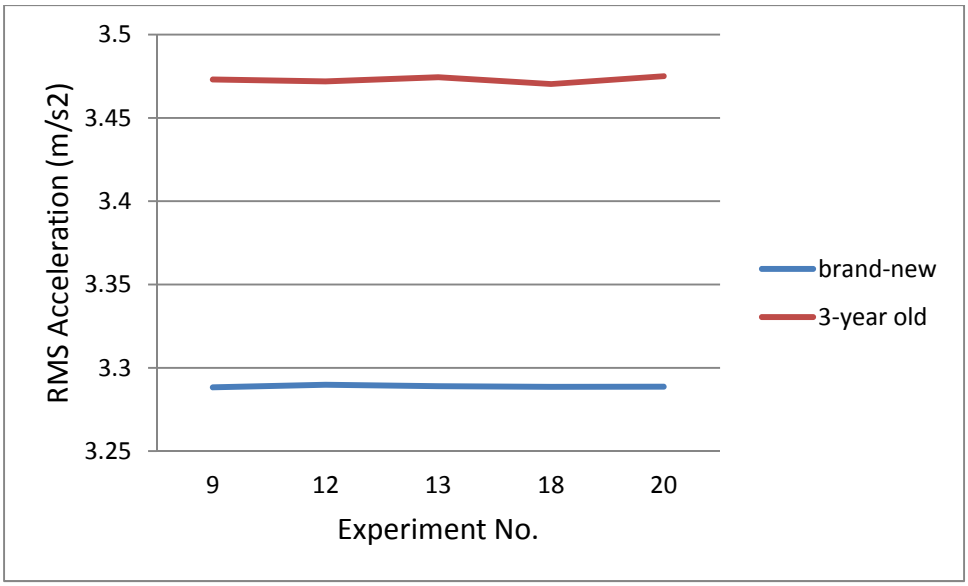

Figure 7.27. Comparison of the vertical (y-direction) RMS accelerations for the five worst accelerations with the nominal values for the 3-year old truck.

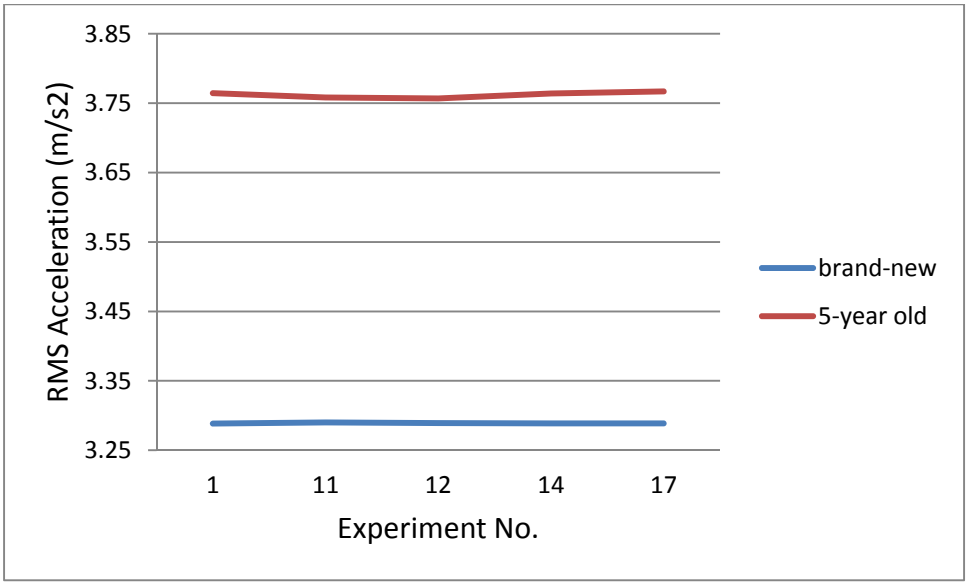

Figure 7.28. Comparison of the vertical (y-direction) RMS accelerations for the five worst accelerations with the nominal values for the 5-year old truck.

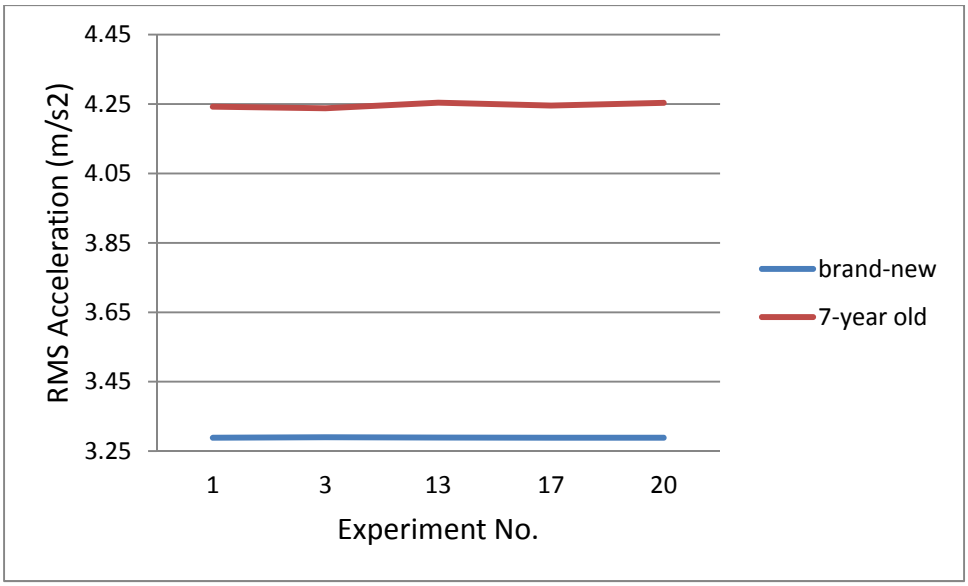

Figure 7.29. Comparison of the vertical (y-direction) RMS accelerations for the five worst accelerations with the nominal values for the 7-year old truck.

7.3. ISO 2631-1 RECOMMENDATIONS FOR EXPOSURE TO WBV

In Sections 7.2, the five worst cases for the 20 experiments in each of the truck age levels were obtained. These results are compared with the ISO 2631-1 WBV exposure limits in the following sections.

ISO 2631-1 acceleration limits comfort zones are summarized in Table 7.4. The RMS values for accelerations that are beyond 2.5 m/s^2 are associated with an extremely uncomfortable condition to the human body under WBVs. This vibration level poses safety and health risks to operators over long-term exposure. Furthermore, operators exposed to WBV with RMS values ≥ 1.0 m/s^2 over 8-hour durations have a high probability of experiencing sacrum, lumbar and cervical problems (ISO, 2004).

Table 7.4. Expected comfort zones to vibrations (ISO 2631-1).

RMS Acceleration (m/s^2)	Comfort Zone
< 0.315	Not uncomfortable
0.315 - .63	A little uncomfortable
0.5 - 1	Fairly uncomfortable
0.8 1.6	Uncomfortable
1.25 - 2.5	Very uncomfortable
> 2.5	Extremely uncomfortable

From Chapter 6, two pairs of a CAT 793 D's rear and front brand-new hydro-pneumatic suspension struts expose the operator to 3.29 m/s^2 and 0.30 m/s^2 RMS accelerations in the vertical and horizontal directions, respectively. Therefore the vertical accelerations are well beyond the very uncomfortable zone according to the ISO 2631-1 limits in Table 7.4. On the other hand, the horizontal accelerations are in the region of not uncomfortable. Therefore, the vertical accelerations in HISLO should be the focus of attention in this area.

However, as discussed in Chapter 6, both the vertical and horizontal accelerations exacerbate with truck ageing. In the following sections, the five worst accelerations in different truck age levels are compared with Table 7.4 to reveal the effect of ageing on WBVs.

7.3.1. The 3-Year Old Suspensions. The five worst vertical accelerations for a 3-year old truck were obtained from experiments No. 9, 12, 13, 18, and 20 with an average RMS value of 3.4729 m/s^2. This acceleration level is 5.6% higher than the bran-new RMS acceleration. Consequently, the already extremely uncomfortable zone for WBVs under HISLO exacerbates even more after 3 years. This increase in WBVs in vertical direction occurs in spite of the ameliorating effects of both the regular scheduled and condition-based maintenance schedules.

In the horizontal direction, the RMS accelerations for the five worst cases reach an average value of 0.3412 m/s^2, which is 12.2 % higher than the average of the brand-new suspensions. Therefore, the comfort zone changes from "not uncomfortable" for a brand-new

truck to “a little uncomfortable” for a 3-year old truck in terms of the operator’s exposure to horizontal accelerations under HISLO conditions.

7.3.2. The 5-Year Old Suspensions. The five worst vertical accelerations for a 5-year old truck were obtained from experiments No. 1, 11, 12, 14, and 20 with an average RMS value of 3.7619 m/s^2. This acceleration level is 14.3% higher than the brand-new RMS acceleration. Consequently, the already extremely uncomfortable zone for WBVs under HISLO exacerbates even more after 5 years. Again, this increase in WBVs in vertical direction occurs in spite of the ameliorating effects of both the regular scheduled and condition-based maintenance schedules.

In the horizontal direction the RMS accelerations for the five worst cases reach an average value of 0.3513 m/s^2, which is 15.4 % higher than the average of the bran-new suspensions. Therefore, the comfort zone changes from “not uncomfortable” for a brand-new truck to “a little uncomfortable” for a 3-year old truck in terms of the operator’s exposure to horizontal accelerations under HISLO conditions.

7.3.3. The 7-Year Old Suspensions. The five worst vertical accelerations for a 5-year old truck were obtained from experiments no. 1, 3, 13, 17, and 20 with an average RMS value of 4.2462 m/s^2. This acceleration level is 29.1% higher than the brand-new RMS acceleration. Consequently, the already extremely uncomfortable zone for WBVs under HISLO exacerbates even more after 7 years. This increase in WBVs in the vertical direction occurs in the spite of the ameliorating effects of both the regular scheduled and condition-based maintenance schedules.

In the horizontal direction, the RMS accelerations for the five worst cases reach an average value of 0.4071 m/s^2, which is 33.9 % higher than the average of the brand-new suspensions. Therefore, the comfort zone changes from “not uncomfortable” for a brand-new truck to “a little uncomfortable” for a 7-year old truck in terms of the operator’s exposure to horizontal accelerations under HISLO conditions.

7.4. IMPORTANCE OF RESULTS

The results obtained in this section have a significant impact on truck suspensions, in the form of design, application, and maintenance. These results are useful to enhance the suspension efficiency and useful life, as well as improving operator's health with respect to harmful effects of prolonged exposures to excessive WBVs, which is a direct result of the under-optimal shock wave attenuation capabilities of ageing hydro-pneumatic suspensions (sentence too long; break and simplify it). Therefore, the results are critical to generate an optimized plan for inspecting, maintaining, and repairing ageing suspension struts in large mining dump trucks in typical surface mining operations.

7.4.1. Impact of Results on Suspension Design. The results of simulating the mathematical ageing model showed clearly that the effectiveness of typical hydro-pneumatic suspension struts in large surface mining trucks deteriorates with time. This deterioration in suspension performance is a direct effect of sub-system (mainly the air spring and oil damper sub-systems) ageing with time. Furthermore, inefficient suspensions introduce all other truck components to excessive levels of shock waves and vibrations due to HISLO, as well as normal truck operations. These vibrations can reduce the effective useful lives of other components due to fatigue (repeated loading and unloading cycles).

7.4.2 Impact of Results on Truck Operator's Health and Safety. The current state-of-the-art technology in suspension struts does not meet the ISO requirements for operator's WBVs exposure under HISLO conditions. A 3.56 m/s^2 vertical acceleration at the seat has severe detrimental effects on operator's health, in the long run. It should be noted again that this level of high WBVs occurs even when the suspension parameters are set to the manufacturers' nominal values for brand-new suspension struts. As demonstrated earlier in this chapter, these detrimental WBVs can increase to more extreme levels (i.e., RMS vertical accelerations of > 4 m/s^2) as a result of ageing, even when the suspensions are regularly inspected, repaired, and maintained. Therefore, in order to improve the operator's health, appropriate strategies and policies should be

formulated and implemented to mitigate the harmful effects of prolonged exposures to WBVs. These strategies can be in the form of improved technologies, efficient maintenance, suspensions rebuilding and replacing and/or reducing the operator's exposure to WBVs by effective counteractions. These are the interesting and important venues for future research studies in this area.

7.5. SUMMARY

The mathematical ageing model set the stage for conducting 600 virtual experimentations in the MSC ADAMS environment. These experiments were conducted to examine the responses of brand-new suspension struts under HISLO. Furthermore, a total of 60 virtual experiments were designed (per the PI model) and carried out (in MSC ADAMS) for different truck ages at 3, 5, and 7 years. The objective was to investigate the effect of ageing suspensions on increasing the WBV levels under HISLO operations. The ageing suspensions have poorer spring-damper parameters than the brand-new ones Therefore, the effects of time-deteriorating suspension parameters on WBVs were examined, that showed the possibility of significant harms to operators under HISLO conditions.

8. SUMMARY, CONCLUSIONS AND RECOMMENDATIONS

In this chapter, firstly a succinct discussion of the previous 7 chapters is summarized. Several conclusions are drawn from each of the 7 previous chapters in section 8.2. The contributions of this PhD dissertation to the body of knowledge in this area are highlighted in section 8.3. Finally, several recommendations for further research in this area are presented, which are based on the limitations of this study.

8.1. SUMMARY

Large scale surface mining operations have deployed large capacity shovels and dump trucks to achieve economic bulk production targets. These large shovels load dump trucks with 100+ tons passes, which cause severe vibrations in the dump trucks. These vibrations are propagated through shockwaves in the truck bodies. A component of the shockwaves generated from these vibrations is propagated into the operator's cabin. The severe magnitudes of the cabin shockwaves expose operators to high levels of whole body vibrations (WBV). Long-term WBV exposures cause musculoskeletal and other diseases of the joints and limbs, and chronic lower back, neck and shoulder pains and injuries [ISO 2631, 1997].

Mining trucks are designed and manufactured with operating lives from 15 to 20 years with effective preventive maintenance (PM) schemes and rebuilds within appropriate time frames. The ability of the suspension mechanism to effectively attenuate the impact of vibrations from HISLO conditions also deteriorates as the truck ages. In cases of poor PM schemes and shovel care practices, the effects can be severely pronounced exposing operators to safety and health risks. Thus, for a sustainable modification of vibration attenuation characteristics of a system, a good knowledge of the time-performance of the suspension system is required for effective PM schemes, replacement of system components and rebuilds.

Research studies on mining truck operators' exposure to WBV have focused on the investigation of dump truck operators' health risks, vibration and suspension system modeling, ergonomic seats, and vibration transmissibility. No fundamental research studies have been carried out on the ageing hydro-pneumatic suspension struts in large mining dump trucks. This study has provided an effort in developing a robust mathematical modeling framework for characterizing the ageing behavior of mining suspensions and their temporal performance. A comprehensive literature survey showed that the suspension performance deteriorates due to effects of two broad categories of continuous-minor-effect and sudden-major-effect processes. The former category encompasses the ageing processes, such as hydraulic oil contamination, oil-nitrogen mixing, and gas accumulator's diaphragm rupture (polymeric deteriorations). The latter category includes discrete shocks, such as the shocks due to HISLO or passing on bumps in haul roads and ramps. Both processes are mathematically modeled to capture the actual underlying physical processes and their effects on suspensions condition.

The effects of these deteriorating processes are compensated for by routine preventive maintenance. Thus, the two major types of maintenance (i.e., scheduled or fixed-interval inspection and maintenance, and condition-based maintenance) were modeled mathematically to capture the ageing process. The proposed mathematical framework was verified and validated using numerical examples. Finally, the ageing model was linked to WBV levels under HISLO in a virtual prototype model for a CAT 793D truck in the MSC ADAMS environment. Several hundred virtual experiments were completed in the ADAMS environment with the objective of determining the effect of suspension ageing in the operator's exposure to WBVs. The experimentations revealed a considerable increase in the RMS accelerations with ageing, which are perceived at the center of mass of the seat in the vertical direction. However, the lateral vibrations were examined to be negligible, which are within the comfort zone of human body in terms of exposure to WBVs. The sections below summarize the detailed procedures used to achieve the objectives of the study.

1. The introduction provides the underlying ageing suspensions problem in large mining dump trucks, as well as, the objectives and scope of the research study. It also outlines the importance of this research and its scientific and industrial contributions.
2. An in-depth literature survey examined the contributions and limitations of previous and current body of knowledge on ageing suspensions. Many researchers have focused on truck operators' health risks, vibration and suspension system modeling, ergonomic seats, and vibration transmissibility. No fundamental research studies have yet been carried out on the ageing hydro-pneumatic suspension struts in large mining dump trucks.
3. The mechanical and thermodynamic operating principles of hydro-pneumatic suspension struts were investigated to estimate the damping ratio and air spring rate and to examine the fundamentals of the underlying mechanics.
4. The PhD research developed the methodology and mathematical modeling scheme of the ageing suspension under different deteriorating phenomenon. Power law functions were used to simulate the ageing effects on suspension performance. Furthermore, preventive maintenance schedules were incorporated in the models for ameliorating the influence of ageing on the shock process.
5. Numerical examples were introduced to examine validity of the proposed models. The model precision was demonstrated through predicting future suspension performance under both ageing and shock phenomena that are typical in surface mining operations.
6. The proposed mathematical model for PI was linked to WBVs for the life of a typical suspension strut in a virtual model of a CAT 793D truck.
7. The effects of suspension ageing in the operator's exposure to WBVs under the HISLO condition were examined for different truck ages.

8.2. CONCLUSIONS

This research study was limited to the study of ageing characteristics of hydro-pneumatic suspension performance in large mining trucks in random fields under HISLO conditions in a typical surface mining environment. However, the theoretical underpinnings of this study can be applied to other mining environments and equipment.

It was revealed that the RMS accelerations increase considerably with truck ageing in the vertical direction. These accelerations reach some extreme values of over 4.0 m/s^2 after 7 years, which makes the HISLO operations extremely detrimental to the operator's health. However, the lateral RMS accelerations remain in the comfort zone for the human body exposure to WBVs. The results of this research will allow the development of a mathematical model that will serve as a guidance to modify the suspension design to manufacture more robust and ageing-resistant suspension struts to absorb the shockwaves beyond the ISO standards and maintain a safe workplace. Hence, the research objectives stated in Section 1.3 have been achieved within the research scope.

From the literature survey the following conclusions can be drawn:

1. The ageing characteristics of hydro-pneumatic suspension struts in large mining trucks have never been studied. This is the first fundamental research study on mining truck suspensions in surface mining operations. This research has created a frontier in the mathematical modeling of ageing behavior of hydro-pneumatic suspensions by modeling both the deteriorating and ameliorating processes that influence the performance of suspension struts in large mining trucks in surface mining operations.
2. This research endeavor provides contributions and understanding into the body of knowledge of dump truck suspension mechanisms. Therefore, the temporal behavior of suspensions and their deteriorating performance in attenuating shockwaves and vibrations in time will be a significant asset to truck manufacturers, as well as mining companies and safety personnel.

From the mechanics and thermodynamic analysis of hydro-pneumatic suspensions, the following conclusions can be drawn:

1. There are two other systems that compete with hydro-pneumatics in the area of suspension systems: the pneumatic and the mechanical suspension. However, the dominant mechanism in today's mining technology is a hydro-pneumatic type. In conventional mechanical springs, the spring rate is constant throughout the whole suspension stroke. In contrast, in both the gas springs and hydro-pneumatic suspensions, the forces versus displacement curves are progressive, which is caused by the physical laws for a poly-tropic change of state of a gaseous medium. In particular, the hydraulically preloaded hydro-pneumatic spring can provide the advantage of increased spring rates near the mechanical end stops thus preventing the suspension from reaching the end-of-stroke stops.
2. For a hydro-pneumatic suspension system, the oil volume is changed during the leveling process, and the gas mass remains constant at all times. This gas mass changes its volume after a load change. A higher load means a smaller gas volume and a higher spring rate. Hence, the system shows progressive spring rate versus sprung mass behavior.
3. The mechanical coil spring with a viscous fluid damper has better friction level. The spring has no friction. The deformation is purely reversible. Therefore, in this suspension element, boundary friction originates only from the friction in the sealing and guiding elements inside the viscous fluid damper. It is a general rule that friction forces from dynamic seals increase with increasing seal differential pressures and sealing edge length.
4. For a hydro-pneumatic suspension system, a level adjustment is quite easily feasible by increasing or decreasing the amount of oil in the system.
5. The geometry of the suspension cylinder(s) plays no role in spring rate equations. The gas fill in the accumulator and the suspended load determine the contour of the force–displacement curve and the spring rate.

From mathematical modeling of the ageing behavior, the following results are drawn:

1. On the one hand, the suspension performance (PI) decreases in between the scheduled maintenance (SM) according to a gradual slow degradation (ageing) process. On the other hand, the PI decreases at random times (e.g., sporadic shocks) or instantaneous sharp decreases (e.g., shocks) at random times.
2. The cumulative PI degradation between the scheduled maintenance points is compensated for by minor routine maintenance and repair actions (e.g., nitrogen gas recharging, oil leakage compensation, repairing malfunctioning valves, and links). In contrast, the sudden sharp decreases in PI that are mainly due to shocks or failure accumulation in sub-systems until reaching a threshold (such as crack growth on oil cylinder or piston) are compensated for by major repair actions. Thus, the first kind of maintenance/repair is scheduled (SM), and the second type is corrective (CM).
3. The major mechanisms that cause PI drop between SMs are due to gas diffusion (thermodynamically) and oil leakage (hydro-mechanically). On the other hand, the effects of major deteriorating mechanisms, such as metal fatigue, elastomer degradation, corrosion, and oil contamination are taken into account in the form of the large non-linear and sharply decreasing curves.
4. The effects of thermodynamically and hydro-mechanically deteriorating mechanisms, as well as the effects of fatigue, material degradation, and oil contamination are mathematically modeled and incorporated in the formula for the temporal functional relationship for the suspension performance.
5. The proposed mathematical framework is solved using a minimum number of experimental data points. Using only, four data points, i.e., for pairs of (t, PI(t)) all model constants and parameters such as a, b, c, d, CSM, and CCM are estimated to capture the dump truck ageing process.
6. Using the validate model, both the rear and front suspension struts configurations were determined for different truck ages until 600 hours.

7. A predictive model for WBVs was extrapolated for the first 35,000 hours of a virtual CAT 793D age. The model shows that WBVs might exceed 4.0 m/s^2 at truck seat, after 7 years of two-shift-per-day continuous operations.

Finally, from the virtual experimentations the following results are drawn:

1. The hydro-pneumatic suspension strut ageing results in deteriorating stiffness-damping parameters. Therefore, the deteriorating suspension performance with time introduces more severe and prolonged WBVs in HISLO operations.
2. The RMS accelerations under HISLO increase significantly with time (suspension ageing). The relatively sharp increase in the vertical accelerations in 7 years introduces severe risks to the truck operators.
3. Even though the vertical accelerations go beyond the extreme level of 4.0 m/s^2 in less than 7 years, the lateral RMS accelerations remain in a safe zone.
4. The RMS accelerations in the vertical direction increased by 5.6% in a 3-year old truck from the nominal RMS accelerations in a brand-new truck under the HISLO operations. Furthermore, the RMS lateral accelerations increased by 12.2% in a 3-year old truck, which is still in the region of comfort zone for the human body exposure to WBVs.
5. The RMS accelerations in the vertical direction increased by 14.3% in a 5-year old truck from the nominal RMS accelerations in a brand-new truck under the HISLO operations. Furthermore, the RMS lateral accelerations increased by 15.4% in a 5-year old truck, which is still in the region of comfort zone for the human body exposure to WBVs.
6. The RMS accelerations in the vertical direction increased by 19.6% in a 7-year old truck from the nominal RMS accelerations in a brand-new truck under the HISLO operations. Furthermore, the RMS lateral accelerations increased by 33.9% in a 7-year old truck, which is still in the region of comfort zone for the human body exposure to WBVs.
7. Although, the two types of regular maintenance and repairs decrease the rate of increase in the vertical RMS accelerations, further major counteractions (e.g., more frequent

suspension rebuilding or replacing) are required for a safer working environment for truck operators.

8. Using the results of the virtual experimentation in the case of the CAT 793 D in the ADAMS environment, appropriate major overhauls, rebuild and replace schedules should be administered to prevent the WBVs from exceeding the pre-specified thresholds.

8.3. CONTRIBUTIONS OF PHD RESEARCH

The PhD research contributes to knowledge and frontier advances in ageing suspension systems of large mining trucks. The contributions include the following.

1. This is the first attempt to study the ageing behavior of hydro-pneumatic suspension struts in large mining dump trucks in surface mining operations.
2. The research originally developed understanding into the mechanisms underlying and governing the ageing process of the suspension systems in very large mining dump trucks using robust mathematical methods.
3. The new knowledge provides a potential basis for developing technologies to be employed in designing and manufacturing more robust suspensions. Thus, the long term health and safety of operators will be improved considerably.

8.4. RECOMMENDATIONS

This research has produced a mathematical basis for analyzing the ageing behavior of suspension struts in large mining trucks. Further studies are required to enhance the work carried out in this study, in the following specific areas.

1. The proposed framework should be examined in the case of real world data. Sensor technologies should be employed in order to collect real-time data from different components of all four hydro-pneumatic suspension struts. These data should be stored during different operations including HISLO, dumping, hauling and maneuvering.

2. Different manufacturers use different state-of-the-art technologies in their suspension struts. These different patented technologies do not have similar time performance behaviors. Therefore, every comprehensive study that seeks to generalize mathematical models should include different truck makes and sizes as well as working conditions.
3. It is known that operators' skills and driving styles have considerable effects on longevity of different components of dump trucks. These parameters and their effects on suspension performance should be taken into account in future studies.
4. A full-life simulation of ageing suspensions demands a significant work load which is over 2800 man-hour in order to undertake 35,000 experimentations in the ADAMS environment. In this study, the data obtained for the first 600 working hours were used to extrapolate the RMS values until 35,000 hours. Therefore, more iterations and experiments are required for defining these relationships more accurately.

APPENDIX

RMS ACCELERATION CURVES FOR TRUCK AGES 3, 5, AND 7 YEARS

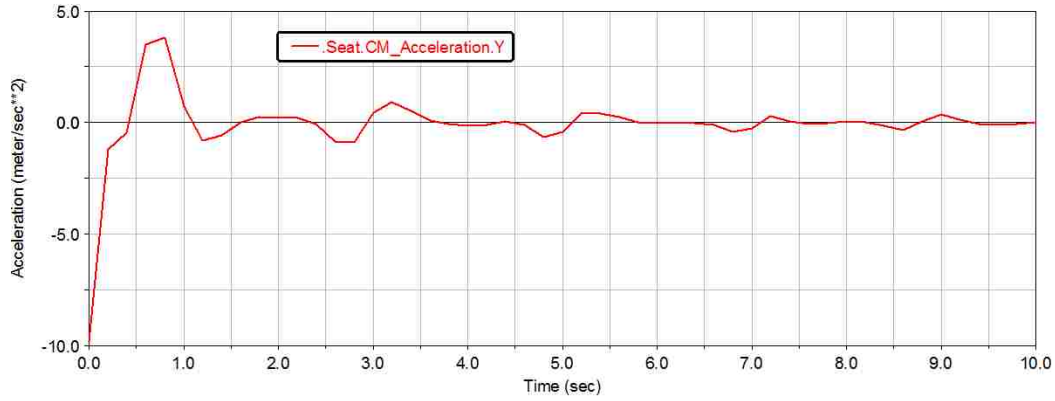

Figure A.1. The RMS values of vertical accelerations for experiment No. 1 in Table 6.5 (3-year old truck).

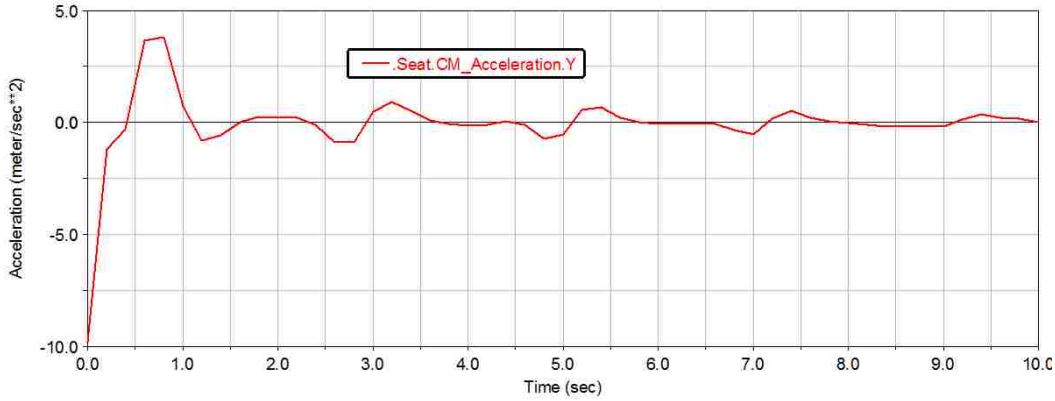

Figure A.2. The RMS values of vertical accelerations for experiment No. 2 in Table 6.5 (3-year old truck).

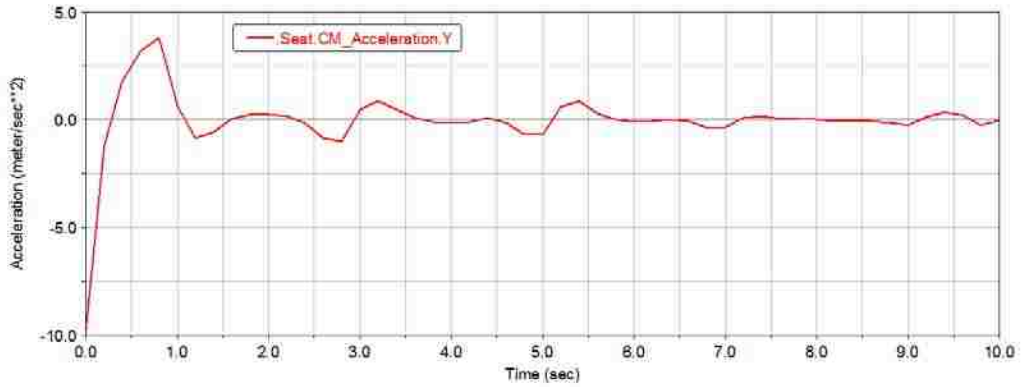

Figure A.3. The RMS values of vertical accelerations for experiment No. 3 in Table 6.5 (3-year old truck).

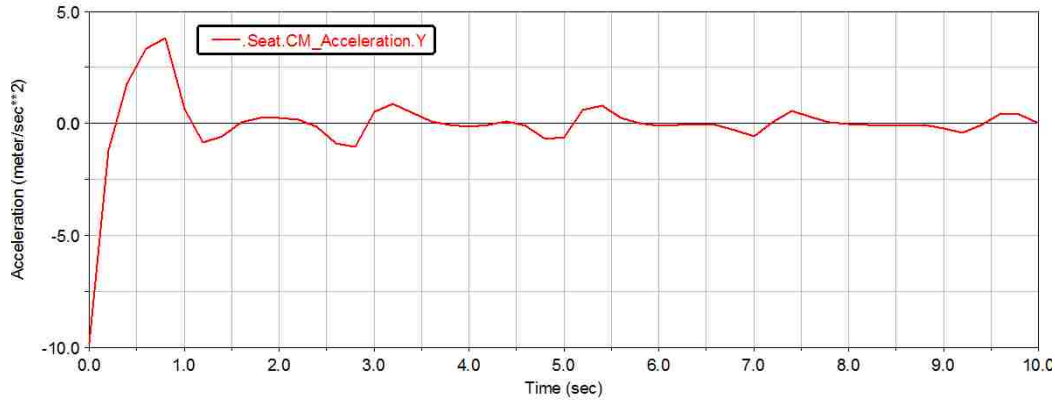

Figure A.4. The RMS values of vertical accelerations for experiment No. 4 in Table 6.5 (3-year old truck).

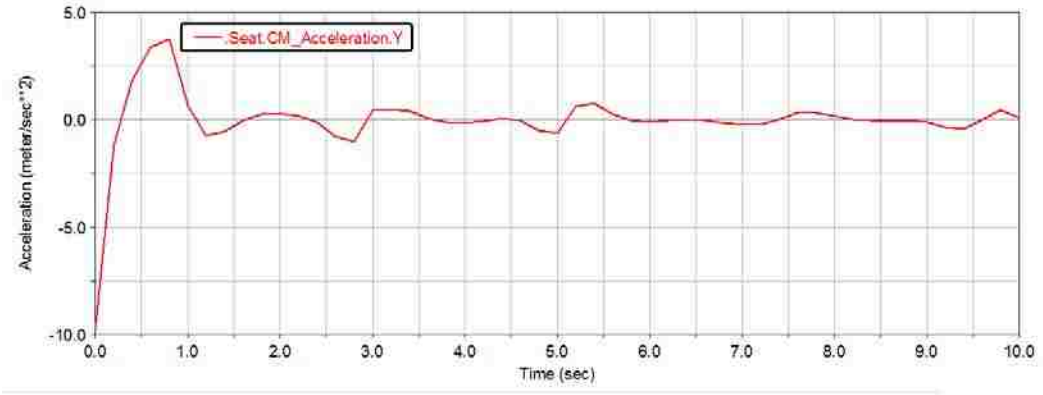

Figure A.5. The RMS values of vertical accelerations for experiment No. 5 in Table 6.5 (3-year old truck).

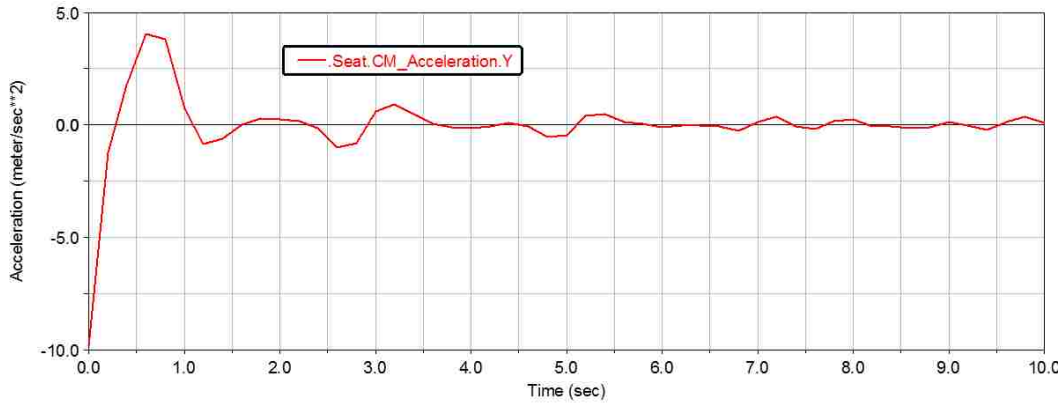

Figure A.6. The RMS values of vertical accelerations for experiment No. 6 in Table 6.5 (3-year old truck).

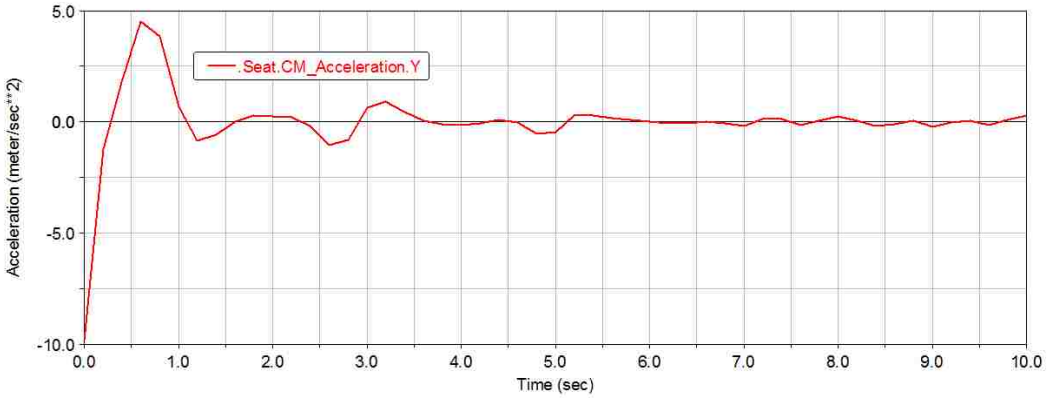

Figure A.7. The RMS values of vertical accelerations for experiment No. 7 in Table 6.5 (3-year old truck).

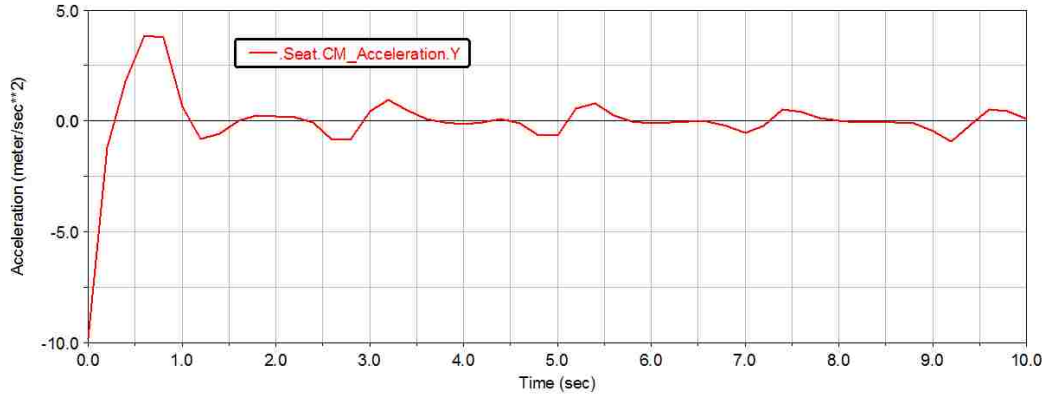

Figure A.8. The RMS values of vertical accelerations for experiment No. 8 in Table 6.5 (3-year old truck).

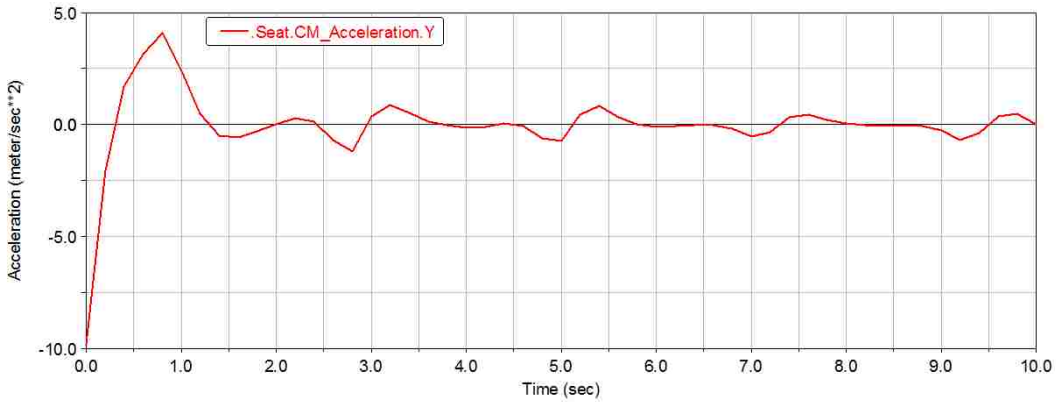

Figure A.9. The RMS values of vertical accelerations for experiment No. 10 in Table 6.5 (3-year old truck).

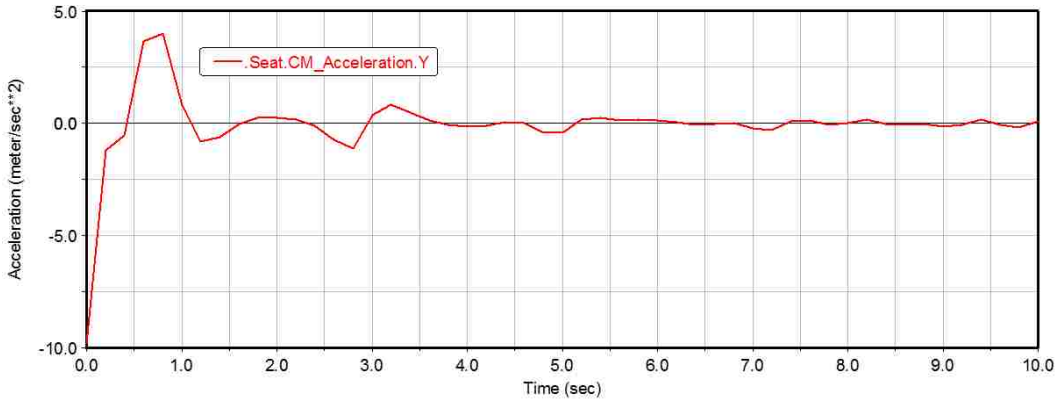

Figure A.10. The RMS values of vertical accelerations for experiment No. 11 in Table 6.5 (3-year old truck).

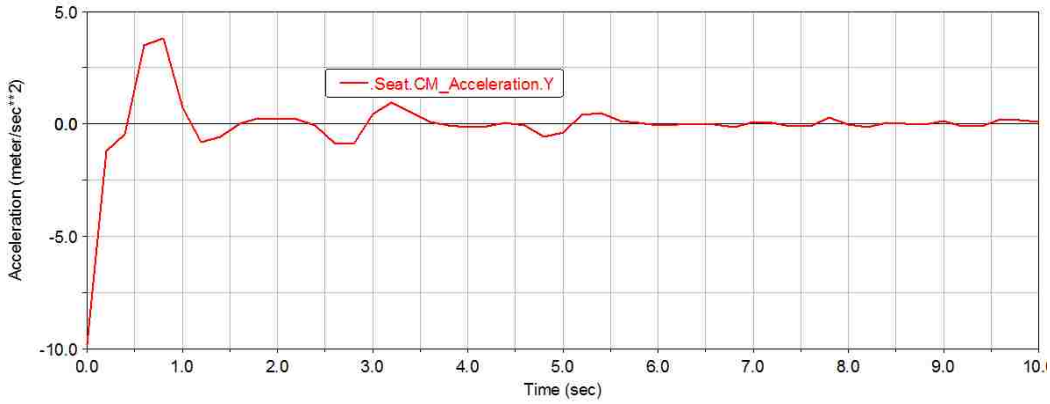

Figure A.11. The RMS values of vertical accelerations for experiment No. 14 in Table 6.5 (3-year old truck).

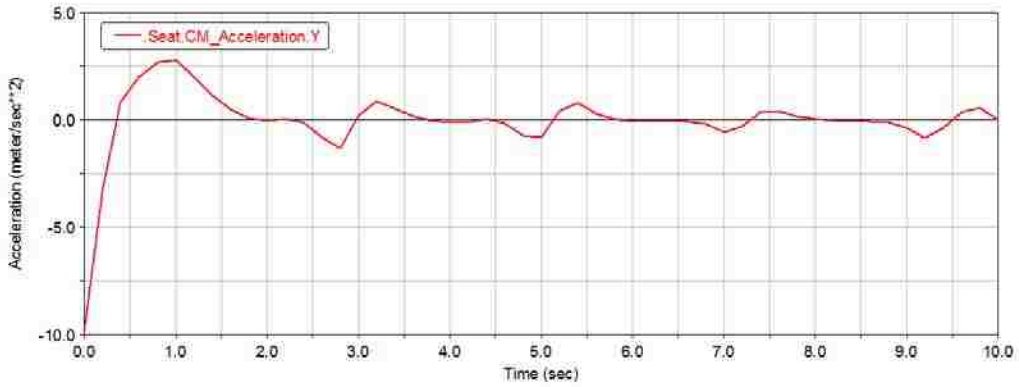

Figure A.12. The RMS values of vertical accelerations for experiment No. 15 in Table 6.5 (3-year old truck).

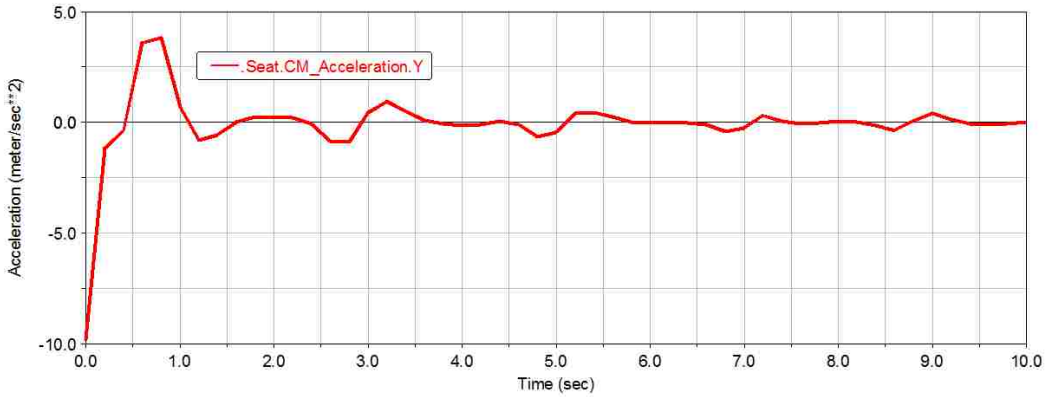

Figure A.13. The RMS values of vertical accelerations for experiment No. 16 in Table 6.5 (3-year old truck).

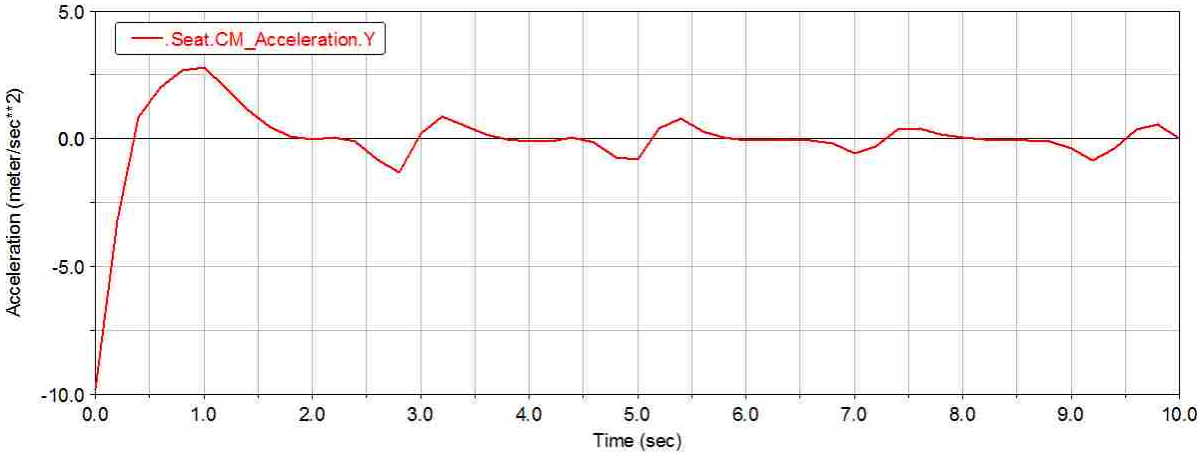

Figure A.14. The RMS values of vertical accelerations for experiment No. 17 in Table 6.5 (3-year old truck).

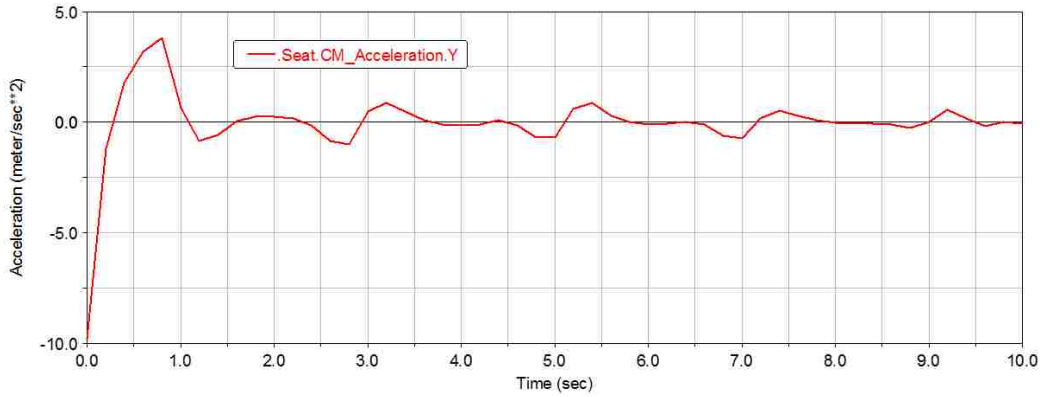

Figure A.15. The RMS values of vertical accelerations for experiment No. 19 in Table 6.5 (3-year old truck).

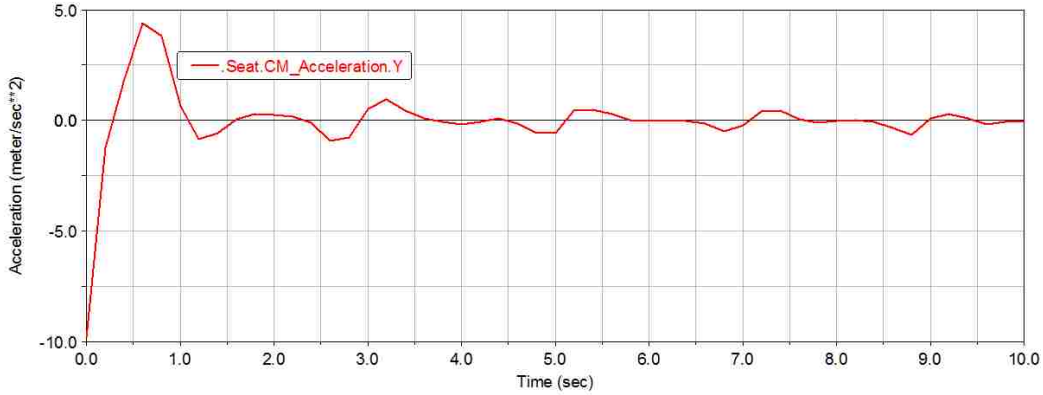

Figure A.16. The RMS values of vertical accelerations for experiment No. 2 in Table 6.6 (5-year old truck).

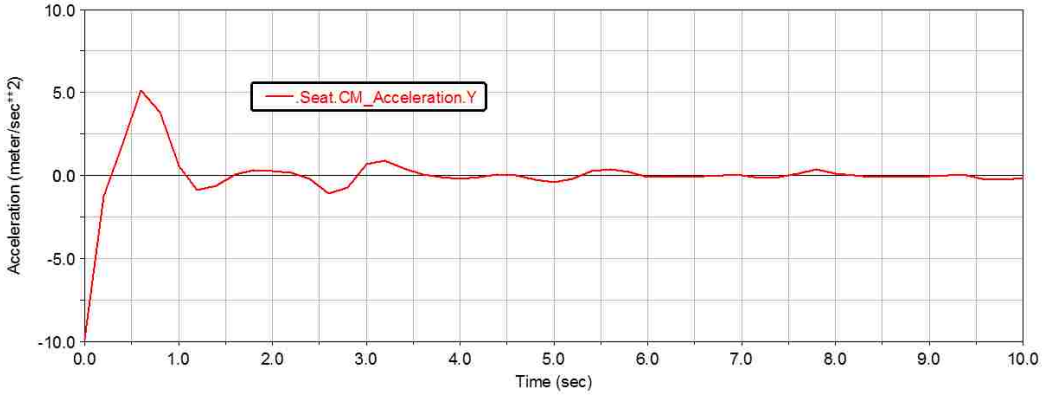

Figure A.17. The RMS values of vertical accelerations for experiment No. 3 in Table 6.6 (5-year old truck).

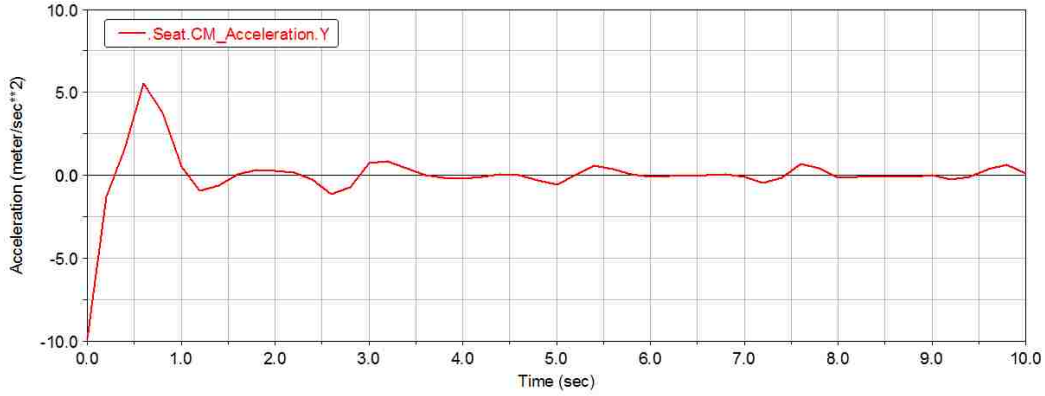

Figure A.18. The RMS values of vertical accelerations for experiment No. 4 in Table 6.6 (5-year old truck).

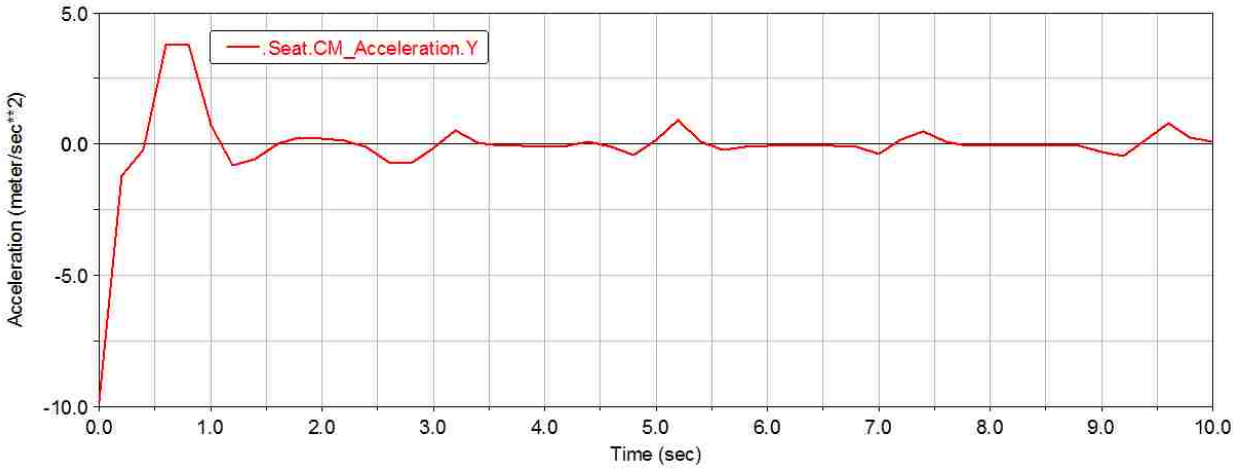

Figure A.19. The RMS values of vertical accelerations for experiment No. 5 in Table 6.6 (5-year old truck).

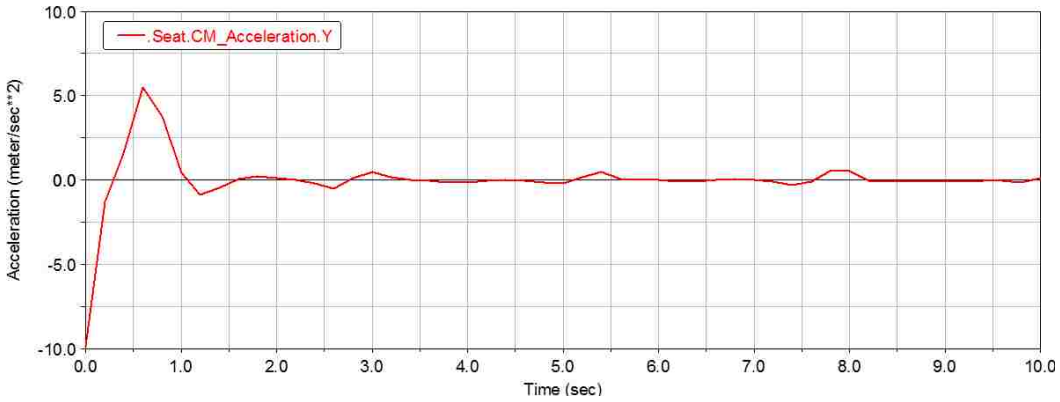

Figure A.20. The RMS values of vertical accelerations for experiment No. 6 in Table 6.6 (5-year old truck).

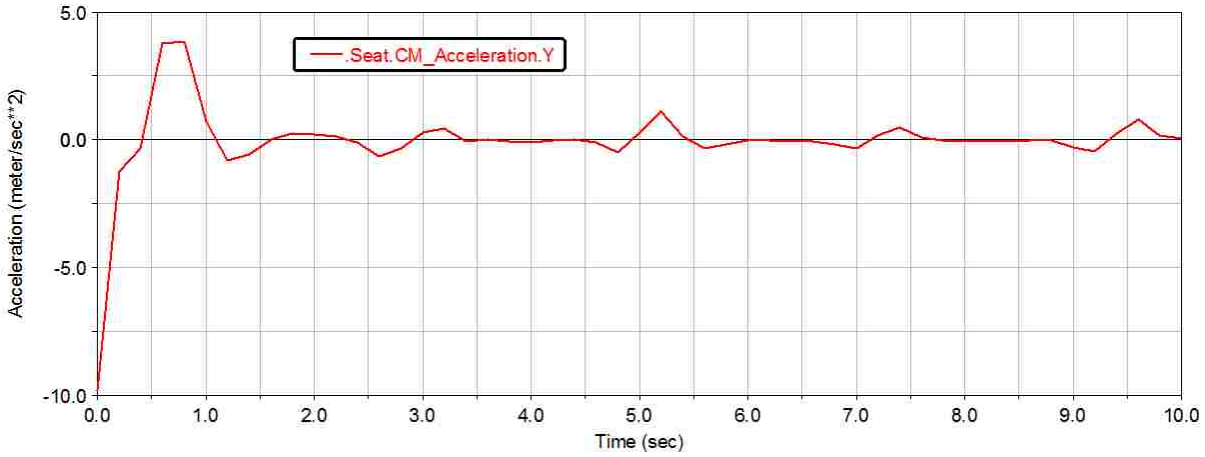

Figure A.21. The RMS values of vertical accelerations for experiment No. 7 in Table 6.6 (5-year old truck).

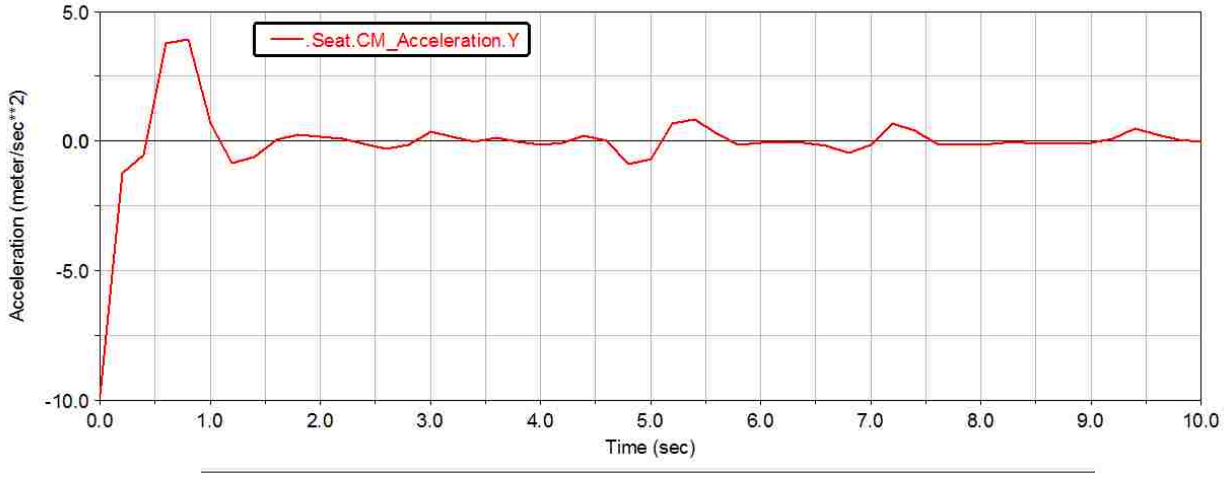

Figure A.22. The RMS values of vertical accelerations for experiment No. 8 in Table 6.6 (5-year old truck).

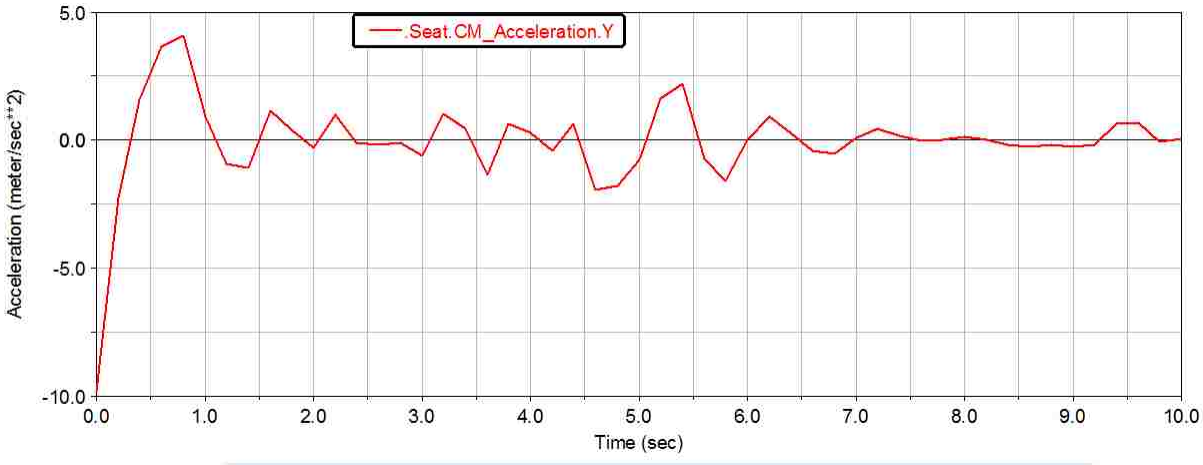

Figure A.23. The RMS values of vertical accelerations for experiment No. 9 in Table 6.6 (5-year old truck).

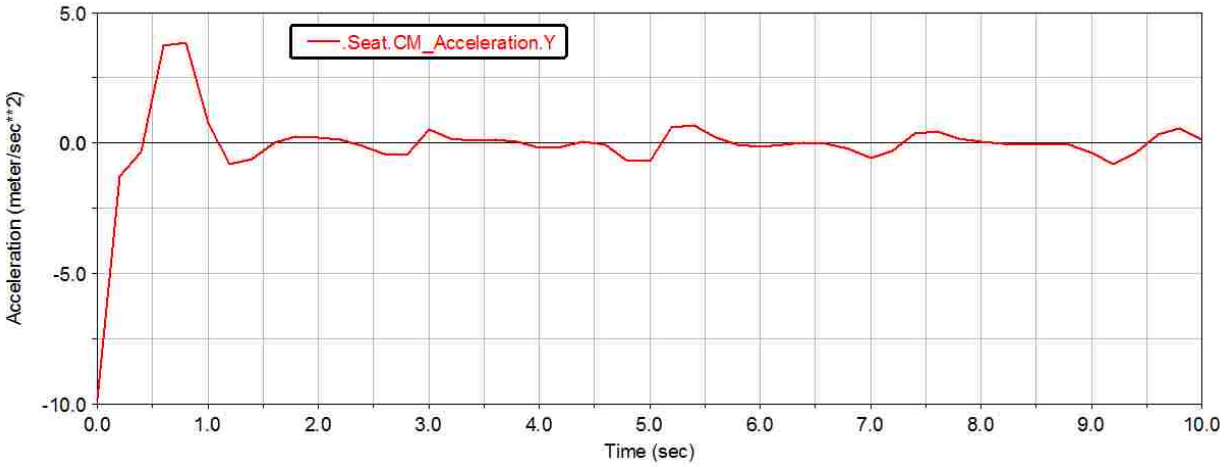

Figure A.24. The RMS values of vertical accelerations for experiment No. 10 in Table 6.6 (5-year old truck).

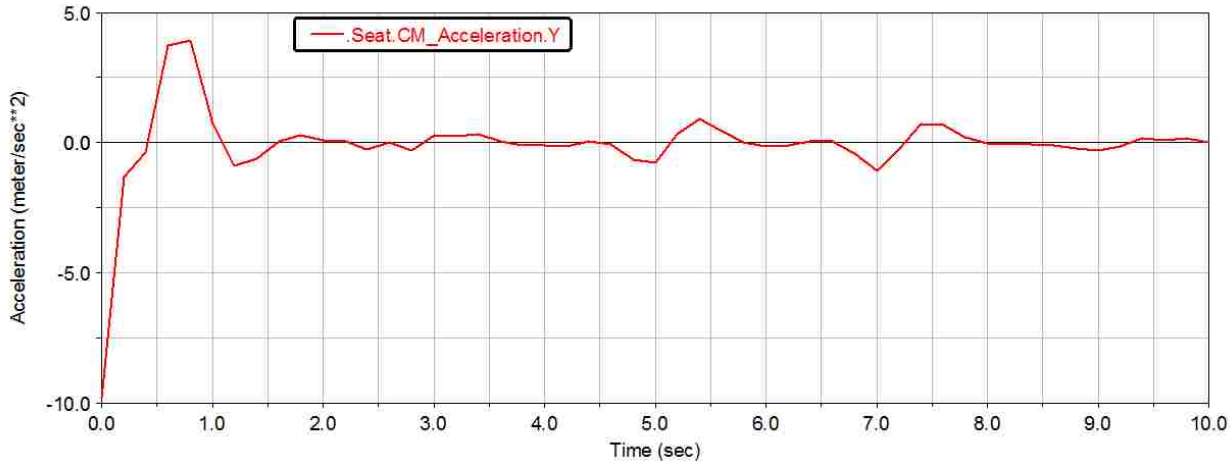

Figure A.25. The RMS values of vertical accelerations for experiment No. 13 in Table 6.6 (5-year old truck).

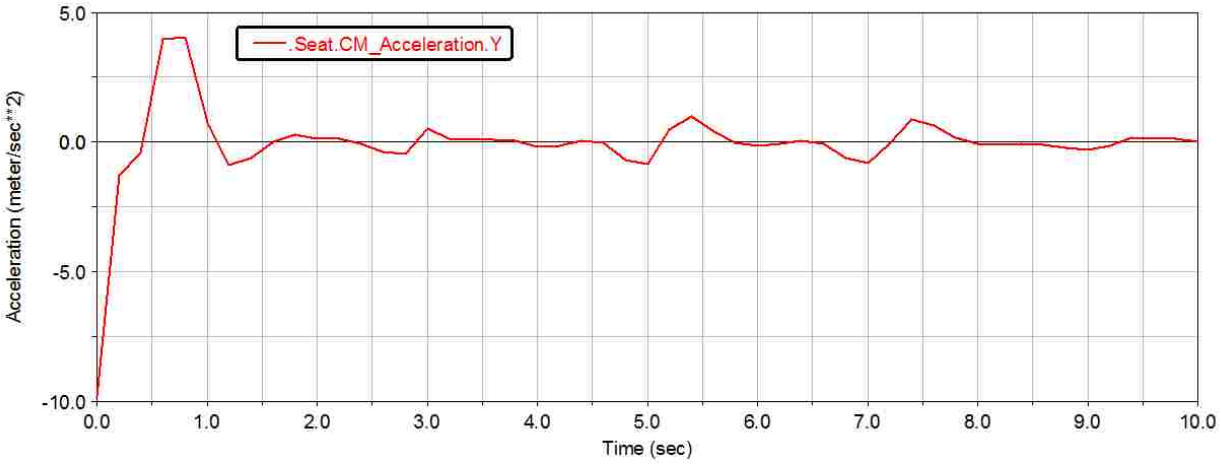

Figure A.26. The RMS values of vertical accelerations for experiment No. 15 in Table 6.6 (5-year old truck).

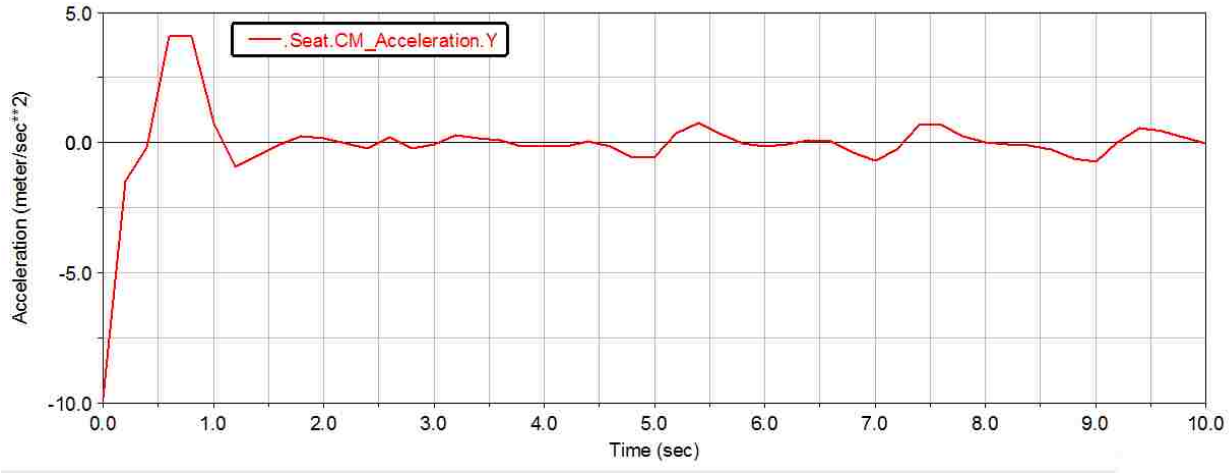

Figure A.27. The RMS values of vertical accelerations for experiment No. 16 in Table 6.6 (5-year old truck).

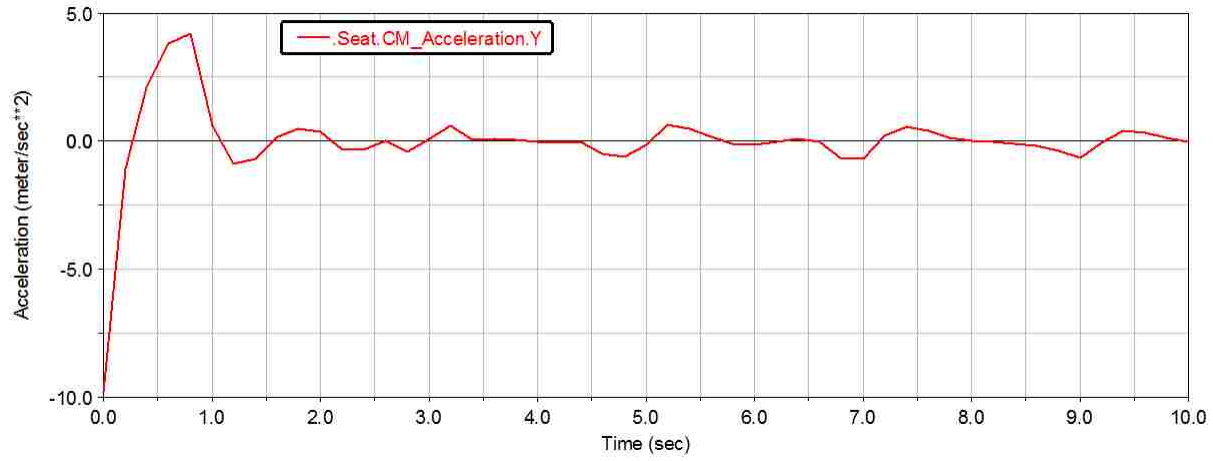

Figure A.28. The RMS values of vertical accelerations for experiment No. 17 in Table 6.6 (5-year old truck).

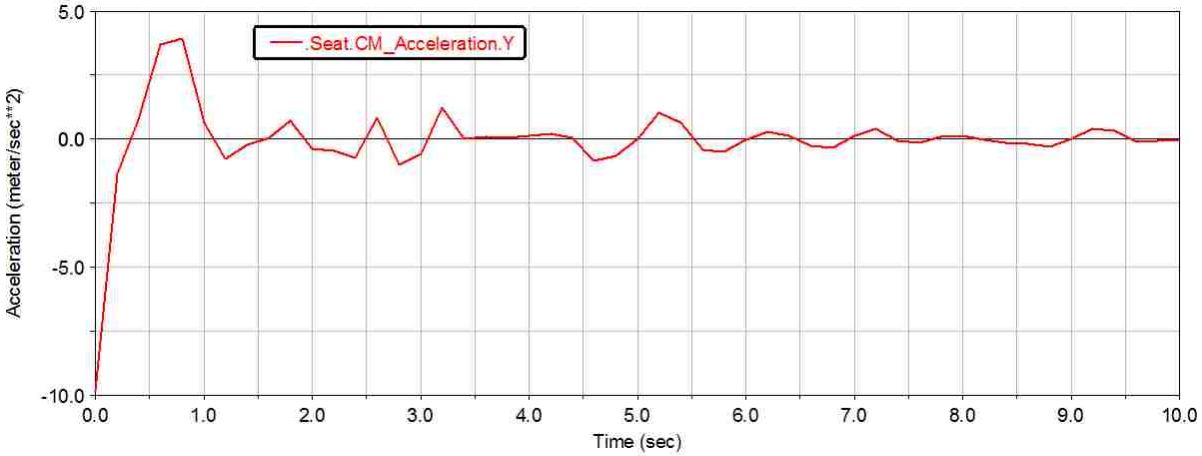

Figure A.29. The RMS values of vertical accelerations for experiment No. 18 in Table 6.6 (5-year old truck).

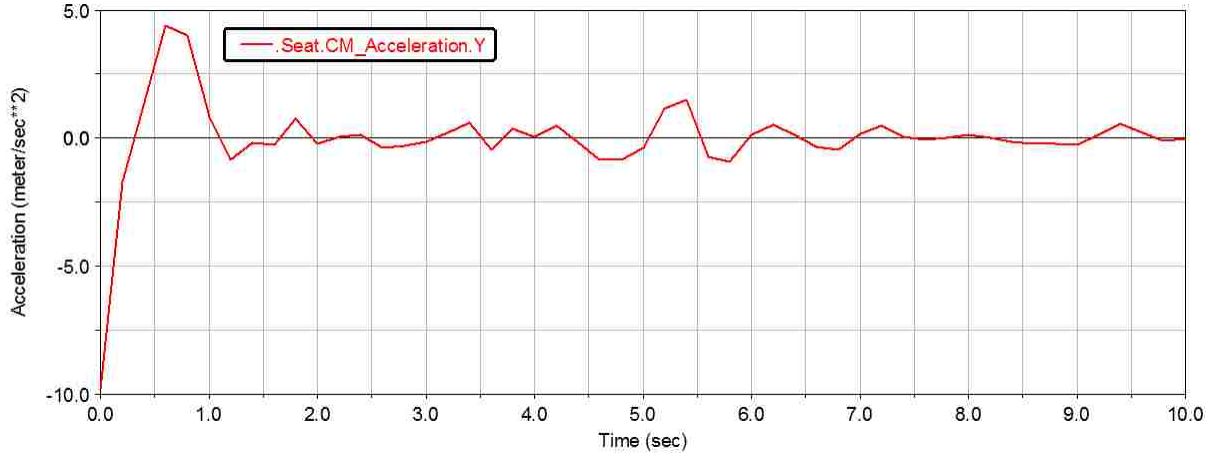

Figure A.30. The RMS values of vertical accelerations for experiment No. 19 in Table 6.6 (5-year old truck).

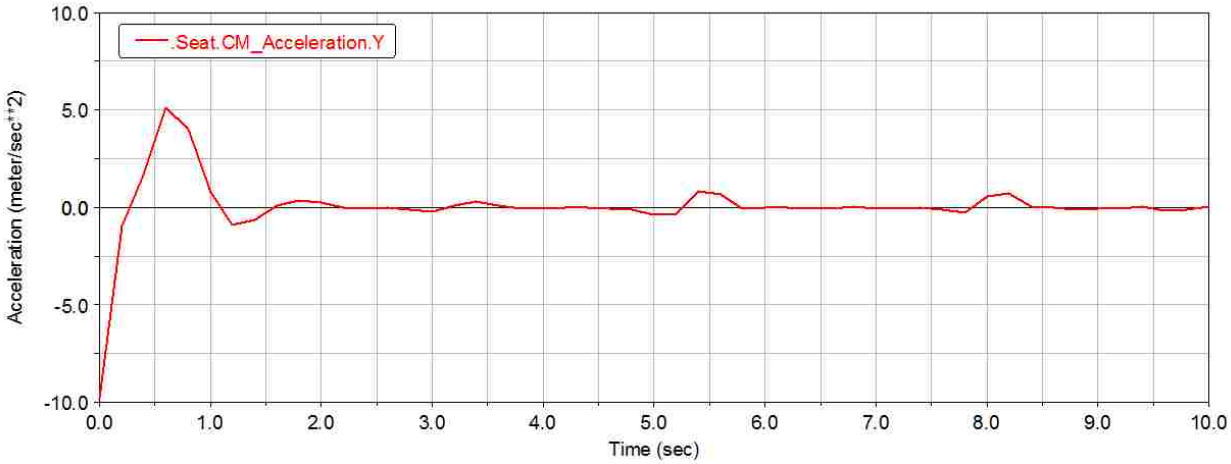

Figure A.31. The RMS values of vertical accelerations for experiment No. 2 in Table 6.7 (7-year old truck).

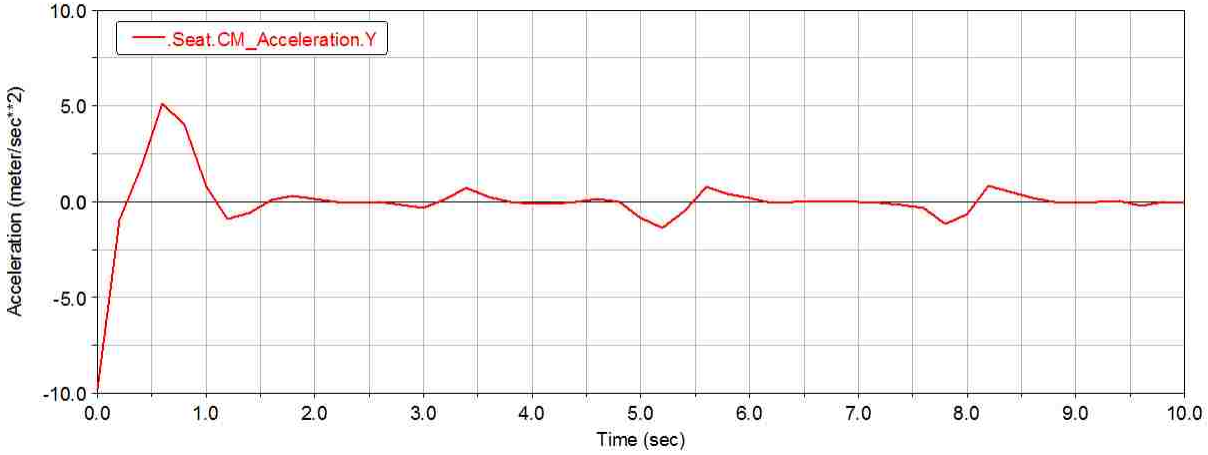

Figure A.32. The RMS values of vertical accelerations for experiment No. 4 in Table 6.7 (7-year old truck).

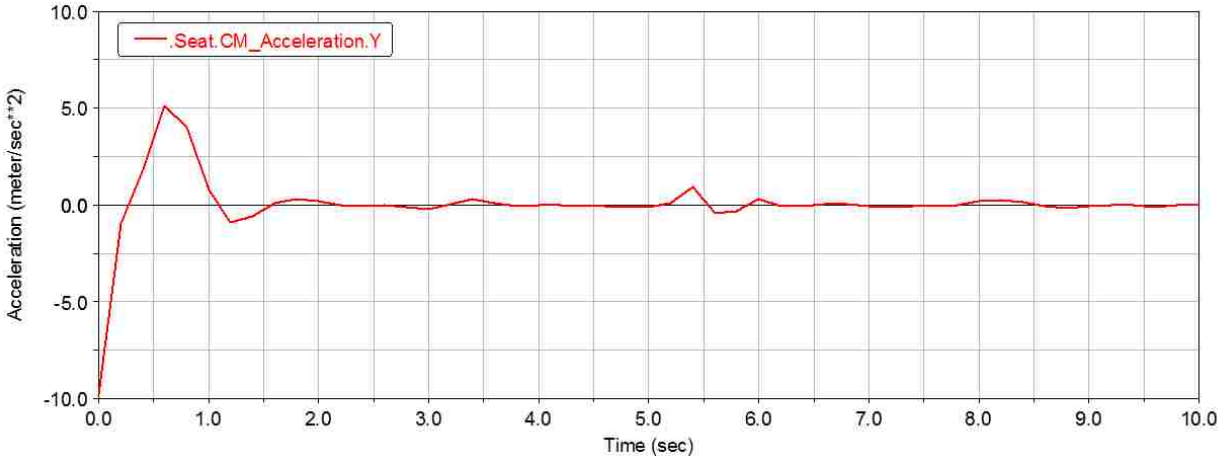

Figure A.33. The RMS values of vertical accelerations for experiment No. 5 in Table 6.7 (7-year old truck).

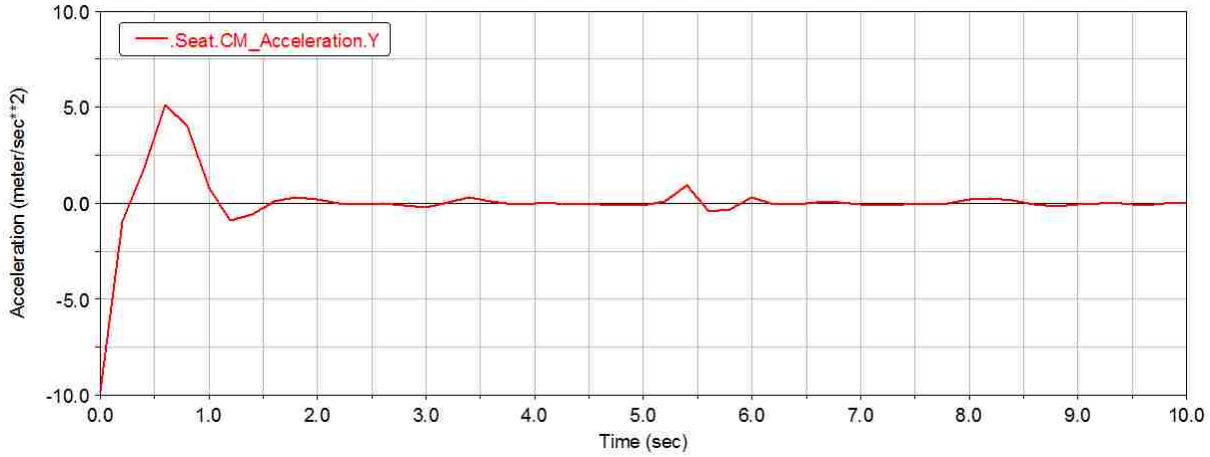

Figure A.34. The RMS values of vertical accelerations for experiment No. 6 in Table 6.7 (7-year old truck).

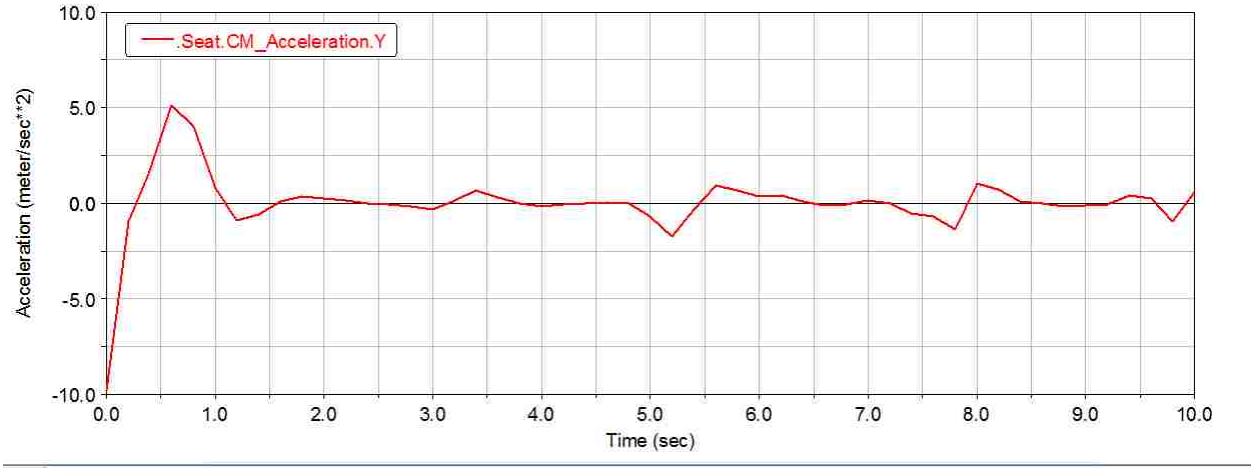

Figure A.35. The RMS values of vertical accelerations for experiment No. 7 in Table 6.7 (7-year old truck).

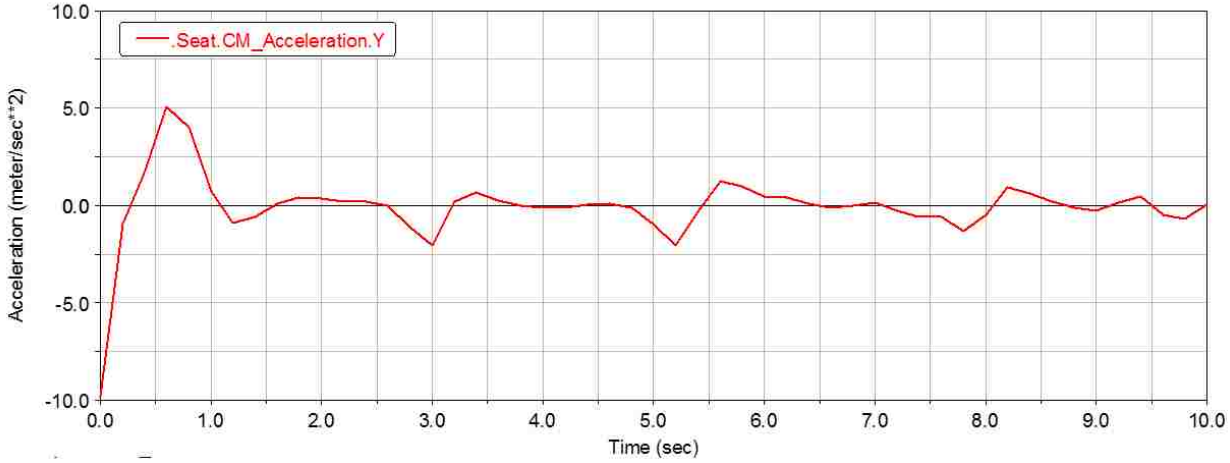

Figure A.36. The RMS values of vertical accelerations for experiment No. 8 in Table 6.7 (7-year old truck).

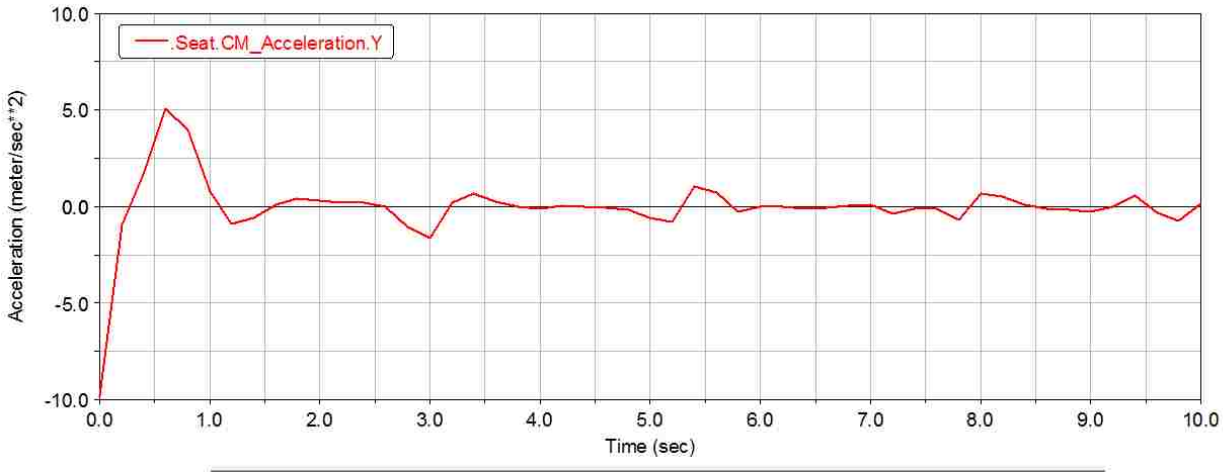

Figure A.37. The RMS values of vertical accelerations for experiment No. 9 in Table 6.7 (7-year old truck).

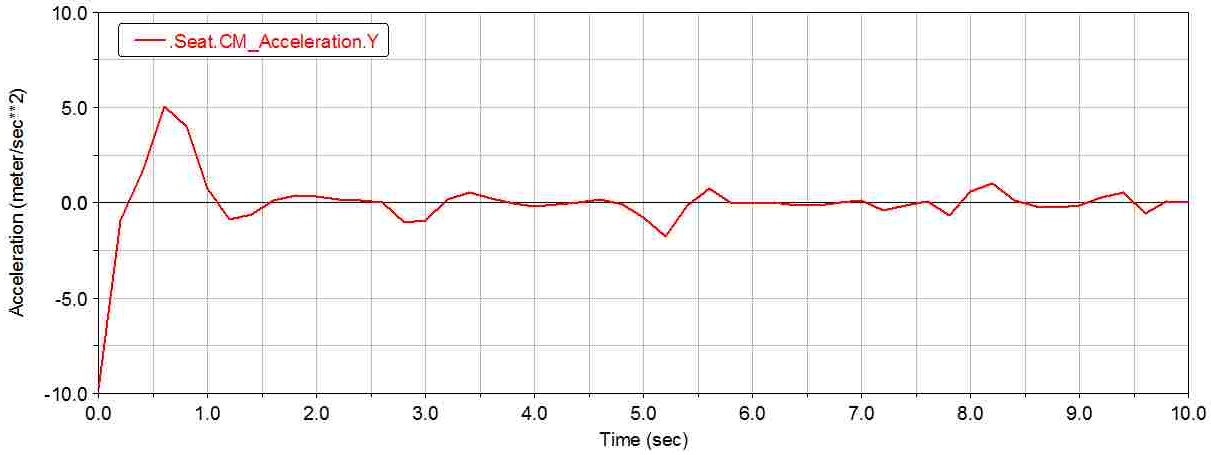

Figure A.38. The RMS values of vertical accelerations for experiment No. 10 in Table 6.7 (7-year old truck).

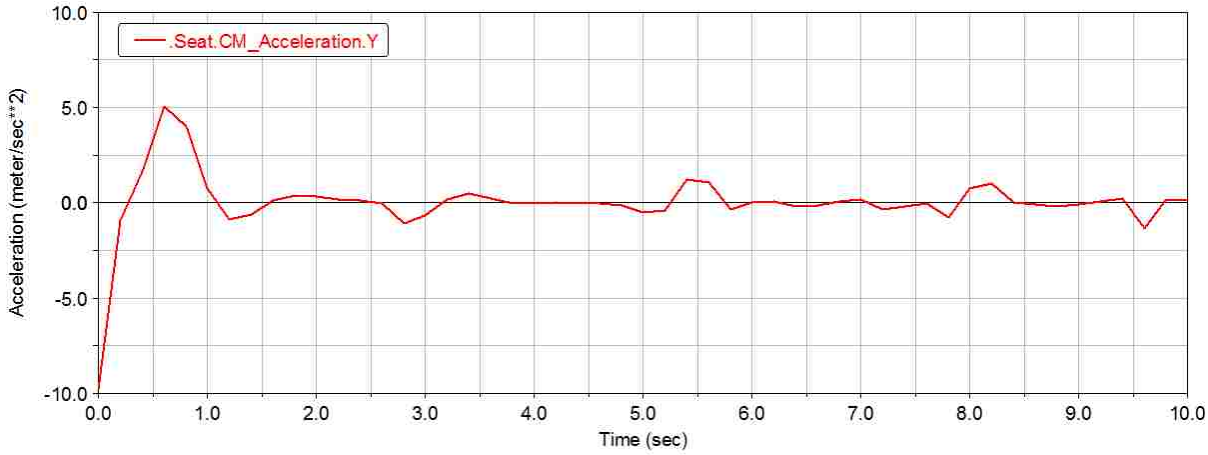

Figure A.39. The RMS values of vertical accelerations for experiment No. 11 in Table 6.7 (7-year old truck).

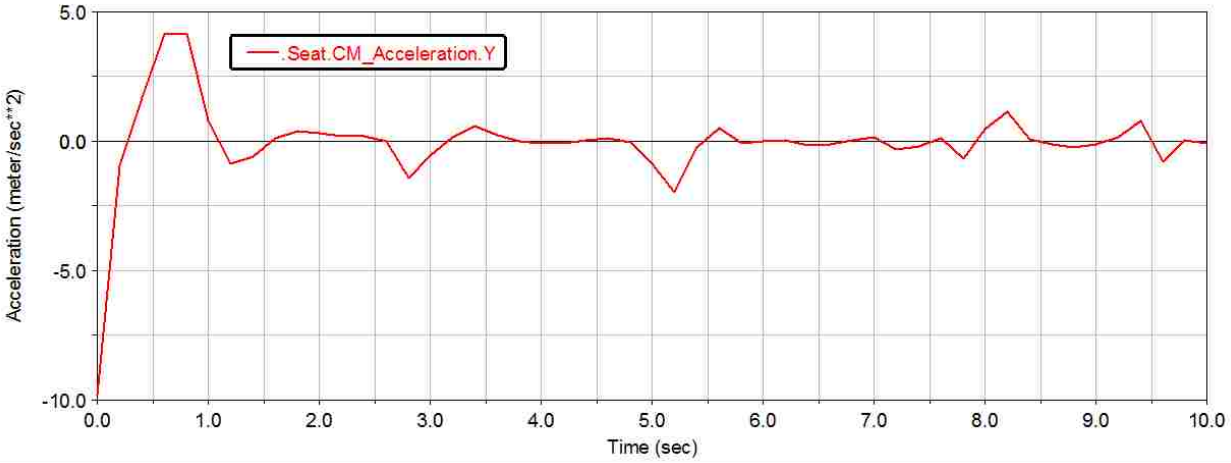

Figure A.40. The RMS values of vertical accelerations for experiment No. 12 in Table 6.7 (7-year old truck).

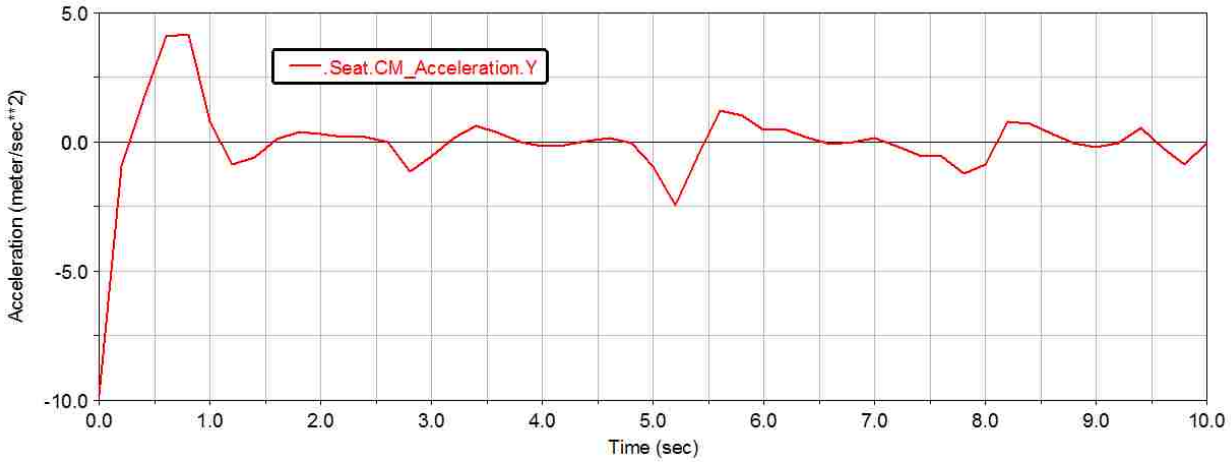

Figure A.41. The RMS values of vertical accelerations for experiment No. 14 in Table 6.7 (7-year old truck).

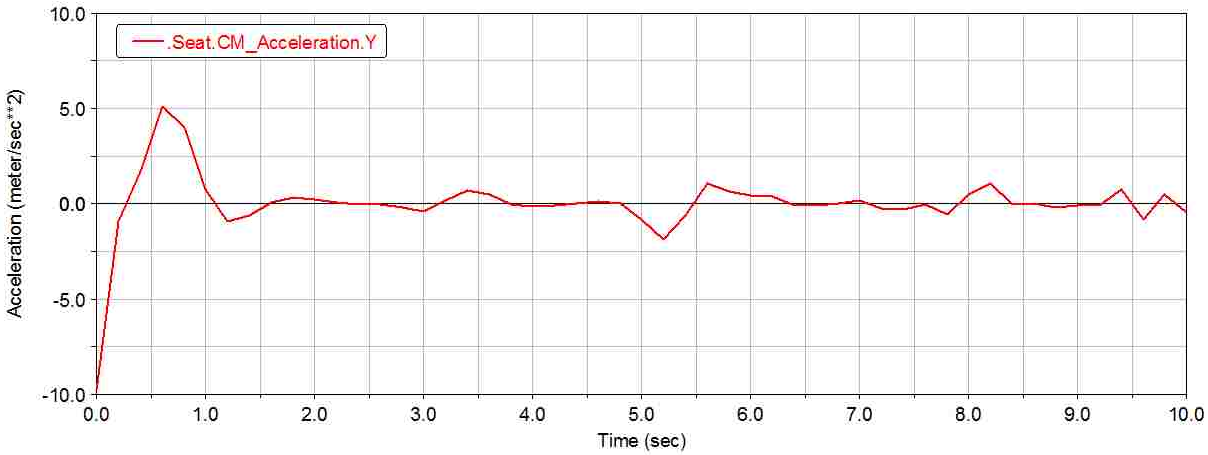

Figure A.42. The RMS values of vertical accelerations for experiment No. 15 in Table 6.7 (7-year old truck).

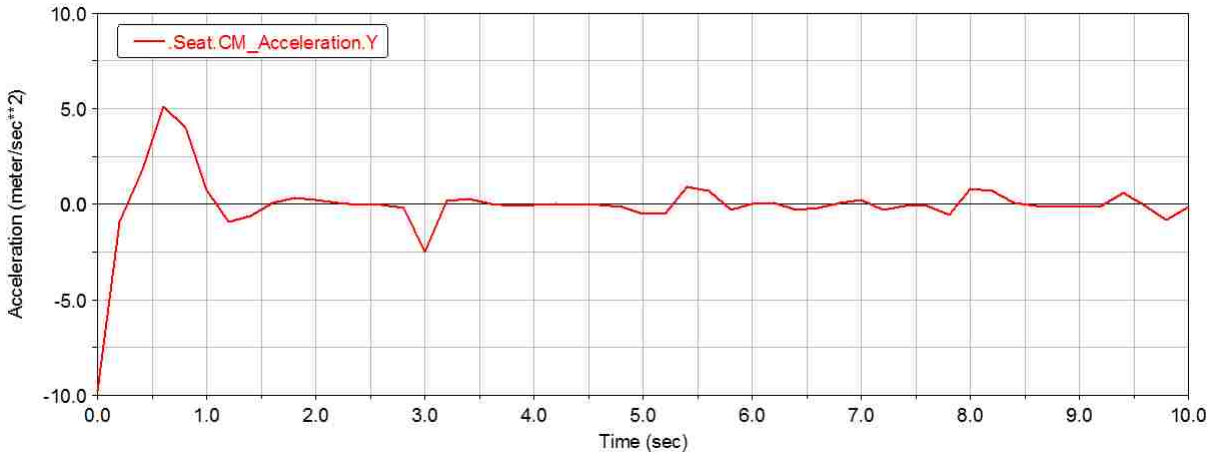

Figure A.43. The RMS values of vertical accelerations for experiment No. 16 in Table 6.7 (7-year old truck).

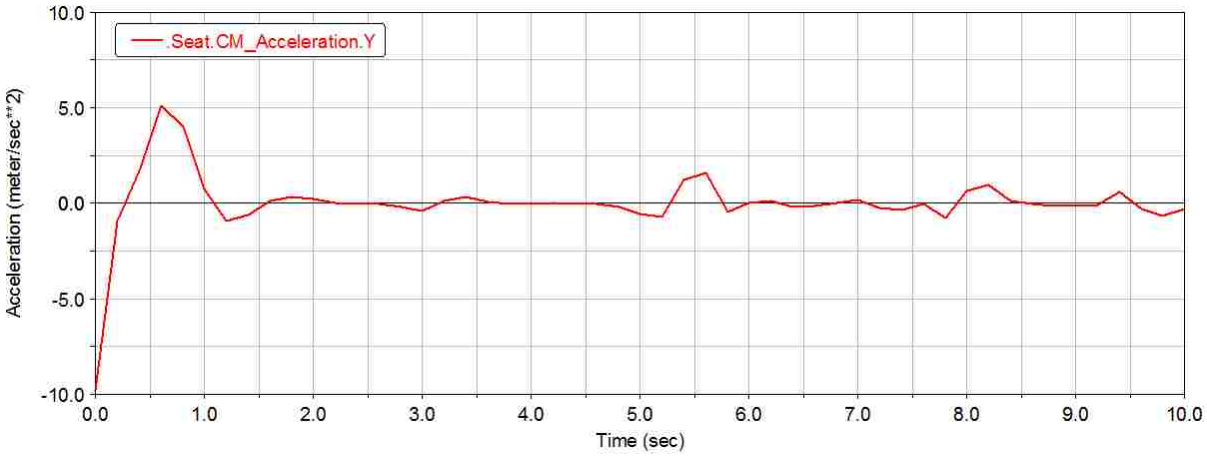

Figure A.44. The RMS values of vertical accelerations for experiment No. 17 in Table 6.7 (7-year old truck).

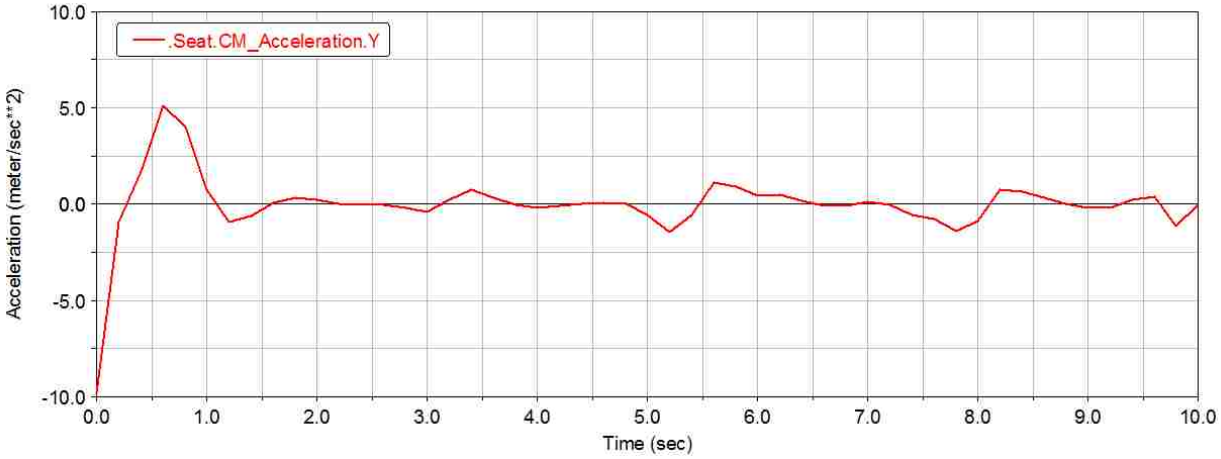

Figure A.45. The RMS values of vertical accelerations for experiment No. 19 in Table 6.7 (7-year old truck).

BIBLIOGRAPHY

Abdeen M. and Abbas W. 2011. *"Prediction the Biodynamic Response of the Seated Human Body using Artificial Intelligence Technique",* International Journal of Engineering, Volume 4, Issue 6, pp. 491 – 506.

Aouad N. 2008. "Mechanics of Dump Truck Vibrations in High Impact Shovel Loading Operations", Ph.D. Dissertation, Missouri S&T, Rolla, MO.

Aziz, S.A.A., Nuawi, M.Z., Mohd Nor, M.J., Daruis, D.D.I. 2014. Study of noise, vibration and harshness (NVH) for Malaysian Army 3-tonne Trucks. Applied Mech. & Matls, 471: 74-80.

Bauer, W. 2010. Hydropneumatic suspension systems. Springer Science & Business Media.

Boileau P.-E., Rakheja S. 1990. "Vibration Attenuation Performance of Suspension Seats for Off-Road Forestry Vehicles", International Journal of Industrial Ergonomics, 5: 275-291.

Bouazara M., Richard M.J., and Rakheja S. 2006. "Safety and comfort analysis of a 3-D vehicle model with optimal non-linear active seat suspension" Journal of Terramechanics, Vol. 43, No. 2: 97–118.

Colquhoun, C. and Draper, J. 2000. "Fatigue Analysis of an FEA Model of a Suspension Component, and Comparison with Experimental Data" NAFEMS Seminar: Fatigue Analysis, Wiesbaden, Germany.

Costa, N. and Arezes, P.M. 2009. "The influence of operator driving characteristics in whole-body vibration exposure from electrical fork-lift trucks" International Journal of Industrial Ergonomics 39: 34–38.

Deb, K., Pratap, A., Agarwal, S., Meyarivan, T. 2002. A fast and elitist multiobjective genetic algorithm: NSGA-II. IEEE. Transactions on Evolutionary Computation; 6 (2):182-197.

Demir, O., Keskin, I., and Cetin, S. 2012. "Modeling and control of nonlinear half-vehicle suspension system: a hybrid fuzzy logic approach" N-linear Dyn., Vol. 67, No. 3: 2139-2151.

Eger, T., Stevenson, J., Boileau, P.-E., Salmoni, A., and VibRG. 2008a. "Predictions of health associated with the operation of load-haul-dump mining vehicles: Part 1—Analysis of WBV exposure using ISO 2631-1 and ISO-2631-5 standards", Int. J. of Ind. Ergon. 38: 726–738.

Eger, T., Stevenson, J., Callaghan, J.P, Grenier, S., and VibRG. 2008b. "Predictions of health risks associated with the operation of load-haul-dump vehicles: Part 2—Eval. of operator driving postures & associated postural loading" Int. J. of Ind. Erg., Vol. 38, No. 9–10: 801–815.

Frimpong, S. 2011. "Engineered Solutions: Dump Truck Vibrations and Impact on Operator Safety in High-Impact Shovel Loading Operations". Proposal funded by CDC-NIOSH, Caterpillar and Peabody Energy. © Missouri S&T, Rolla, MO: 28 p.

Frimpong, S. and Aouad, N. 2009. "Dump Truck Vibrations in High-Impact Shovel Loading Operations". Proceedings of CAMI Conference. Banff, AB.

Goh, Y M., Booker, J D., McMahon, C A. 2005. "Uncertainty modeling of a suspension unit" Proceedings of the Institution of Mechanical Engineers, 219. 6 : 755-771.

Gómez, J. F., Aguilar; Rosales, J. J., Bernal, J. J., and Guia, M. 2012. "Mathematical modelling of the mass-spring-damper system - A fractional calculus approach" Acta Universitaria, Vol. 22, No. 5: 5 – 11.

Griffin, M. J. 1990. "Handbook of Human Vibration". © Academic Press, London

Howard, B., Sesek, R., and Bloswick, D. 2009. "Typical whole body vibration exposure magnitudes encountered in the open pit mining industry", Work (Reading, Mass.), Vol. 34, No. 3: 297-303.

Huston, D.R., Johnson, C.C., Wood, M.A. and Zhao, X. 1999. "Vibration Attenuating Characteristics of Air-Filled Seat Cushions" J. of Sound and Vibration 222(2): 3313-327.

ISO, 2004. Mechanical Vibration and Shock: Evaluation of Human Exposure to Whole Body Vibration; Part 1: General Requirements (ISO 2631-1). © ISO, Switzerland.

Kijima, M. (1989). Some results for repairable systems with general repair, Journal of Applied Probability, 26: 89-102.

Lardner, T.J. 2002. "Resonance & the Ageing Spring". J. of Applied Mechanics, Vol. 69: 397-398.

Leelavathy, K.R., Raju, R., and Gokul, R.S. 2011. "Whole Body Vibration and Back Disorders among Vehicle Operators" European J. of Scientific Research, Vol.61, No.3: 328-340.

Mcmanus, S. J., Clair, K.A., Boileau, P.E., Boutin, J. and Rakheja, S. 2002. "Evaluation of Vibration and Shock Attenuation Performance of a Suspension Seat with a Semi-Active Magnetorheological Fluid Damper". J. of Sound and vibration 253(1): 313-327.

Nouri, K., Loussifi, H., and Braieck, N.B. 2011. "Modelling and wavelet-based identification of 3-DOF vehicle suspension system" J. of Software Engineering and Applications (JSEA), Vol. 4, No. 12: 672 – 681.

Patil, M., and Palanichamy, M.S. 1998. "A mathematical model of tractor occupant system with a new seat suspension for minimization of vibration response". Appl. Math. Modelling, Vol. 12: 63-71.

Puff, R., de Bortoli, G.D.M., Bosco, R. Jr. 2010. "Fatigue Analysis of Helical Suspension Springs for Reciprocating Compressors". Int. Compressor Eng. Conference, Purdue, IN: 1298-1.

Rajapakse, N.I., Happawana, G.S., and Hurmuzlu, Y. 2007. "Suppression of heavy-truck driver-seat vibration using sliding-mode control and quantitative feedback theory", Proc. IMechE Vol. 221 Part I: J. Systems and Control Engineering: 769-779.

Rodríguez, G.A., Chacón, J.M., Donoso, A., Rodríguez, A.G. 2011. "Design of an adjustable-stiffness spring: Mathematical modeling and simulation, fabrication and experimental validation". Mechanism and Machine Theory 46: 1970–1979.

Savić, D. A., Bicik, J., & Morley, M. S. 2011. A DSS Generator for Multiobjective Optimisation of Spreadsheet-Based Models. Environmental Modelling and Software; 26(5):551-561.

Seidel H. 2005. "On the relationship between whole-body vibration exposure and spinal health risk". Industrial health, Vol. 43, No. 3: 361-377.

Smets, M., Eger, T.R., and Grenier, S.G. 2010. "Whole-body vibration experienced by haulage truck operators in surface mining operations: A comparison of various analysis methods utilized in the prediction of health risks". Applied Ergonomics 41: 763–770.

Smith, S. D., Smith, J. A., and Bowden, D. R. 2008. "Transmission characteristics of suspension seats in multi-axis vibration environments". Int. J. of Ind. Erg., Vol. 38, No. 5: 434 – 446.

N. Srinivas and K. Deb, "Multiobjective function optimization using nondominated sorting genetic algorithms," Evol. Comput., vol. 2, no. 3, pp. 221–248, Fall 1995.

Trangsrud, C., Law, E.H., and Janajreh, I. (2004), "Ride Dynamics and Pavement Loadings of Tractor Semi-Trailors on Randomly Rough Roads," SAE International, Vehivle Dynamics & Chassis Development, SP-1904, 2004-01- 2612, pp. 23-46.

van Noortwijk, J.M. 2009. A survey of the application of gamma processes in maintenance Reliability Engineering and System Safety, 94 (1):2-21.

Walsh, P.L. and Lamancusa, J.S. 1992. “A Variable Stiffness Vibration Absorber for Minimization of Transient Vibrations”. J. of Sound and Vibration 158(2): 195-211.

Wang, W., Rakheja, S., Boileau, P-É. 2008. "Relationship between measured apparent mass and seat-to-head transmissibility responses of seated occupants exposed to vertical vibration". J. of Sound and Vibration, Vol. 314, No. 3: 907 – 922.

Whitaker, L.R., Samaniego, F.J. 1989. Estimating the reliability of systems subject to imperfect repair. Journal of the American Statistical Association, 84 (405): 301-309.

VITA

Saeid R Dindarloo obtained his Bachelor of Science in Mining Engineering from Amirkabir University of Technology, Iran from 2002 to 2006. He holds a Master of Science in Mining Engineering from Amirkabir University of Technology, Iran. In August 2012, he joined the PhD program in Mining Engineering at Missouri University of Science and Technology in Rolla, MO, formerly known as University of Missouri Rolla. During his PhD candidacy, he worked as a research assistant on mining truck suspension modeling as part of the Heavy Mining Machinery Research Group under the guidance of Dr. Samuel Frimpong. In May 2016 he received his PhD in Mining Engineering from Missouri University of Science and Technology.